

Technology Development Plan

August 2019

Contents

1 - INTRODUCTION	1
2 - CRYOCOOLERS.....	2
2.1 Cryocoolers to Achieve 4.5 K.....	2
2.1.1 Cryocooler Requirements	2
2.1.2 Cryocooler State-of-the-Art	3
2.1.3 Advancements Planned to Reach TRL 5 and 6.	4
2.2 Sub-Kelvin Cooling.....	5
2.2.1 Sub-Kelvin Cooling Requirements	5
2.2.2 Sub-Kelvin State-of-the-Art.....	6
2.2.3 Advancements Planned to Reach TRL 5 and 6.	6
2.3 Cryocooler Schedule and Cost.....	7
3 - FAR-INFRARED DETECTORS FOR OSS AND FIP	8
3.1 Transition-Edge-Sensed (TES) Bolometers	11
3.1.1 TES Foundations	11
3.1.2 TES State-of-the-Art	12
3.1.3 Theoretical Predictions for Current TES Technologies.....	13
3.1.4 TES Challenges.....	14
3.1.5 TES Development Plan	14
3.2 Cryogenic Readout Electronics for TES bolometers.....	15
3.2.1 Direct Microwave Multiplexing	15
3.2.2 Hybridized Time-Frequency Division Multiplexing with Microwave Multiplexing	16
3.2.3 Code Division Multiplexing and Frequency Division Multiplexing Variants.....	17
3.3 Kinetic Inductance Detectors	18
3.3.1 Foundations: Physics of Photon Detection	18
3.3.2 KID State-of-the-Art.....	19
3.3.3 KID Challenges.....	20
3.3.4 KID Development Plan	23
3.4 Quantum Capacitance Detector	25
3.5 Warm Readout Electronics	26
3.5.1 Power vs. TRL.....	27
3.6 Schedule for FIR Array Development, Down Select Strategy, and Cost Estimate.....	29
4 - Mid-Infrared Arrays.....	30
4.1 Mid-IR Array Requirements	30
4.2 Mid-IR Detector Technology State-of-the-Art	30
4.3 Mid-IR Array Challenges	32
4.4 HgCdTe Detector Array Technology Development.....	32
4.4.1 HgCdTe Detector Development Plan.....	33
4.4.2 HgCdTe Detector Manufacturing.....	35
4.5 Si:As Detector Development Plan	37
4.6 HgCdTe Detector Testing	38
4.7 TES Development Plan	39

4.8 Schedule for MIR array development and Down Select Strategy.....	40
5 - Cost Summary.....	40

APPENDICES

Appendix A: TES Detector Development Labor Plan and Budget	
Appendix B: MKID Detector Development Labor Plan and Budget	
Appendix C: Mid-IR Detector Development Labor Plan and Budget: HgCdTe and TES Bolometers	
Appendix D: <i>Origins</i> Space Telescope Sub-Kelvin Cryocooler Technology Development	
Appendix E: Far-IR Detector Readout Electronics for the <i>Origins</i> Space Telescope	
Acronyms and Definitions	
References	

1 - INTRODUCTION

The *Origins Space Telescope's* (*Origins*) significant improvement over the scientific capabilities of prior infrared missions is based on its cold telescope (4.5 K) combined with low-noise far-IR detectors and ultra-stable mid-IR detectors. A small number of new technologies will enable *Origins* to approach the fundamental sensitivity limit imposed by the natural sky background and deliver groundbreaking science. This report describes a robust plan to mature the *Origins* mission-enabling technology from current state-of-the-art (SOA) to Technology Readiness Level (TRL) 5 by 2025 and to TRL 6 by mission PDR. Entry TRLs corresponding to today's SOA are 3 or 4, depending on the technology in question. Potential mission-enhancing technology is not described in this report, except where the enhancement naturally extends an effort to develop enabling technology. Mission enhancing technologies include lighter weight optics, smaller far IR-spectrometers, and improvements to heterodyne detectors.

Cryocooler advancement is needed to cool the telescope to 4.5 K and the detectors in the far-infrared instruments to sub-Kelvin temperatures. Cooling the entire observatory reduces its self-emission, and cooling the far-infrared detectors reduces their noise, and both are required to reach astronomical background-limited performance.

Figure 1 shows the detector sensitivity needed to reach natural background-limited performance, expressed as Noise Equivalent Power (NEP). The NEP required for imaging is $\sim 3 \times 10^{-19} \text{ W Hz}^{-1/2}$, whereas the NEP needed for the far-infrared spectrometer OSS with its spectral resolution of $R=300$ is $3 \times 10^{-20} \text{ W Hz}^{-1/2}$.

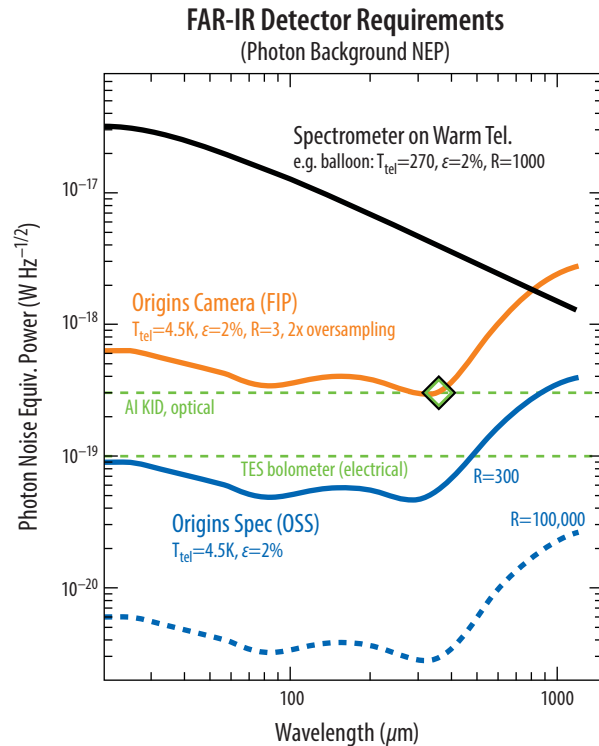


Figure 1: Sensitivity (i.e., NEP) requirements for far-IR instrumentation. Curves show the photon shot noise — improving detectors beyond this produces diminishing gains. The most demanding application is the *Origins* spectrometer (OSS), for which the photon NEP is as low as $3 \times 10^{-20} \text{ W Hz}^{-1/2}$. Horizontal lines show published measurements (aluminum KID from the SRON group, TES bolometers at $1 \times 10^{-19} \text{ W Hz}^{-1/2}$ were measured at JPL and SRON).

Table 1: Detector characteristics for *Origins* instruments

Inst.	Temp (K)	λ_{\min} (μm)	λ_{\max} (μm)	$R=\lambda/\Delta\lambda$	N_{pix}	Sensitivity	Saturation Limits	Notes
FIP ¹	50 mK	50	250	3	6,500	NEP= $3 \times 10^{-19} \text{ (W/Hz}^{1/2})$	50 μm: 1 Jy 250 μm: 5 Jy	2 bands, total power mode and polarimetry mode
OSS ¹	50 mK	25	588	200	10^4 6 arrays	NEP= $3 \times 10^{-20} \text{ (W/Hz}^{1/2})$	5 Jy @ 128 μm for R=300	6 bands R~ 4×10^4 FTS mode
MISC Transit Spectrometer ²	50 mK 30K	2.8	20	Up to 295	10^4 or 4×10^6	NEP= $3 \times 10^{-18} \text{ (W/Hz}^{1/2})$ 5 ppm stability over a few hours	K~3.0 mag 30 Jy @ 3.3 μm	Detector stability limiting (5 ppm aimed for the short and mid wavelength band)

¹ Superconducting detectors will be used for the direct detection instruments (FIP, OSS) that operate at wavelengths beyond 25 μm. These instruments need arrays with $\sim 10^4$ pixels, which could be achieved by use of a mosaic of arrays with several 10^3 pixels. This method has been demonstrated in existing FIR instruments (e.g., SOFIA/HAWC+). For OSS, each detector couples to an R=300 band at the focus of the grating modules. This sets the sensitivity requirement; the medium- high-resolution modes use the same grating just with an FTS inserted in front.

² The baseline detector technology for the long wavelengths channel of the mid-IR transit spectrometer will be arsenic-doped silicon impurity band conduction (Si:As IBC) detectors. These are being used in JWST/MIRI (Ressler et al., 2008) in a 1 k x 1 k format. For the transit spectrometer's two shorter wavelength channels, the baseline detector technology is HgCdTe, which will be developed to provide the required performance parameters. TES detectors are also investigated for MISC-T stability requirements.

While the noise requirements for the Transit Spectrometer's mid-IR detectors are nominally not a challenge (the required NEP is $\sim 3 \times 10^{-18} \text{ W Hz}^{-1/2}$, which is routinely achieved with existing FIR detectors), stability over several hours must be addressed to meet *Origins* requirements. *Origins*' required stability over several hours of uninterrupted source monitoring is 5 ppm.

Table 1 lists the detector requirements for *Origins* instruments, including wavelength range, number of pixels, and sensitivity as measured by NEP.

Managing the Technology Development Program

During the technology development program, a dedicated technology Program Manager will hold an overall 25% contingency to be applied to critical needs for any of the technology development efforts. The Program Manager is also in charge of the technology review processes and the technology down-selection process. The *Origins* Program Office will also have a systems engineer who will assure alignment of the *Origins* requirements with the technological developments. This organizational structure will continue from the beginning of pre-Phase A through Phase A.

As risk reduction, the individual technology development plans discussed below include funded schedule contingency. As further risk mitigation, different technologies are being developed in parallel for far-IR detectors, mid-IR detectors, and 4.5 K cryocoolers. The sub-K cooler development reaches TRL 6 before Phase A, leaving significant schedule margin.

This document describes the cost associated with maturing the technology during pre-Phase A. Phase A costs are accounted for in the *Origins* Cost Report. The complete mission lifecycle cost of the *Origins* Space Telescope is summarized in section 4.5 of the *Origins* Mission Concept Study Report.

Note that for the schedules shown in this volume, we have defined Program Year which is defined as starting in the middle of the calendar year. We have assumed that the Pre-Phase A activities start in mid 2021, *i.e.*, the beginning of PY 2021.

2 - CRYOCOOLERS

Origins requires 4.5 K mechanical coolers for all instruments and telescope, and sub-Kelvin coolers for the OSS and FIP instruments. If MISC-T selects bolometers for the long wavelength mid IR channel, then another sub-Kelvin cooler will be required.

2.1 Cryocoolers to Achieve 4.5 K

2.1.1 Cryocooler Requirements

Taking advantage of radiation to deep space can enable achieving low temperatures. However, due to the T^4 decrease in cooling power per area – and parasitic heat from the spacecraft, Earth, and Sun – radiators colder than $\sim 30 \text{ K}$ are not practical. In the past, the InfraRed Astronomy Satellite (IRAS), the Cosmic Background Explorer (COBE), the Infrared Space Observatory (ISO), *Spitzer*, and the *Herschel* instruments used liquid helium to cool to $<6 \text{ K}$ and Mid-course Space eXperiment (MSX) and the Wide-field Infrared Survey Explorer (WISE) used solid hydrogen to cool telescopes to $<12 \text{ K}$. Stored cryogenics have limited life, are bulky, and drive ground testing and on-orbit operations. For these reasons, mechanical cryocoolers have been developed over the last several decades to replace stored cryogenics.

The baseline *Origins* design assumes high-reliability, relatively low-vibration mechanical cryocoolers. Four such cryocoolers will each provide 50 mW of cooling power at 4.5 K, 100 mW of cooling at 20 K, and 5 W of cooling at 70 K, all with an input power (bus power) of 450 W or less. These requirements were derived to be straightforward extensions on present day cryocoolers. The requirements are somewhat flexible to allow more qualified cryocooler vendors to participate. Therefore, while the total cooling power at 4.5 K is fixed at $4 \times 50 = 200 \text{ mW}$, and the total input power is fixed at $4 \times 450 = 1800 \text{ W}$, the number of cryocoolers and the intermediate stage temperatures can vary. 4.5 K was cho-

sen as the base temperature to limit the in-band emission from the telescope. While a temperature lower than the cosmic microwave background at 2.7 K provides the least noise, for low emissivity optics, 4.5 K represents a reasonable compromise, allowing use of some existing cryocoolers, as well as limiting input power to the cryocoolers. See Figure 2 for a comparison of telescope emission for various temperatures and sky background.

Origins is designed with high thermal conductance materials in low-temperature regions. Consequently, the 4.5 K, 20 K, and 35 K regions are all nearly isothermal. Cooling these areas at one location produces only small gradients. Therefore, concepts such as broad area cooling are not required. What is required, however, is a scheme to transfer relatively-cold fluid where it is produced (e.g., at the spacecraft) to where it is needed at the telescope, instruments, and surrounding structure. Fortunately, the scheme used by the James Webb Space Telescope (JWST)/Mid InfraRed Instrument (MIRI) cooler also works for *Origins*, and the *Origins* system has been modeled after it. Two of the five cooler concepts need some method to mimic this (e.g., by providing a separate circulating loop). Soft mounted compressors of the type for the MIRI cooler have been shown to produce exported vibration ~ 0.1 N. *Origins* performed a rough simulation of the effect on the telescope, using 4 simultaneously operating coolers each producing this level of vibration. The results indicated that the stability requirements for the most sensitive instrument were met by a factor of more than 5. See Section 2.8 of the main report for details.

2.1.2 Cryocooler State-of-the-Art

Mechanical cryocoolers at TRL 7+ include *Planck* (Planck Collaboration, 2011), JWST/MIRI (Petach, 2014), and Hitomi (ASTRO-H) (Fujimoto, 2018). Note that while the quoted performance of the JT cryocooler on Hitomi was 4.5 K, the actual cooler temperature under full load was 4.3-4.4 K, so a considerable margin exists on achieving the telescope temperature of 4.5 K. Domestic coolers that could achieve 4.5 K are considered to be TRL 4-5, having been demonstrated as a system in a laboratory environment under NASA's Advanced Cryocooler Technology Development Program (ACT-DP) (Ross, 2006; Figure 3) or are a variant of a high TRL cooler (JWST/MIRI). The JWST/MIRI cryocooler engineering unit was tested with a simple substitution of the rare isotope ^3He for the typical ^4He , which produced significant cooling at temperatures below 4.5 K (Petach, private communication). Mechanical cryocoolers for higher temperatures have already demonstrated impressive on-orbit reliability (Ross, 2007; Figure 4). The moving components of a 4.5 K cooler are similar (expanders) or are exactly the same (compressors) as those that have flown. Further development of these coolers to maximize cooling power per input power (<9000 W/W at 4.5 K) for small cooling loads (50-200 mW), while minimizing mass, is desired. There is also a need to minimize the exported vibration from the cooler system. The miniature reverse-brayton cryocoolers in development at Creare (Breedlove, 2014) are examples of high efficiency, reliable coolers with negligible exported vibration. These coolers are at TRL 6 for 80 K, TRL 4-5 for 10 K, and TRL 3 for 4 K operation.

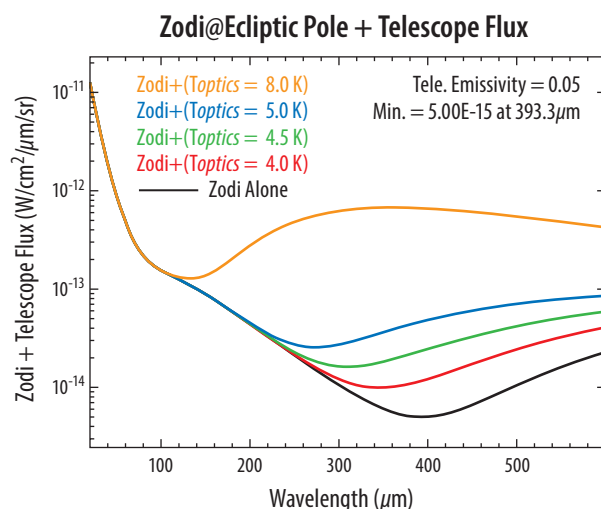
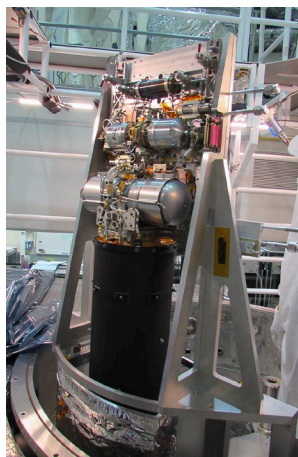


Figure 2: A comparison of telescope emission (effective emissivity = 0.05) vs. sky background in the mid to far infrared.

NGAS JWST/MIRI



Ball 10 K



Lockheed ACTDP



SHI Hitomi/SXS

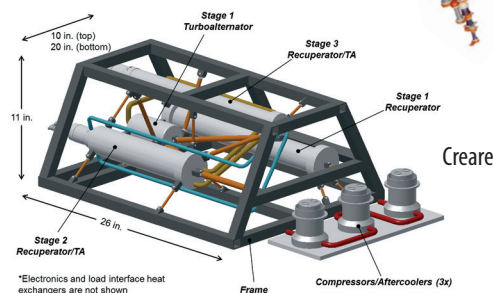


Figure 3: Five vendors have developed cryocoolers that have reached TRL 4+ and need only small improvements to meet the *Origins* 4.5 K cooling requirements.

2.1.3 Advancements Planned to Reach TRL 5 and 6.

The TRL 7 JWST/MIRI cryocooler is designed to cool a primary load at 6.2 K and an intercept load at 18 K. It does this using a precooled helium Joule Thompson loop that compresses ^4He from 4 to 12 bar, precools it to 18 K with a three-stage pulse tube cryocooler, then circulates it to a remote heat intercept at 18 K and an isenthalpic expander that provides cooling at 6.2 K. The only change required to lower the temperature to 4.5 K is to lower the return pressure from 4 bar to 1 bar. To maintain the required mass flow, the compressor swept volume must be increased to accommodate the lower density of the lower pressure helium, and the pressure ratio must be increased to maintain the pressure drop. This can be achieved by upgrading the JT compressor used in the MIRI cooler. One way this can be done is by augmenting the existing MIRI JT compressor with a second JT compressor of the same design but with larger pistons to act as the first stage in a two-stage compressor.

The Lockheed four-stage pulse tube cryocooler has demonstrated the required heat removal at the temperatures required for *Origins* in a TRL 4 design (Olson, 2005). However, for *Origins*, 4.5 K is required in a location that is remote from the compressor. This will require development of a separate 4.5 K cooling loop. This could be realized using a HST/NICMOS cooling loop driven by a “fan.”

The Ball Aerospace (Ball) 4.5 K cooler design uses a similar architecture to the NGAS JWST/MIRI cryocooler with a Stirling-type displacer (rather than a pulse tube) and a JT with a long loop for remote cooling. The Ball design lacks a system-level demonstration to reach TRL 5 (Glaister, 2007).

Creare is currently funded through an SBIR Phase II contract to demonstrate a 4.5 K turbo-expander. This will demonstrate a TRL 4 component of the system and is the lowest TRL component of the Creare design. During *Origins* Pre-Phase A funding the turbo-expander will be combined with other components (2 other turbo-expanders, three recuperators and compressors) to attain TRL 5. A TRL-6 version will be designed as an ETU of the *Origins* flight coolers.

Creare is developing a 4.5 K stage for its miniature turbine reverse-Brayton cryocoolers under SBIR funding. This expansion stage is similar to the one used for a single stage cooler flown on HST/NICMOS and the two-stage 10 K design currently at TRL 5.

Recent Long-Life Space Cryocooler Flight Operating Experience as of May 2016



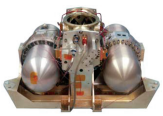
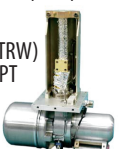

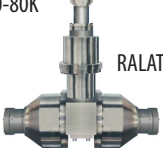
Cooler/Mission	Hours/Unit	Comments	
Air Liquide Turbo Brayton (ISS MELFI 190K)	85,600	Turn on 7/06, Ongoing, No degradation	
Ball Aerospace Stirling			
HIRDLS (60K 1-stage Stirling)	83,800	8/04 thru 3/14, Instr. failed 2009; Data turned off 3/14	
TIRS cooler (35K two-stage Stirling)	27,900	Turn on 3/6/13, Ongoing, No degradation	
Creare Turbo Brayton (77K NICMOS)	57,000	3/02 thru 10/09, Off, Coupling to Load failed	
Fujitsu Stirling (ASTER 80K TIR system)	141,700	Turn on 3/00, Ongoing, No degradation	
JPL Sorption (PLANCK 18K JT (Prime & Bkup))	27,500	FM1 (8/10-10/13 EOM); FM2 failed at 10,500 h	
Mitsubishi Stirling (ASTER 77K SWIR system)	137,500	Turn on 3/00, Ongoing, Load off at 71,000 h	
NGAS (TRW) Coolers			
CX (150K Mini PT (2 units))	161,600	Turn on 2/98, Ongoing, No degradation	
HTSSE-2 (80K mini Stirling)	24,000	3/99 thru 3/02, Mission End, No degradation	
MTI (60K 6020 10cc PT)	141,600	Turn on 3/00, Ongoing, No degradation	
Hyperion (110K Mini PT)	133,600	Turn on 12/00, Ongoing, No degradation	
SABER on TIMED (75 Mini PT)	129,600	Turn on 1/02, Ongoing, No degradation	
AIRS (55K 10cc PT (2 units))	121,600	Turn on 6/02, Ongoing, No degradation	
TES (60K 10cc PT (2 units))	102,600	Turn on 8/04, Ongoing, No degradation	
JAMI (65K HEC PT (2 units))	91,000	4/05 to 12/15, Mission End, No degradation	
GOSAT/IBUKI (60K HEC PT)	63,300	Turn on 2/09, Ongoing, No degradation	
STSS (Mini PT (4 units))	52,800	Turn on 4/10, Ongoing, No degradation	
OCO-2 (HEC PT)	14,900	Turn on 8/14, Ongoing, No degradation	
Himawari-8 (65K HEC PT (2 units))	12,800	Turn on 12/14, Ongoing, No degradation	
Oxford/BAe/MMS/Astrium/Airbus Stirling			
ISAMS (80K Oxford/RAL)	15,800	10/91 thru 7/92, Instrument failed	
HTSSE-2 (80K BAe)	24,000	3/99 thru 3/02, Mission End, No degradation	
MOPIIT (50-80K BAe (2 units))	138,600	Turn on 3/00, lost one disp. at 10,300 h	
ODIN (50-80K Astrium (1 unit))	132,600	Turn on 3/01, Ongoing, No degradation	
AATSR on ERS-1 (50-80K Astrium (2 units))	88,200	3/02 to 4/12, No degradation, Satellite failed	
MIPAS on ERS-1 (50-80K Astrium (2 units))	88,200	3/02 to 4/12, No degradation, Satellite failed	
INTEGRAL (50-80K Astrium (4 units))	118,700	Turn on 10/02, Ongoing, No degradation	
Helios 2A (50-80K Astrium (2 units))	96,600	Turn on 4/05, Ongoing, No degradation	
Helios 2B (50-80K Astrium (2 units))	58,800	Turn on 4/10, Ongoing, No degradation	
SLSTR (50-80K Airbus (2 units))	1,400	Turn on 3/16, Ongoing, No degradation	
Planck (4K JT using 2 Astrium Comp.)	38,500	5/09 thru 10/13, Mission End, No degradation	
Raytheon ISSC Stirling (STSS (2 units))	52,800	Turn on 4/10, Ongoing, No degradation	
Rutherford Appleton Lab (RAL)			
ASTR 1 on ERS-1 (80K Integral Stirling)	75,300	7/91 thru 3/00, Satellite failed	
ASTR 2 on ERS-2 (80K Integral Stirling)	112,000	4/95 thru 2/08, Instrument failed	
Sumitomo Stirling Coolers			
Suzaku (100K 1-stg)	59,300	7/05 thru 4/12, Mission End, No degradation	
Akari (20K 2-stg (2 units))	39,000	2/06 to 11/11 EOM, 1 Degr., 2nd failed at 13 kh	
Kaguya GRS (70K 1-stg)	14,600	10/07 thru 6/09, Mission End, No degradation	
JEM/SMILES on ISS (4.5K JT)	4,500	Turn on 10/09, Could not restart at 4,500 h	
Sunpower Stirling			
RHESSI (75K Cryotel)	124,600	Turn on 2/02, Ongoing, Modest degradation	
CHIRP (CryoTel CT-F)	19,700	9/11 to 12/13, Mission End, No degradation	

Figure 4: On orbit mechanical cooler lifetimes. Almost all cryocoolers have continued to operate normally until turned off at the end of instrument life. (Ross, 2007, updated). Note that there are 8766 hours in one year.

The Sumitomo Heavy Industries (SHI) 4.5 K cryocooler flown on Hitomi had a lifetime goal of 5 years. Lifetime is expected to be limited by bearing friction and contamination. Reliability and lifetime will be improved by using a non-contacting suspension system (similar to displacers) and by improving the cleanliness of the critical internal parts and working fluid. This will extend expected life from 5 to 10 or more years. This development is in progress at SHI.

2.2 Sub-Kelvin Cooling

2.2.1 Sub-Kelvin Cooling Requirements

The FIP instrument requires: 3 μ W of cooling at 50 mK plus 125 μ W at 0.6 K for a heat rejection temperature at 4.5 K with a heat rejected of 4 mW average.

The OSS instrument requires: 3 μW of cooling at 50 mK plus 125 μW at 0.6 K plus 500 μW at 1.6 K for heat rejection temperature of 4.5 K and a heat reject power of 8 mW average. These cooling powers are the current best estimates (CBE) from the up-scoped design for these instruments (*Origins* Mission Concept Study Report, Section 3). The cooling required is over and above any internal sub-Kelvin cooler requirements and inefficiencies. For the baseline designs (*Origins* Mission Concept Study Report, Section 3), the requirement for low temperature heat lift will be lowered by almost a factor of 2. It is also required that the sub-Kelvin cooler capability would provide a factor of 2 margin for the baseline design. In other words the sub-Kelvin coolers must be capable of providing 6 μW of cooling at 50 mK and 250 μW of cooling at 0.6 K. Superconducting detectors and their readout systems are very sensitive to small/time varying magnetic fields. Typically, a detector package will provide its own shielding to deal with external fields on the order of 30 μT , so the magnetic field generated by the sub-Kelvin cooler must be $<30 \mu\text{T}$.

2.2.2 Sub-Kelvin State-of-the-Art

For detector cooling to 50 mK, adiabatic demagnetization refrigerator (ADRs) are currently the only proven technology, although some work has been funded by ESA to develop a continuously recirculating dilution refrigerator (DR). A single shot DR flown on Planck produced 0.1 μW of cooling at 100 mK for ~ 1.5 years (Collaudin, 1999; Planck Collaboration, 2011), while a three-stage ADR used on Hitomi produced 0.4 μW of cooling at 50 mK with an indefinite lifetime (Shirron, 2015). The *Origins* temperature stability requirement at the 50 mK stage (2.5 μK rms over 10 min) is similar to that of Hitomi. The Hitomi design and temperature readout system easily meet ($<0.4 \mu\text{K}$ rms) this requirement (Figure 5).

2.2.3 Advancements Planned to Reach TRL 5 and 6.

In contrast, a TRL 4 Continuous ADR (CADR) has demonstrated 6 μW of cooling at 50 mK with no life-limiting parts (Shirron, 2002). This technology is currently being advanced toward TRL 6 by 2020 through SAT funding (Tuttle, 2017; Figure 5). Demonstration of a 10 K upper stage for this machine, as is planned, would enable coupling to a higher temperature cryocooler, such as the one produced by Create, that has a near-zero vibration technology (Breedlove, 2014). The CADR is modular and allows additional continuous cooling at other temperatures. It can be configured as the base four-stage design, producing 6 μW of cooling at 0.05 K, with one or two additional stages to

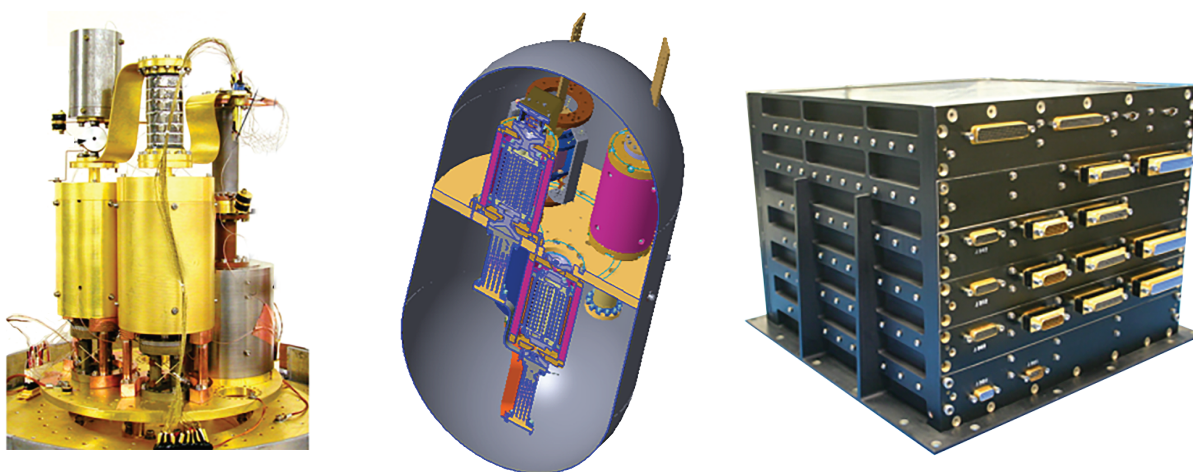


Figure 5: Left: Laboratory Continuous ADR (CADR) provides 6 μW of cooling at 50 mK, Center: CADR under development at NASA will provide 6 μW of cooling at 50 mK and also has a precooling stage that can be operated from 0.3 to 1.5 K. The drawing shows a notional enclosing magnetic shield for $< 1 \mu\text{T}$ fringing field. Overall dimensions are 445 mm tall by 225 mm diameter. Right: ADR Controller flown on Hitomi. The *Origins* CADR will use duplicates of the controller cards and temperature readout cards from this.

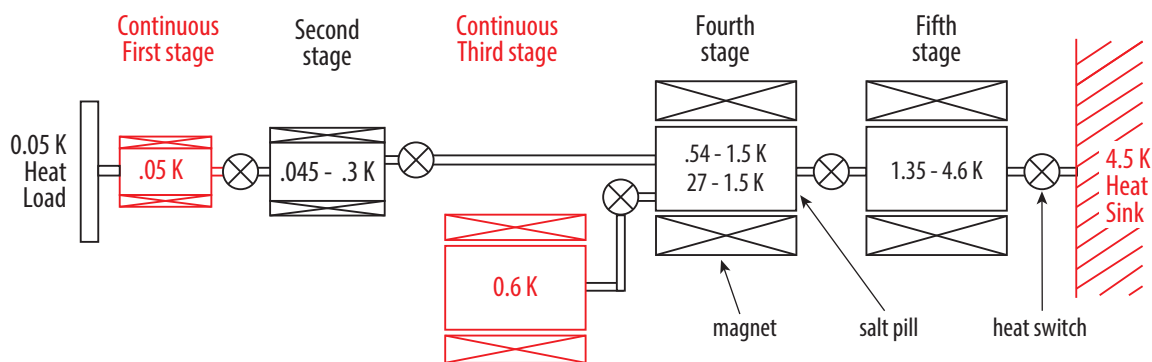


Figure 6: A schematic representation of the FIP and OSS CADR. The ADR stages are synchronized to move heat from the 50 mK and 0.6 K stages to the 4.5 K stage, where it is lifted by the 4.5 K cryocooler(s). Salt pill operating temperature range is indicated. The average cooling power for each continuous stage and heat rejection to the sink are indicated in red, as they called out in instrument requirements.

provide additional cooling at higher temperatures. The design includes a surrounding magnetic shield, resulting in less than 1 μT external field. The large gray pill-shaped structure in Figure 5 is the notional magnetic shield and will easily meet the requirement.

The CADR design is aided by software that accurately simulates its operation. This allows users to vary salt pill sizes, materials, operating temperatures, magnetic field strengths, and heat switch conductances to approach an optimum design. The CADR for the *Origins*/FIP instrument, shown schematically in Figure 6, will include five stages made of elements nearly identical to those used in the new 2019 CADR. The CADR for the *Origins*/OSS instrument will have an additional two stages, similar to stages 4 and 5 (not shown), to provide 1 mW (factor of 2 higher than requirement) of cooling at 1.3 K. The first and third stages will remain continuously at 0.05 and 0.6 K, respectively. The fourth stage cools to absorb heat from the second and third stages on alternate cycles. Each stage cycles between maximum and minimum magnetic field in ~ 20 -30 min.

The five *Origins* ADR stages use two different magnetocaloric materials: gadolinium-lithium-fluoride (GLF) and chrome-potassium-alum (CPA). Performance of these materials in an actual ADR are well understood and accurately modeled. Based on the design study, the two cooling power values are 100% higher than the corresponding heat load predictions.

The flight control electronics for this ADR is based on the flight-proven Hitomi ADR controller, and has achieved TRL 6 by employing the same cards used in the Hitomi flight unit (Figure 4).

The CADR components are modular, so the CBE design (Figure 4) may be easily rearranged to better conform with volume constraints. Heat straps shown exiting the magnetic shield are notional and a penetration that prevents fringing magnetic field from reaching the outside of the shield is underway. This notional CADR design has an estimated mass of 21 kg, including 9 kg for the outer magnetic shield.

The electronics box (Figure 5) includes eight thermometry channels per card, with adjustable excitation and resolution that provides complete temperature readout for the host instrument, as well as CADR control.

2.3 Cryocooler Schedule and Cost

Top-level schedules for the 4.5 K cryocooler and the sub-Kelvin cooler technology development are provided Figures 7a and 7b, respectively. We expect to perform Task 1 in Figure 7a similarly to the way the Advanced Cryocooler Technology Development Program (ACTDP) was executed, with several vendors sharing a total funding of about \$10M per year over a 4-year span. This effort will conclude in 2025 with a single vendor selected to qualify the TRL 5 cooler to TRL 6 during Phase A at a cost of \$2.5M per year.

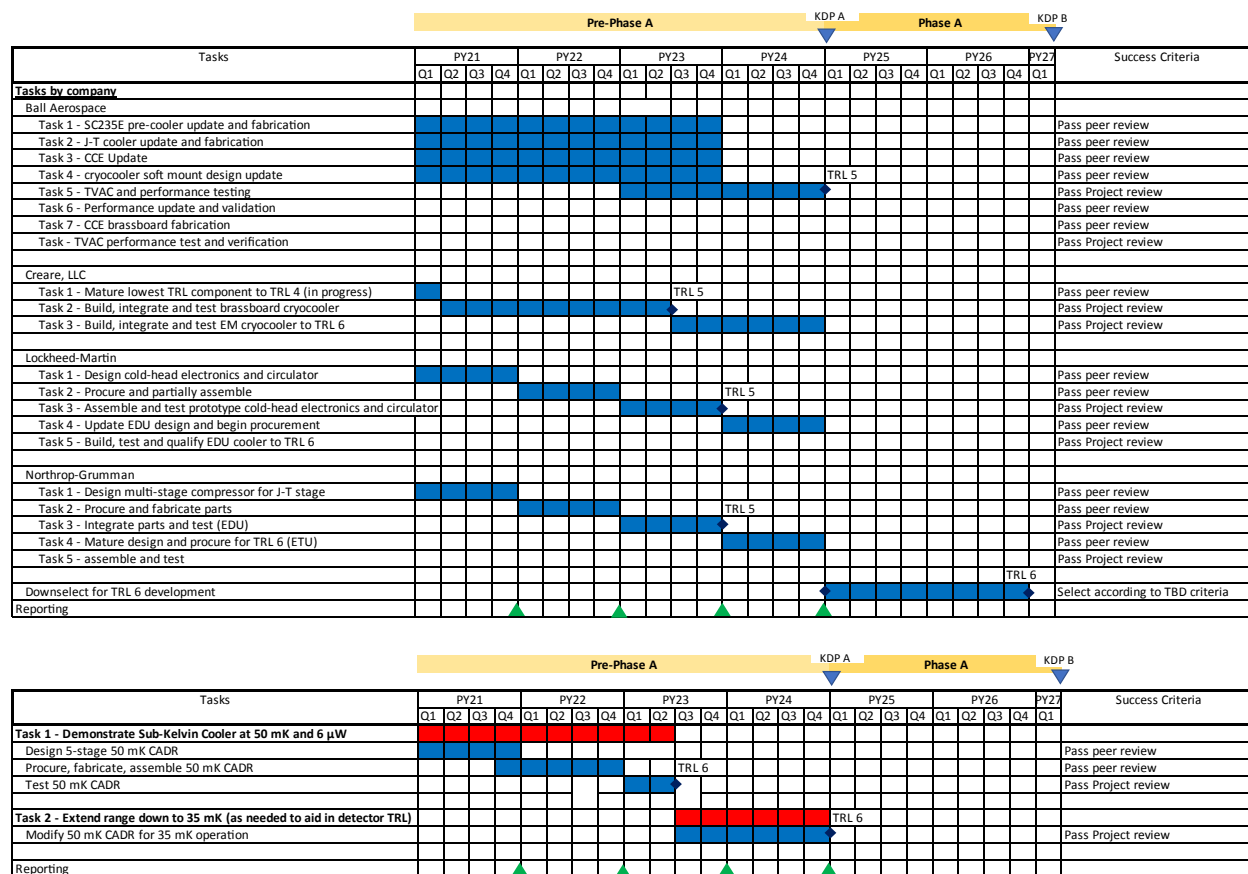


Figure 7: (a, top) The 4.5 K cryocooler and (b, bottom) sub-Kelvin cooler for *Origins* can be raised to TRL 6 before *Origins* instrument PDR in 2027.

As shown in Figure 7b, the CADR development is broken into two Tasks. Task 1 is an extension of the ongoing 10 K to 0.05 K SAT effort with the following changes: The 10 K to 4 K stages will be eliminated from the design. A 4.5 K ADR stage will be directly connected via a mounting plate and thermal strap to a 4.5 K cryocooler. A 0.6 K continuous stage will be added to the design to provide an intermediate heat sink as shown in Figure 6. This 0.6 K stage will have its own thermal strap, along with a strap to the 0.05 K stage, extending out of the magnetic shield to be connected to a 0.6 K heat station or to the 0.05 K detector arrays. Design, fabrication, assembly, and test will lead to a TRL 6 level version of the 50 mK CADR.

Task 2 will be implemented to aid in achieving the required NEP on the Far IR detector arrays. The CADR from Task 1 will be modified to allow higher cooling power at lower temperature. The TRL 4 unit shown in Figure 5 demonstrated continuous cooling of 1.5 μ W at 35 mK. In Task 2 the system will be redesigned to handle 6 μ W of load at 35 mK to meet *Origins* requirements. At the end of Task 2, this lower temperature CADR will be qualified to TRL 6. If it is not necessary to improve the detector NEP by lowering the operating temperature, Task 2 becomes margin on the Task 1 developments.

3 - FAR-INFRARED DETECTORS FOR OSS AND FIP

Unlike the near-IR and mid-IR detector arrays, far-IR to millimeter-wave detectors suitable for astrophysics and cosmology have not yet identified a commercial application and hence development efforts are led by science-driven teams. These groups are typically centered at NASA or national agencies in Europe and Japan, and often include close collaboration with universities. This approach has

produced the sub-K direct detectors used on the *Herschel* and Planck missions, as well as those now flying on SOFIA.

Excellent reviews of detector technologies include Richards (1994), Zmuidzinas and Richards (2004), Irwin and Hilton (2005), Zmuidzinas (2012), Farrah (2017), and Mauskopf (2018). The semiconductor bolometer (Schultz *et al.*, 2008) and photoconductor detectors (Birkmann *et al.*, 2004; Rieke *et al.*, 2004) used for previous space missions, including *Herschel* and *Spitzer*, have been replaced by superconducting detectors. However, multiplexing constraints for the readout of a large number of detectors requires the use of new types of superconducting detectors. The most mature types of those are the Transition-Edge-Sensed (TES) bolometers and the Kinetic Inductance Detectors (KIDs). However, other technologies are currently being explored, for example the quantum capacitance detector (QCD), which has a lower TRL but the capability for photon counting (Echternach *et al.* 2018). A more comprehensive description of detector needs for FIR space missions is detailed in Staguhn (2018).

The detectors for *Origins*' OSS and FIP instruments require development to meet the requirements listed in Table 2. Arrays capable of taking advantage of the cryogenic telescope's low-background and performing dispersed spectroscopy must be substantially more sensitive and larger than any that have

Table 2: *Origins* Far-IR Detector Requirements

Parameter	Value
Wavelength Range	25–600 μm (6 bands in OSS)
NEP	3×10^{-19} (FIP) to 3×10^{-20} (OSS)
Saturation	5 Jy @ 128 μm
Speed	< 10 ms
Array Size	1 kilopixel + mosaicking to $\sim 10^4$
Optical Efficiency	>70%
Mux Density	>500 / GHz
Yield	>70%
Stability	NEP down to 0.1 Hz
Crosstalk	< -10 dB peak; < -3 dB integrated
Cosmic Ray Dead Time	< 10%
Dynamic Range	>1000
Pixel Pitch	0.5 mm (short λ) to 1 mm (long λ)

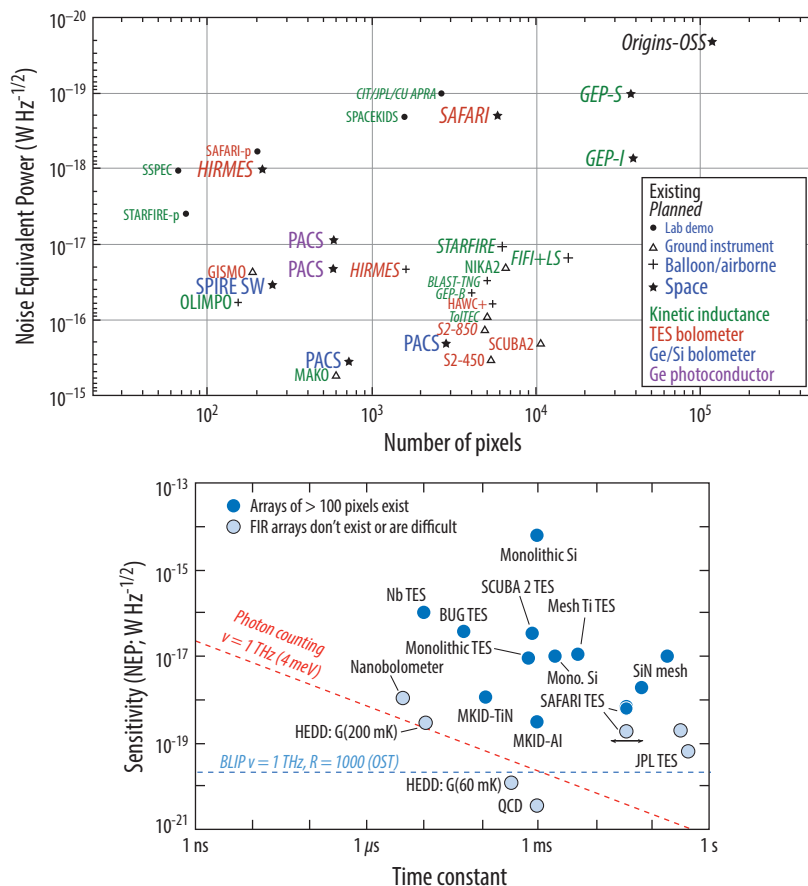


Figure 8: (top left) The past decade has shown the steady progress of far-IR detector technology toward larger, more sensitive arrays. The number of pixels is the total number needed for the missions, however, these pixels maybe realized in a number of smaller arrays. *Origins*/OSS captures the requirements for *Origins*, and of these demonstrations, SpaceKIDs are the closest in this 2D metric. (BLAST-TNG: Lourie *et al.*, 2018; CIT/JPL/CU APRA: Hailey-Dunsheath *et al.*, 2018b; FIFI+LS: Fischer *et al.*, 2018; GEP-I, GEP-S: Glenn *et al.*, 2018; GISMO: Staguhn *et al.*, 2006; HIRMES: Richards *et al.*, 2018; MAKO: Swenson *et al.*, 2012; McKenney *et al.*, 2012; NIKA2: Adam *et al.*, 2018; OLIMPO: Masi *et al.*, 2019; PACS: Poglitsch *et al.*, 2010; SAFARI-p: Hijmering *et al.*, 2016; SAFARI: Audley *et al.*, 2018; SCUBA2: Holland *et al.*, 2013; SPACEKIDs: Baselmans *et al.*, 2017; SPIRE: Griffin *et al.*, 2010; SSPEC: Redford *et al.*, 2018; STARFIRE-p: Barlis *et al.*, 2018; Hailey-Dunsheath *et al.*, 2018a; STARFIRE: Aguirre *et al.*, 2018; TolTEC: Austermann *et al.*, 2018.) Credit: J.Zmuidzinas

Figure 9: (bottom left) Detector speed requirements for photon vs sensitivity. Credit: J.Zmuidzinas

been used scientifically to date. Moreover, the *Origins* sensitivity requirements are not levied by even the most ambitious possible ground-based or sub-orbital platforms. Thus, the situation that played out for *Herschel* and *Planck*, for which the Boomerang balloon experiment was an important stepping stone, will not work fully for *Origins*. There are funded far-IR instruments for a balloon (TIM, previously STARFIRE) and SOFIA (HIRMES) maturing over the next few years, and these will help mature some of the new readout and system-level aspects, but demonstrating the *Origins* sensitivities at array scale requires a dedicated program.

In terms of format, OSS has a total of 60,000 pixels in the six arrays, with a potential upscope to 120,000, a factor of ~ 15 -30 more than was fielded in *Herschel*, so new readout schemes must be employed. As illustrated in Figures 8, 9, and 10, existing demonstrations have shown that appropriate sensitivities can be obtained, and array formats in the 10^4 pixel range are within reach, since current technologies can be tiled. Readout electronics development is described in Section 3.2.

Currently, NASA's far-IR detector development work is supported through the grants program, and in some cases, internal investments from NASA Centers (primarily JPL and GSFC). Both provide 2-3 years of support for small teams, typically ~ 1 full-time-equivalent (FTE) divided between design, fabrication, and testing. This program can be effective for initial, single-pixel demonstrations; a good example is the quantum capacitance detector development at JPL, supported initially as a JPL Research & Technology Development, then matured with a 3-year NASA grant. However, this grants program cannot support maturation of any detector array to the point at which it could be proposed for flight. Even Strategic Astrophysics Technology (SAT) grants, though they can have slightly larger budgets (up to 3 FTE), carry at most a 3-year term, which is insufficient to engage a team and the necessary infrastructure, develop expertise, and accomplish the range of tasks required.

A dedicated far-infrared detector program for *Origins'* FIP and OSS instruments will provide a strategic NASA investment outside of the grants program. This program will focus on fabrication of

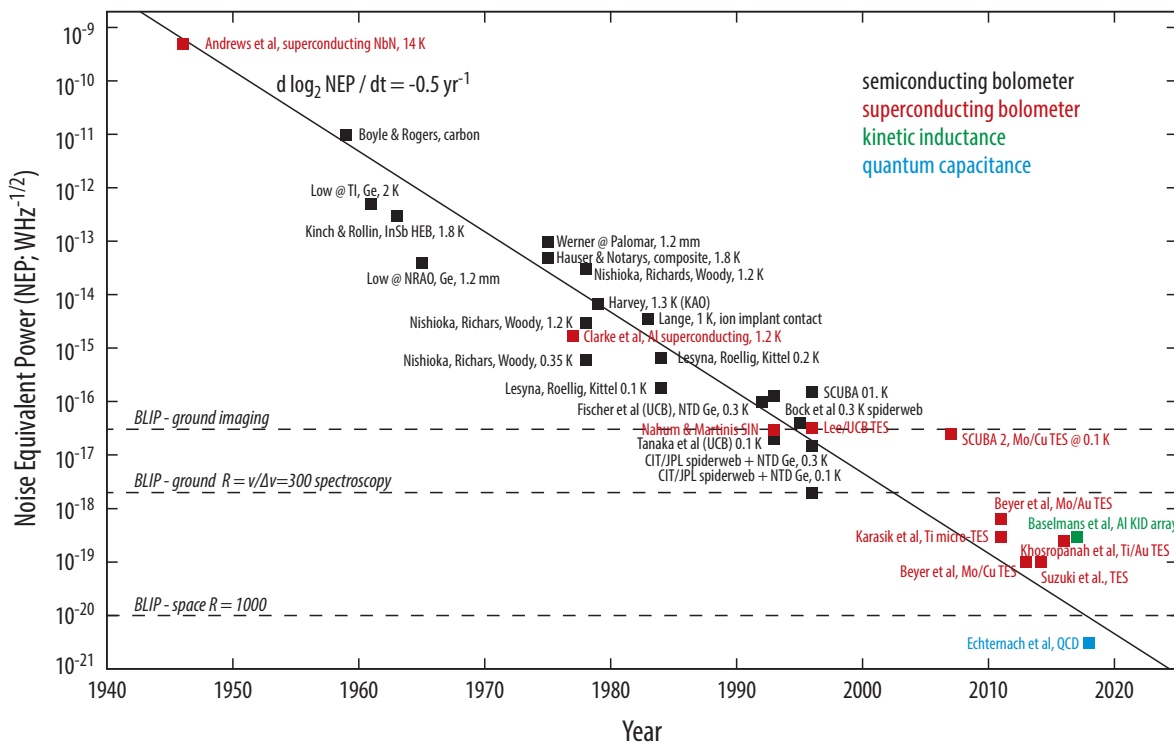


Figure 10: The sensitivity for far-infrared detectors has been steadily improving by factors of 2 per year and the projected technological improvement matches *Origins'* required far-infrared detector needs. Credit: Jonas Zmuidzinas, Caltech/JPL

far-infrared detector arrays that meet the technical requirements of the OSS and FIP instruments and programmatic needs of the *Origins* mission. *Origins*' strategy for developing far-infrared detectors is to pursue two technology paths, TES bolometers and KIDs, and to also fund promising lower TRL technologies such as the quantum capacitance detectors with ~20% of the program budget. This approach is chosen to mitigate mission risk of inadequate detector development in time for mission implementation. Unlike a traditional grant-based program, we will implement a review and progress assessment program, so that a technology that meets *Origins* requirements can be chosen as early as possible. For example, if during the initial phases of the program, one of the lower TRL technologies takes off and appears more likely to achieve the requirements than KIDs or TES bolometers, then resources can be redirected to maturing that technology. The *Origins* roadmap shows a credible path using the two NASA Centers already focusing on far-IR detectors: JPL (KIDs) and GSFC (TES). These Centers offer key aspects not available at universities: integrated fabrication capabilities, critical mass of expertise with long-term researchers, and, importantly, sufficient experience in managing large projects to ensure steady progress toward the milestones.

The *Origins* team envisions this development as a collaboration with other US labs, universities, and international groups.

3.1 Transition-Edge-Sensed (TES) Bolometers

3.1.1 TES Foundations

A Transition Edge Sensor (TES) is a superconducting device deposited on a thermally well-insulated membrane with an absorber that converts the incoming radiation into heat. Irwin (1995) realized that such a device, if voltage biased, acts as a self-regulating bolometer, since over a wide range of bias currents and radiation loads, it will remain on the superconducting transition. When infrared radiation is absorbed in the bolometer and converted to heat, warming the detector of heat capacity C above its nominal temperature, T_{bias} occurs (Figure 11). This temperature change will result in a resistance change, which is measured electrically with Superconducting QUantum Interference Devices (SQUIDS) (Chervenak *et al.*, 1999) that measure the change in current through the device due to the resistance change. As a consequence of the increased resistance, the dissipated Joule heat is reduced by exactly the amount of the heat dissipated by the photons, leaving the device on its transition. This effect is called “electrothermal feedback.” The heat is conducted away through a thermal conductance, G , to a heat sink at T_{bath} . A superconducting transition at temperature T_C yields an extremely sharp but continuous change in resistance from near zero to the normal state resistance (Figure 12).

The response time of a bolometer is typically the thermal time constant, $\tau = C/G$. However, TES bolometers can be faster than this due to the electrothermal feedback. When biased onto the transition, power is dissipated in the thermistor as $P = V^2/R$.

When optical power is applied, the thermistor warms up, increasing its resistance. The bias power drops (since the bias voltage is held constant), bringing the TES back toward the stable bias point. The measured change in current is then proportional to the Photon Energy deposited in the

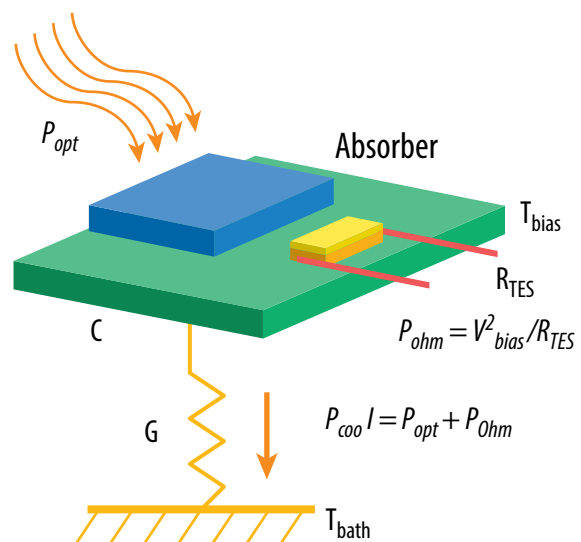


Figure 11: Operation of a TES bolometer.

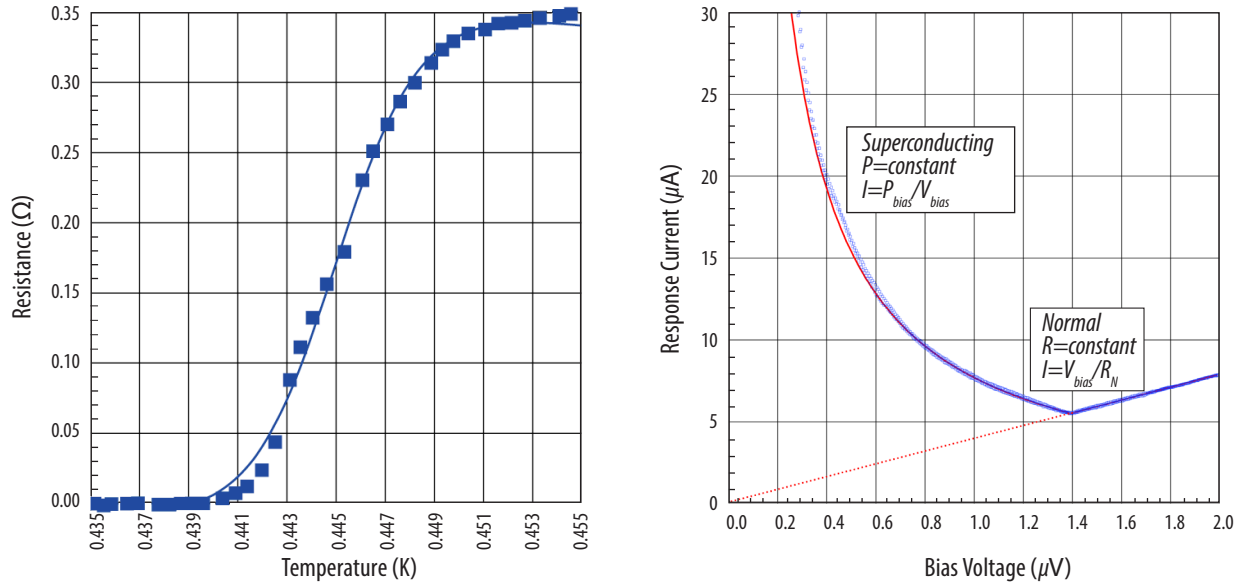


Figure 12: left: Resistance as a function of temperature for several devices of slightly different bilayers, resulting in different transition temperatures. right: Voltage-current characteristic of an ideal superconducting transition edge sensor (solid line) compared with measurements from a detector (points).

absorber. This is true over the entire range of the TES, making it a very linear device. (To be precise: this is only true if the TES is really voltage biased; also, the small temperature increase over the transition (Figure 12) adds a second order term, but this value is very small and easily calibrated).

The effective time constant is then approximately $\tau_{\text{eff}} = \tau_n / a$, where n is the temperature index of the thermal conductance. Additionally, at low frequencies ($(\omega \tau_{\text{eff}})^2 \ll 1$), the Johnson noise is suppressed through the action of the electrothermal feedback by a factor of $(n/a)^2$. The end result is that the intrinsic noise of a TES bolometer is typically dominated by the phonon noise alone.

Superconducting transitions can be tuned to the desired temperature in several ways. To produce a thermistor with a tunable TC and a known resistance, superconducting-normal bilayers are manufactured. The transition temperature of other materials, such as AlMn, can be tuned by their thickness. Both methods have been used successfully.

3.1.2 TES State-of-the-Art

TES detectors are TRL 4 (Figures 13 and 14). In terms of noise performance, the state-of-the-art of laboratory ultra-low noise TES detectors were built at SRON (Figure 15). The group has demonstrated individual TES pixels with NEPs in the low $10^{-19} \text{ W}/\sqrt{\text{Hz}}$. The best performance SRON recently published comes from an ultra low noise (NEP= $1 \times 10^{-19} \text{ W}/\sqrt{\text{Hz}}$) TES with a time constant of $<1 \text{ ms}$ (Suzuki *et al.*, 2016).

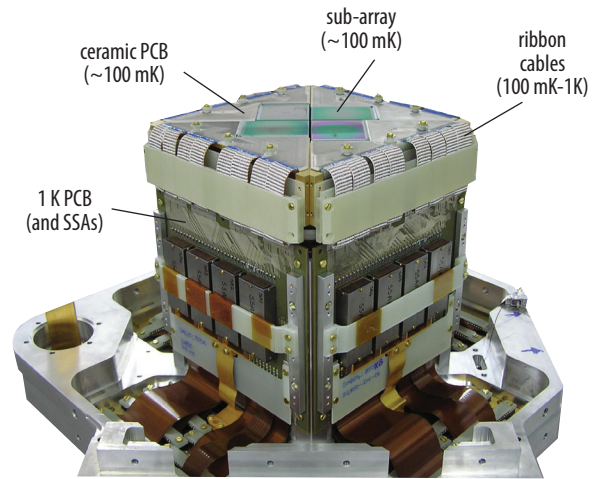


Figure 13: The TES bolometer arrays used for each of the two wavelength channels of SCUBA-2 consist of a mosaic of four 1280-pixel tiles.

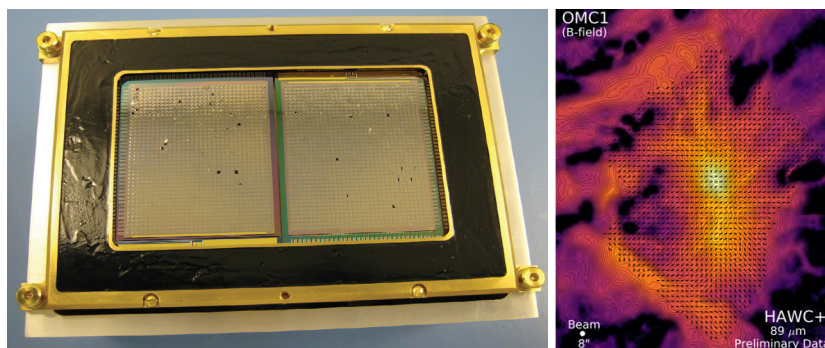


Figure 14: The SOFIA HAWC instrument uses three 1280-pixel Backshort-Under-Grid TES bolometer arrays developed at GSFC (Staguhn et al., 2016). The inset (right) shows HAWC+ polarimetry data obtained on the Orion molecular cloud.

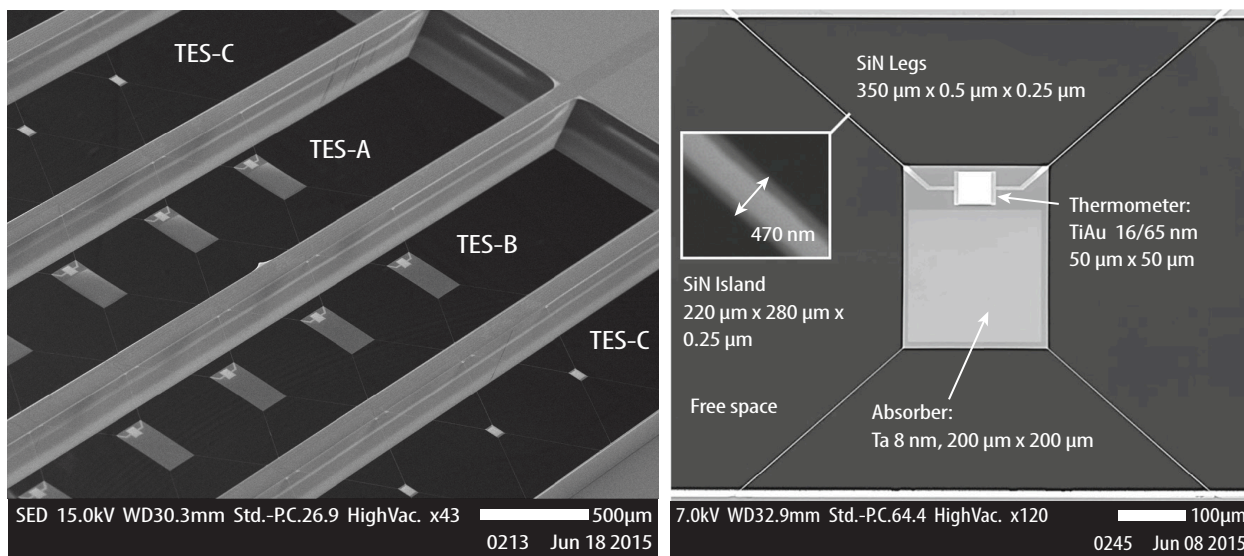


Figure 15: Left: Test array of TES bolometers produced as part of the detector development program for the SRON-led SAFARI/SPICA instrument. Right: Close-up of a single pixel showing the silicon nitride thermal suspension, 8 nm tantalum film used as the optical absorber, and 50 x 50 μm^2 TiAu TES.

3.1.3 Theoretical Predictions for Current TES Technologies

Thermal isolation of TES bolometers is generally achieved by increasing the lengths of the beams suspending the bolometer membrane. The state-of-the-art performance of the SRON TES pixel in Figure 15 is a product of this approach. As shown in Figure 16, scaling the performance of an SRON-like TES pixel to a lower bath and critical temperature suggests a path exists for meeting *Origins*/OSS requirements. The models in Figure 16 also indicate that achieving increased thermal isolation of a bolometer can significantly relax the requirements on the cryogenic system.

Below 100 mK, the phonon thermal wavelength exceeds 1 μm in silicon nitride (and single-crystal silicon) beams. Thus, sub-micron features etched in a dielectric beam can serve to reduce the phonon thermal conduction with a coherent phonon filter structure. The natural outcome of a phononic structure is compactness, which is extremely desirable for achieving a high pixel filling-fraction in a photon-starved instrument. An additional advantage of a phononic filter is the reduced sensitivity of the conductance to variations in surface conditions (*e.g.*, roughness). These properties enable a viable path for producing uniform ultra-low-noise TES bolometers for *Origins*. As currently studied at GSFC (PI Karwan Rostem), using a device suspended with legs that have phononic filters, a TES critical temperature of 90 mK would be sufficient to meet the required OSS detector sensitivities.

The design and fabrication of phononic filter isolation beams is currently implemented through an APRA program (Rostem *et al.*), and described in detail by Rostem *et al.*, 2016, Bartlett *et al.*, 2019, and Olsson *et al.* (2015). This small effort has led to a greatly improved understanding of phonon transport at low temperatures and a leap in phononic filter design and fabrication. As shown in Figure 16, the NEP requirement for OSS can be achieved with a phononic-isolated TES bolometer at ~ 90 mK with a 50 mK bath temperature. The test pixel structure fabrication described in Olsson *et al.* (2015) suggests scalability to 10^4 pixel arrays is possible and well matched to standard techniques employed in electron-beam lithography.

3.1.4 TES Challenges

To construct TES detectors that enable FIP and OSS performance requires designing and fabricating detectors that obtain high sensitivity and high pixel count simultaneously with high yield and uniformity across the wavelength range of interest. Fortunately, the sensitivity and format are separable problems, and in the last few years, solutions have been demonstrated in the laboratory. Four steps to making these new detectors are:

1. Design and fabricate a single pixel at the sensitivity needed for FIP.
2. Design and fabricate a single pixel at the sensitivity needed for OSS.
3. Design and fabricate an array 1/3 the size needed for FIP with sensitivity required by FIP.
4. Design and fabricate an array 1/3 the size needed for OSS with sensitivity required by OSS.

3.1.5 TES Development Plan

Superconducting transition-edge-sensed (TES) bolometers are high heritage and have demonstrated NEPs as low as 1×10^{-19} W Hz $^{-1/2}$ at JPL and SRON. Attaining lower NEPs is possible in two ways: either base temperatures must be reduced from the canonical 50 mK (a reduction to 35 mK is discussed in Section 3.1.3) and/or the leg isolation needs to be improved, for example, with phonon-choke micro-fabricated structures studied in an APRA program at GSFC (Rostem *et al.*). A principal disadvantage of TES systems, particularly for the formats required for OSS, is the complexity of focal plane assembly for TES systems, in particular hybridization with superconducting quantum interference devices (SQUIDS), typically one per detector. An ongoing SAT project (Staguhn *et al.*) is aimed at simplifying this process. A key TES technology development is to demonstrate this hybridization at the scale needed for *Origins*. Section 3.2 describes the readout electronics technology development required that is scalable to large array sizes for TES.

To push the TES bolometers to the much-lower *Origins* sensitivities, and to larger array sizes, requires a dedicated program between 2021 and 2025:

1. Task 1 (Year 2021): Develop extremely dark test environments for the FIR detectors. This task requires very thorough test cryostat design. All electrical signal lines going into the cryostat must be RF filtered to prevent miniscule amounts (less than one zepto-Watt) of electromagnetic power from being transmitted to the test packages. Vibrational energy also must be kept away from the

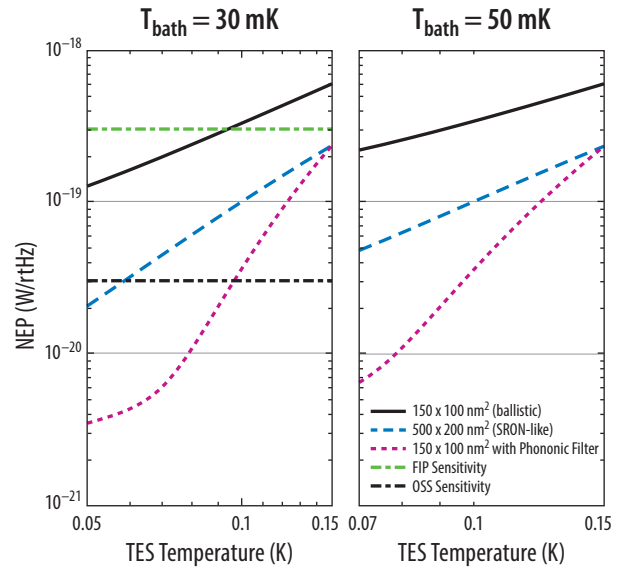


Figure 16: Sensitivity (NEP) plots for TES bolometers for various thermal isolation structures. At a bath temperature of 35 mK, a SRON type detector with T_c of 55 mK provides a viable path for achieving OSS sensitivity by reducing the bath temperature, which can be done with current ADR technology (Section 2.2).

detectors, so sophisticated vibration insulation (e.g., stiffness-controlled suspensions, eddy-current dampers) is mandatory. The team will avoid introducing thermal radiation from any surface by keeping the temperatures of all structures in the detector FOV below 2 K and, based on a surface's position and temperature, by using extremely black surfaces in combination with highly reflective ones. Extremely low dissipation cryogenic readout systems, with as many dissipationless components as possible, in well-shielded electronics boxes are also required. Multi-stage magnetic field shielding elements are also essential.

2. Task 2 (Year 2021): Design and fabricate a single TES pixel that meets the FIP NEP requirement, $<10^{-19}$ W/Hz^{-1/2}. Test the single pixel in the new cryostat environment.
3. Task 3 (Years 2021 and 2022): Design and fabricate a single TES pixel that meets the OSS NEP requirement, $<3 \times 10^{-20}$ W/Hz^{-1/2}. Test the single pixel in the new cryostat.
4. Task 4 (Years 2022, 2023, and 2024): Design and build arrays based on the single pixels that meet FIP NEP requirements and have multiplexing scalable to *Origins* requirements, 1000 pixels per 4 GHz of readout band, and at least 80% operability.
5. Task 5 (Years 2023 and 2024): Integrate the microwave multiplexed readout at FIP array size.
6. Task 6 (Years 2024 and 2025): Design and build arrays based on the single pixels that meet OSS NEP requirements and have multiplexing scalable to *Origins* requirements, 1000 pixels per 4 GHz of readout band, and at least 80% operability.

These performance demonstrations will qualify the devices as TRL 5. The team will then perform subsequent environmental testing, primarily vibration and cosmic ray testing, in 2026 and 2027, to meet TRL 6 by the end of 2027.

3.2 Cryogenic Readout Electronics for TES bolometers

Creating the large TES FIR arrays needed for the *Origins* instruments will require readout electronics development. The electronics on the warm spacecraft side are similar to those required for the KIDs and QCDs, and this aspect benefits from rapid development for industrial and military stakeholders and is described separately below (Section 3.5). Among the 3 far-IR detector technologies, the TES bolometers have unique requirements in the cold focal plane – specifically the TES bolometers require cold amplification with a SQUID at or near the focal plane. This aspect must be incorporated into a multiplexing circuit, and three approaches will be considered in the first two years of the development schedule to identify the best path forward for the TES readout electronics. The state-of-the-art and development needs for each type of readout electronics are detailed in Sections 3.2.1, 3.2.2 and 3.2.3. The readout electronics operate at the cold temperatures of the instruments.

3.2.1 Direct Microwave Multiplexing

In this approach, TES resonators are coupled to a corresponding microwave resonator circuit of a specific frequency (Figure 17). The resonators are connected in parallel over a shared transmission line. The signals from each are thus frequency-division-multiplexed (FDM) over a 4 GHz bandwidth and

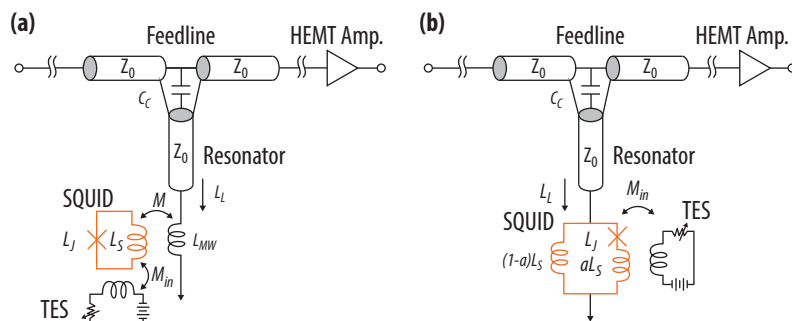


Figure 17: TES to Microwave Resonator coupling.

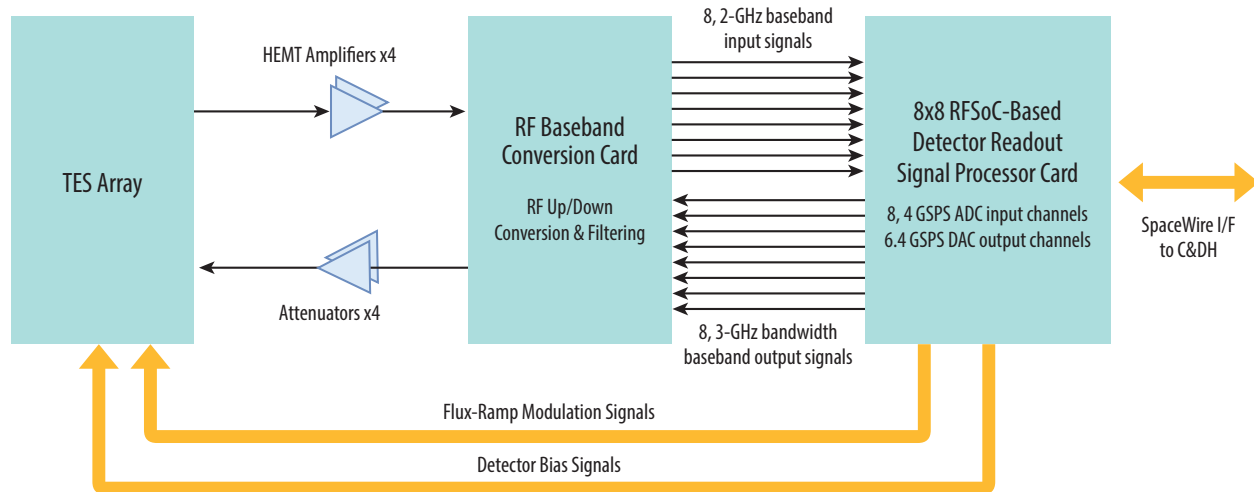


Figure 18: Block diagram showing the flow of signals from the detectors on e.g. FIP to the warm electronics on *Origins*.

spaced evenly in frequency to occupy the full bandwidth. The resulting RF signal occupies 4 to 8 GHz in the microwave spectrum, commensurate with the bandwidth of a single HEMT cryogenic amplifier. Current research has demonstrated up to 2000 microwave resonators occupying 4 GHz bandwidth can be effectively read out by warm electronics that are akin to a communications system or radar receiver. Readout involves down-converting the 4 GHz FDM signal, digitizing it, and applying a digital filterbank to isolate the TES signals at each resonant frequency (Figure 18). The TES signals are then acquired, coherently averaged, and passed to a C&DH system where telemetry operations packetize and transmit the resulting data. Using this methodology, the TES array only requires a small set (~10 or fewer) of DC bias current signals for the entire array and a slow (~100 Hz) common flux-ramp modulation signal to linearize the detector array.

A microwave multiplexed TES readout where each TES has its own microwave resonator is the least bandwidth-efficient packing approach, but the one with the highest TRL; it has been demonstrated in the lab (<https://www.xilinx.com/products/silicon-devices/soc/rfsoc.html>) and has the lowest complexity. Since ~2000 resonators fit within a 4 GHz processing bandwidth, and ~10,000 resonators need to be read, a total of five RF signals need to be connected to corresponding HEMT amplifiers and transmitted downstream for signal processing.

The two detector arrays of the upscoped FIP design are combined into a set of two 4 GHz bandwidth RF signals. These signals are down-converted and split into four 2 GHz bandwidth signals.

A new enabling technology developed by Xilinx Inc. is the RF System-on-Chip (RFSoc). This key technology combines eight 4 GSPS RF-Sampling ADCs, eight 6.4 GSPS RF-Sampling DACs, a quad-core ARM-A₉ microprocessor, and Xilinx Ultrascale+ digital logic into a digital chip. At 200 MHz, this chip utilized ~30 W. The FIP RF signals are all sampled and processed simultaneously by a single RFSoc. The detector feedback and row current signals used to control the TES arrays can also be controlled by the RFSoc and a combination of digital electronics on the same board. In 2017, Xilinx demonstrated this technology in a related environment. Bringing this technology from TRL 3 to TRL 5 will require additional investment.

3.2.2 Hybridized Time-Frequency Division Multiplexing with Microwave Multiplexing

In this approach, an entire array of TES elements is coupled to a single microwave squid multiplexer rather than to just a single TES element (Figure 19). In theory, a 32-TES array using Time-Frequency Division Multiplexing (TDM) can be coupled to a single resonator circuit that is read out in a man-

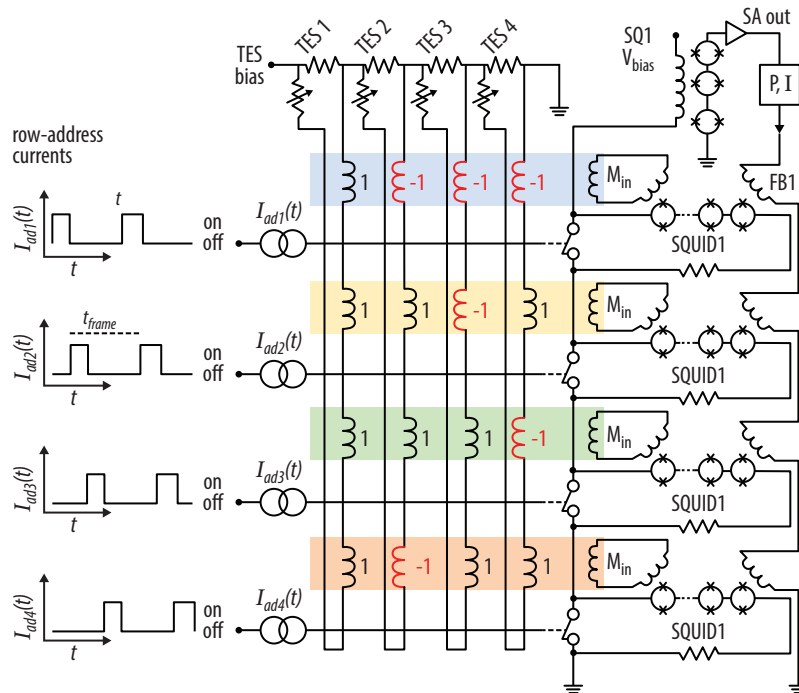


Figure 19: Hybridized Time-Frequency Division Multiplexing scheme.

ner similar to microwave kinetic inductance detectors. Resonators are spaced evenly over the 4 GHz bandwidth, and each acts as a carrier that modulates an entire TDM array that is coupled to it. This method is lower-TRL, yet more frequency efficient because TES element packing increases by a factor of the array size times the number of resonator elements. Comparing to just 2000 TES in the direct microwave multiplexed scheme, the hybridized method can carry $32 \times 2000 = 64,000$ TES signals in the same amount of bandwidth, with every TES array employing the same TDM scheme. This method has a higher complexity because it requires not only bias currents, but row-address modulating currents that control TDM for all 2000 arrays, as well as resonator demodulation signal processing. So while bandwidth packing efficiency is superior in this scheme compared with direct TES coupling to microwave MUXes, hardware complexity is higher to accommodate the additional current signals, and processing complexity is also higher because every TDM array must now be read out simultaneously while demultiplexed in frequency. Since the OSS instrument requires many more TES pixels than FIP, it is recommended to use this methodology for readout for this instrument.

3.2.3 Code Division Multiplexing and Frequency Division Multiplexing Variants

Code Division Multiplexing (CDM) is a very promising technology. Using CDM, the same TDM row address current signals used for TDM of TES array elements can be used to read out TES elements simultaneously as opposed to serially. This method requires modulating the currents using Walsh-Hadamard encoding for every row address signal. If the Walsh matrix used for encoding is set to the identity matrix, this method is identical to TDM. Otherwise, multiple TES rows are read out simultaneously by decoding the resulting signal using an inverse Walsh matrix.

Conceivably, CDM is also compatible with microwave multiplexing, as described in Section 3.2.2. CDM has the highest complexity, but also offers the densest packing of TES elements while ameliorating the noise penalty incurred as the number of TES elements grows in the array.

3.3 Kinetic Inductance Detectors

3.3.1 Foundations: Physics of Photon Detection

In contrast to TESs, which operate at the superconducting transition temperature T_C , kinetic inductance detectors (KIDs) operate at temperatures well below T_C . In KIDs, almost all conduction electrons in the material are in the form of Cooper pairs. In contrast to ordinary electrons in a normal metal, Cooper pairs do not suffer scattering and can therefore carry current with no dissipation, leading to the phenomenon of superconductivity.

Superconductivity has a limited frequency range. The pairs have a binding or “gap” energy of E_g , corresponding to a photon frequency of ν_g . This “gap frequency” is the minimum energy required for a photon to break a Cooper pair (Figure 20 left). At frequencies below ν_g , a single photon cannot break a Cooper pair, so the material cannot efficiently absorb energy and thus behaves as a superconductor. However, for frequencies above ν_g , the material can readily absorb energy and behaves as an ordinary (dissipative), normal metal.

KIDs make use of both of these behaviors. As illustrated in Figure 20 (center), a simple meandered thin-film superconducting trace can serve as an efficient radiation absorber for frequencies above the gap, ν_g , provided the area filling factor and normal-state sheet resistance of the superconductor are chosen appropriately. Simultaneously, the meander behaves as a low-loss superconducting inductor for frequencies below the gap, ν_g . For an ordinary inductor, the stored energy is given by $1/2 LI^2$, where I is the current. For a KID, the inductance L has two components: the ordinary magnetic inductance corresponding to energy in the magnetic field, and the kinetic inductance corresponding to the kinetic energy of the Cooper pairs carrying the current. Like the energy in the magnetic field, the kinetic energy represents stored energy that can be recovered because the pairs do not scatter and the kinetic energy is not lost. By combining the meandered inductor with a simple interdigitated capacitor (Figure 20), an LC circuit is formed whose resonant frequency is given by $\omega^{-1/2}$. The resonance can be very sharp (high Q) because the inductor is superconducting and has low loss.

Because the kinetic inductance derives from the motion of Cooper pairs, it is sensitive to the pair density. Meanwhile, absorption of above-gap radiation causes breaking of Cooper pairs, which reduces their density and increases the kinetic inductance. In turn, the increased kinetic inductance causes the resonance

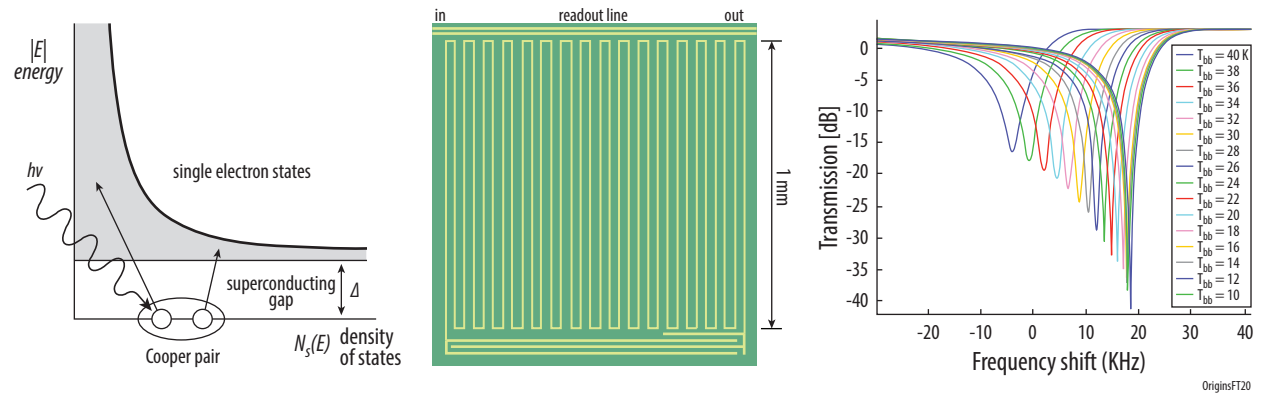


Figure 20: Left: photon energy absorbed by a superconductor leads to breaking a Cooper pair (C) into single electrons. This process occurs when the photon energy exceeds the binding energy of a Cooper pair. As illustrated, this process is analogous to photon absorption in a semiconductor, where the photon energy must exceed the bandgap. Center - close-up of a simple KID pixel consisting of a meandered inductor (L) that doubles as a radiation absorber and an interdigitated capacitor (CIDC). These form an LC resonant circuit that is weakly coupled to a common readout line. Right: the 1 GHz resonant frequency of this KID pixel shifts downward in response to the intensity of the radiation. The curves show measured data for a KID illuminated with blackbody radiation passed through a $\lambda=200\ \mu\text{m}$ bandpass filter. The intensity is controlled by the blackbody temperature, which was varied from 10 K to 40 K. A 10 kHz shift represents a fractional change of $10\ \text{kHz}/1\ \text{GHz} = 10^{-5}$. Credit: P. K. Day, JPL.

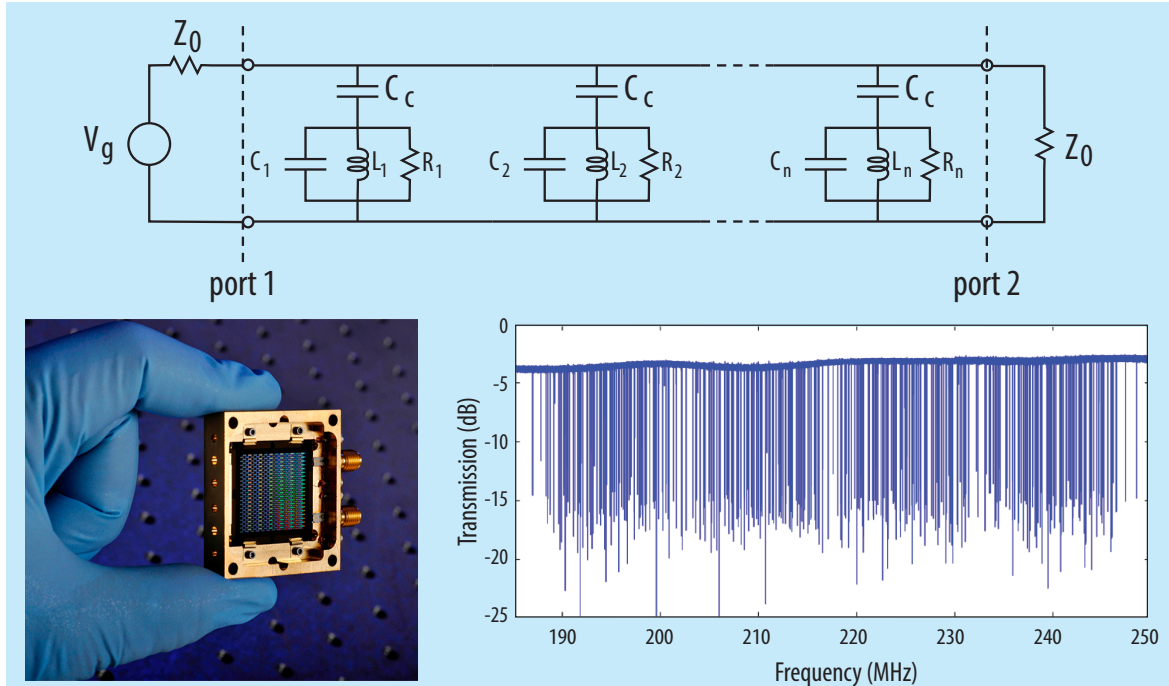


Figure 21: Top: KID arrays are read out using frequency-domain multiplexing. Each KID pixel is weakly coupled to a common readout line using a small coupling capacitance C_c and is assigned a unique resonant frequency, typically by adjusting the geometry of the capacitor. The signal generator at port 1 produces the superposition of frequencies needed to excite all the resonators. The output signal at port 2 is sent to a cryogenic low-noise amplifier, represented by its input impedance, Z_0 . Left: Photograph of a 432-pixel KID array. The two connectors on the right represent ports 1 and 2, and attach to the common readout line on the array. Right: A frequency sweep reveals 415 sharp resonances produced by the 432 pixels in the array, corresponding to a fabrication yield of 96%. Credit: C. McKenney, Caltech/NIST.

frequency to shift downward. This is the fundamental detection mechanism for KIDs, and is illustrated using experimental data in Figure 20 (right). Breaking of pairs increases the density of single electrons, which do scatter, increasing the resistive dissipation. This broadens the resonances and reduces their depth.

The narrow resonance produced by a single KID leads to the simple scheme for frequency-domain multiplexing shown in Figure 21. The capacitor geometry is adjusted so each KID has a unique resonance frequency. The readout electronics generate a superposition of frequencies to excite the array, and then separate these frequencies in the output signal from the array to isolate the response of individual pixels. This task is now tractable as a result of advances in electronics, especially digital signal processing using FGPAs. Figure 22 shows an example of KID readout electronics, a submillimeter-wavelength KID camera, and an astronomical image taken with KIDs.

3.3.2 KID State-of-the-Art

Kinetic Inductance Detectors (KIDs) are TRL 4. They have been demonstrated on the ground at the Caltech Submillimeter Observatory (Swenson *et al.*, 2012) and IRAM 30 m (Catalano *et al.*, 2018) telescopes. New instruments soon to be in the field include the TolTEC millimeter-wave camera (Austerman *et al.*, 2018) and the BLAST-TNG balloon experiment (Lourie *et al.*, 2018). Higher sensitivity KID arrays are funded for balloon-borne spectroscopy on TIM (formerly STARFIRE; Figure 23, Aguirre and collaborators). In addition to these instruments, the European consortium SPACEKIDs development program (Baselmans *et al.*, 2017) has funded KID development, explicitly targeting the very high sensitivity (low NEP) of space. Of the existing demonstrations (Figure 10), SPACEKIDs (Baselmans *et al.*, 2017) is the closest to meeting *Origins*' sensitivity requirements (Tables 2 and 3). The SPACEKIDs devices (Figure 24) already meet the NEP needed for FIP, but OSS requires a $10\times$

Table 3: Detector requirements for *Origins* versus results achieved for SPACEKIDS (Baselmans et al., 2017).

	Tile Size (pixels)	λ (μm)	NEP ($\text{W Hz}^{-1/2}$)	MUX (pix/GHz)	Pitch (μm)	t_{det} (ms)	Min. Yield	Dynamic Range	Crosstalk (dB)	1/f knee (Hz)	Cosmic Ray Deadtime
SPACEKIDS	961	350	3×10^{-19}	240	1600	1.5	83%	10^5	-30	0.2	< 5%
<i>Origins</i> -FIP	8000	50–250	3×10^{-19}	1,500	500	< 3	80%	2000	-17	< 0.1	< 2%
<i>Origins</i> -OSS	16000	25–588	3×10^{-20}	1,500	400 x 700	< 3	80%	10,000	-17	< 0.1	< 2%

Minimum tile sizes for GEP-I/GEP-S shown; actual arrays could be multiples thereof. Tiles with $12 \times 120 = 1,440$ pixel format are envisioned for GEP-I bands 1–18. GEP-S bands 1 & 2 assume arrays with 112×70 format, which could consist of tiles with $28 \times 35 = 980$ pixels. The dynamic range is specified for a 1 Jy calibration source, e.g., an asteroid (Müller et al., 2014; Baselmans et al., 2017). Techniques to mitigate electrical and optical crosstalk, and cosmic ray susceptibility, have been demonstrated (Noroozian et al. 2012; Baselmans et al., 2017; Yates et al., 2017).



Figure 22: Left – Example of KID readout electronics: a ROACH-1 system. The circuit boards in the foreground contain fast digital to analog (DAC) converters that generate the multifrequency analog signal that excites the KID array and the analog to digital (ADC) converters that digitize the return signal from the KID array. The FPGA, underneath the cooling fan in the background, performs the digital signal processing needed to separate the individual KID frequencies. Center – The MAKO KID cryostat alongside a laboratory electronics rack. Right – A $\lambda=350$ μm image of the moon taken with MAKO at the Caltech Submillimeter Observatory.

improvement. KIDs are close to the tile size needed for FIP/OSS and the *Origins* approach would be to use a number of tiles to fill the instruments' FOVs.

3.3.3 KID Challenges

Comparing *Origins* KID focal plane requirements with the current state-of-the-art, the team identified specific advances required to achieve TRL 5 by 2023, including sensitivity, wavelength range, multiplexing, and pixel pitch.

Sensitivity: Sensitivity is the most important challenge for KIDs. The SPACEKIDS devices already meet the NEP needed for FIP, but OSS requires a 10 \times improvement.

The easiest way to improve KID's sensitivity is to increase its responsivity (frequency shift per absorbed power) while maintaining its fixed electrical noise. The frequency noise (electrical noise) of a KID is typically set by the two-level-system (TLS) fluctuators in the capacitance. The increase in responsivity can be achieved by reducing the detector active volume (V) below the ~ 100 μm^3 used by SPACEKIDS. For a given material, the frequency shift scales as the quasiparticle density, so the power-to-frequency response scales as $1/V$ and the NEP scales as V . In a lumped-element KID, the active region is the inductor, so the design problem is simply to create an inductor with a sufficiently-small volume that couples to the radiation effectively.

Groups worldwide, including the Caltech/JPL group contributing to the *Origins* study (Figure 23), are developing smaller-volume lumped-element KIDs. These devices have a volume of 35-70 cubic microns depending on the film thickness used. Figure 25 shows designs that extend this approach to create volumes as low as 10 μm^3 . Scaled from the much larger KIDs demonstrated in SPACEKIDS, with a correction for the larger TLS noise expected for the reduced readout power, these 10 μm^3 devices would meet the sensitivity requirement for OSS.

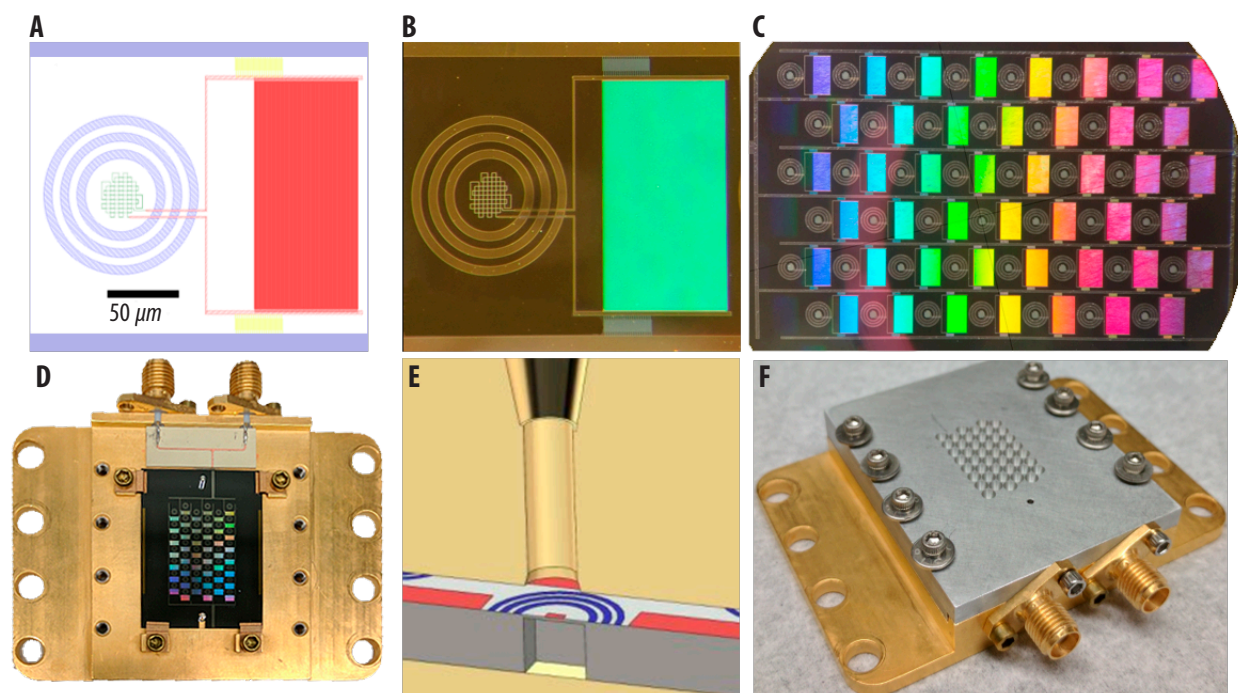


Figure 23: Lumped-element KIDs under development for the TIM balloon experiment. (A) Diagram of the mask layout for a single resonator. The meandered inductor (green) is surrounded by an optical choke structure (blue). An interdigitated capacitor (red) sets the resonance frequency of the pixel, and two coupling capacitors (yellow) allow readout via microstrip feedlines. (B) A microscope image of a single pixel. All pixel elements of the prototype array are patterned with 40 nm aluminum film. (C) A microscope image of the 45-pixel prototype array, as fabricated. (D) The array in its enclosure. The back side of the die is bare silicon and lies flat on the gold-plated package surface. The die is 30mm × 22mm. (E) A CAD model of the detector package. The optical power is coupled into a feedhorn and travels through a circular waveguide that is terminated by the inductor. The final design will have a backside etch to provide a backshort. (F) The prototype feedhorn block installed above the 45-pixel array.

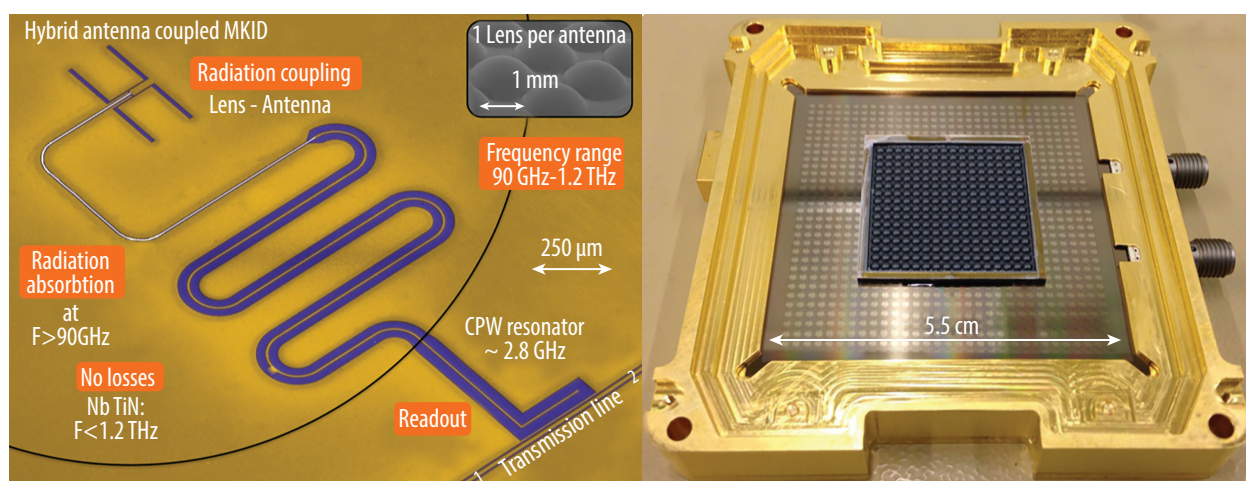


Figure 24: The European SPACEKIDs consortium has demonstrated a 1000-pixel fully-multiplexed array of antenna-coupled KIDs operating at $\lambda=300 \mu\text{m}$. Left: The pixel design incorporates a lens-fed twin-slot planar antenna coupled to a transmission-line KID. Right: A sub-scale microlens array is used to illuminate a portion of the KID array.

A particular challenge is to maintain the material quality as film thickness and feature sizes are reduced. The KID response is dependent on the quasiparticle lifetime (τ_{QP}), and the SPACEKIDs devices exhibit $\tau_{QP} \sim 500 \mu\text{s}$; this long value is the result of careful attention to deposition conditions to insure a high-purity aluminum film, and even longer lifetimes may be possible. By contrast, the low-volume devices (Figure 25) have much smaller τ_{QP} , $\sim 35 \mu\text{s}$. While this discrepancy is not fully understood, the most likely explanation is disorder in the material, which may be addressed with changes to the fabrication process. The sputtering deposition devices employed may be modified in a number of ways that could potentially improve the film quality, including varying the film thickness or the deposition rate. Additionally, shifting to electron beam evaporation from ultrapure targets should produce clean films with longer quasiparticle lifetimes (Barends *et al.*, 2009).

The lifetime may also benefit from operating at much lower temperatures ($\sim 100 \text{ mK}$) than has been traditionally used with KIDs (operated thus far at 220–300 mK for convenience). Measurements at these lower temperatures (still above the 50 mK *Origins* focal plane temperature) are in the near-term plan. These smaller volume, improved lifetime approaches are summarized in Table 4.

Wavelength Range: To support the *Origins* wavebands, particularly the short wavelength band of the OSS spectrograph that reaches down to 25 microns, requires absorber-coupled detectors. The antenna-coupling used for the $\lambda = 350 \mu\text{m}$ SPACEKIDs design will not work because the antennas are lossy above the niobium gap frequency (720 GHz). The lumped-element devices from the Caltech/JPL group have begun to address this need (Figure 25).

Table 4: Approaches to low-NEP KIDs for *Origins*.

Parameter	Existing 350 ¹	Increase τ^2	Reduce Volume: OSS at 350 μm^3	Reduce Volume: OSS at 30 μm^4
Temperature [mK]	210	100	100	100
τ_{QP} [μs]	35	800	800	800
Linewidth [nm]	400	400	150	150
V_L [μm^3]	76	76	10	34
f_{res} [MHz]	300	300	310	1250
Response R_k [W^{-1}]	1.2×10^9	2.7×10^{10}	2.1×10^{11}	6.0×10^{10}
Noise due to TLS (S_{xx})	2.1×10^{-17}	1.8×10^{-17}	4.7×10^{-17}	1.1×10^{-17}
NEP	4×10^{-18}	1.3×10^{-19}	3×10^{-20}	5×10^{-20}

350 μm designs include: (1) the fabricated/characterized STARFIRE detector, (2) the same device with an increased τ_{QP} and reduced temperature, and (3) a subsequently reduced inductor volume. The GEP design includes (4) a 30 μm optimized device patterned with a 150 nm wide inductor.

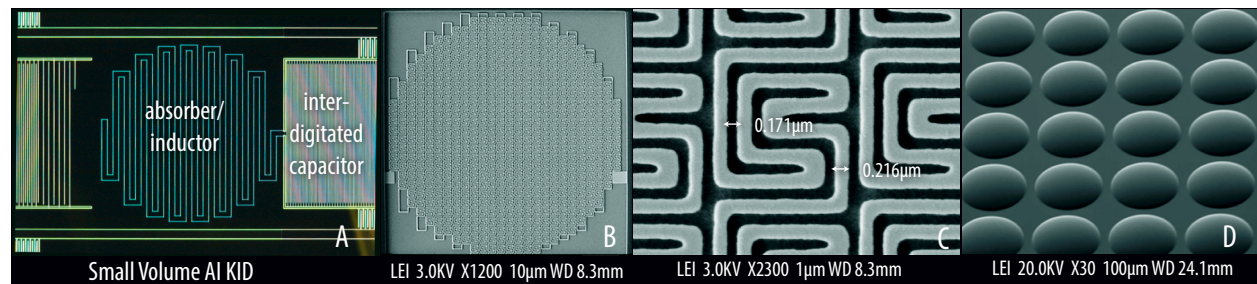


Figure 25: KID designs suitable for the *Origins* wavebands. (A) This $\lambda > 100 \mu\text{m}$ design (Swenson *et al.*, 2012; McKenney *et al.*, 2012; Stacey *et al.*, 2014) uses a meandered inductor that acts as an efficient single-polarization absorber. A microlens focuses the far-IR radiation onto the absorber. Dual-polarization designs have also been demonstrated. An interdigitated capacitor completes the resonant circuit and sets the radio-frequency (RF) readout frequency. (B) This modified absorber/inductor design provides high absorption efficiency at $\lambda = 10 \mu\text{m}$, (even shorter than is required for *Origins*) and is shown in close-up in (C). (D) Illustrates prototype silicon microlenses produced at JPL/MDL (Lee *et al.*, 2013); adopting hexagonal close packing increases the optical fill factor to 91%. Over 5,000 such microlenses have been produced on a 100 mm diameter silicon wafer.

Multiplexing: This is a natural strength of KIDs, and *Origins* arrays are a straightforward adaptation of existing devices. The *Origins* instruments system design accommodates a minimum detector-multiplexing factor of 500 pixels per GHz of readout bandwidth. This is only a 2× increase in multiplex factor relative to SPACEKIDs, and is straightforward based on a 2× reduction in readout frequency, from 6 GHz to 3 GHz (band center). In fact, KID development for STARFIRE is targeting resonant frequencies below 1 GHz, which would offer multiplex factors of 1500 pixels per GHz. Even lower frequencies can offer even denser muxing: 6,500 per GHz have been demonstrated at 200 MHz readout frequency (Swenson *et al.*, 2012). Further improvements are likely using post-fabrication resonator trimming methods (Liu *et al.*, 2017; Shu *et al.*, 2018), which can adjust resonant frequencies after fabrication to eliminate frequency-space collisions arising from lithography errors and material variation.

Pitch: The pixel pitch, or more precisely the per-pixel area, is an important consideration for KIDs because it sets the size of the capacitor, which translates to the readout frequencies, in particular for small-inductor devices. The smallest pixel pitch in OSS is $400 \times 700 \mu\text{m}$, while FIP has a 500-micron square pitch; therefore, both require a per-pixel area of $\sim 0.25\text{--}0.3 \text{ mm}^2$. These are smaller than those for SPACEKIDs, which have a relatively large $1,600 \mu\text{m}$ pitch. However the large SPACEKIDs footprint is driven by its optics/antenna design, and *Origins* requirements can be met with area-efficient resonator designs and narrow meandered inductors possible with deep-UV lithography (JPL/MDL 2018). Smaller pixels generally have higher readout frequency, which presents an engineering design trade space of pitch versus readout frequency.

3.3.4 KID Development Plan

Recent, ongoing, and future key technology demonstrations that lead to *Origins*' requirements are listed in Table 5 and summarized in Figures 8 and 10. The table represents a pathway from the current state-of-the-art (SPACEKIDs, TIMp) wavebands, detector counts, and sensitivities through to meeting *Origins* requirements.

A recently-selected, 3-year CIT/JPL/CU NASA APRA program will demonstrate kilopixel-scale KID arrays meeting *Origins* KIDs requirements (Hailey-Dunsheath *et al.*, 2018). A small KID array was flown on the Italian OLIMPO balloon payload (Masi *et al.*, 2019) and the BLAST-TNG 3.3 kilopixel KID focal plane is scheduled for an Antarctic balloon flight in 2019 (Lourie *et al.*, 2018). Kilopixel-scale, far-infrared, aluminum KID arrays can also be fully demonstrated using the recently-selected TIM NASA balloon payload (Aguirre and Collaboration, 2018) and/or through the proposed KID upgrade for the FIFI-LS/SOFIA instrument (Fischer *et al.*, 2018).

To demonstrate detector technology to the sensitivities required for *Origins*, a dedicated program between 2021 and 2025 (*Origins*-TD in Table 5) will undertake multiple tasks. The final year is under

Table 5: Major KID technology demonstrations leading to *Origins*.

Project	Date	Type	Detector Count (pixels)	NEP ($\text{W Hz}^{-1/2}$)	Wavelength (μm)
SPACEKIDs	2014–17	Lab	1,000	3×10^{-19}	350
STARFIRE-p	2017–18	Lab	45	4×10^{-18}	350
APRA	2019–22	Lab	1,000	1×10^{-19}	10–350
FIFI+LS	2018–22	SOFIA	9,856	$< 1.5 \times 10^{-17}$	51–206
STARFIRE	2019–23	Balloon	3,600	$< 1 \times 10^{-17}$	240–420
<i>Origins</i> -TD	2020–23	Pre-phase A	2,000	1×10^{-19}	25–588
<i>Origins</i> -TM	2023–25	Pre-phase A	2,000	1×10^{-19}	25–588
Probe or SPICA	2026+	TBD	5k–50k	1×10^{-19}	10–250
<i>Origins</i> -FIP	2030+	Flagship	10,000	3×10^{-19}	50–250
<i>Origins</i> -OSS	2030+	Flagship	60,000	3×10^{-20}	25–588

The SPACEKIDs (Baselmans *et al.* 2017) and STARFIRE-p (Barlis *et al.* 2018) programs are already completed. The APRA (Hailey-Dunsheath 2018) and STARFIRE (Aguirre and Collaboration 2018) programs were selected for funding by NASA, and FIFI+LS (Fischer *et al.*, 2018) has been proposed. All rows below SPACEKIDs are, or are expected to be, NASA funded for *Origins*.

Origins program Phase A. At the end of the program the packaged detector arrays covering the long wavelength 300-588 μm and short wavelength 25-50 μm will advance to TRL 5.

1. Task 1.1 (Year 2021): Pursue improved aluminum film quality to increase quasiparticle lifetime that is important for low-NEP MKIDs. Film quality can be assessed independently of the very-low NEP through the use of large-volume devices, and/or lifetime measurements via generation-recombination noise as a function of temperature. A 800 μs lifetime is targeted to be able to generate devices sufficiently sensitive for OSS.

Task 1.2 (Year 2021): Design and test Quantum Capacitance Detector (QCD) array with a two pixel types; one optimized for 350 μm , the other for 35 μm wavelength photon detectors. Show that demonstrated performance of $<3 \times 10^{-20} \text{ W/Hz}^{-1/2}$ is achieved for detection at 35 and 350 μm at an operating temperature in the range of 50-100 mK.

2. Task 2 (Year 2021): Develop an RF-shielded, light-tight, low-background test facility in a dilution-cooled cryostat for 2000 pixel format array(s). The first tests will be dark, but testing will quickly expand to include optical measurements with a cryogenic black body and a range of band-pass filters inside the cryostat. The system will eventually include filtration to enable coupling to sources outside the cryostat for full spectral and beam shape characterization. This facility naturally works for both QCDs and KIDs.
3. Task 3.1 (Years 2021 and 2022): Fabricate low-volume feedhorn or lens-coupled devices (both KIDs and QCDs), building on the models shown in Figure 25. The *Origins* top-level design steps are presented in Table 4. Screening for basic yield and resonant frequencies can be done quickly in existing test facilities.

Task 3.2 (Years 2021 and 2022): Design, build and test prototype packaging for detector arrays designed as part of Task 3.1 for the long wavelength 300-600 μm and short wavelength 25-50 μm bands.

4. Task 4.1 (Beginning mid-Year 2022): Test the low-NEP MKID and QCD devices, in 100-500 pixel array formats. Full characterization includes noise measurements while dark (un-illuminated) as a function of bath temperature, and response and noise as a function of applied power from the cryogenic blackbody.

Task 4.2 (Beginning of Year 2023): Latest date for down select detector approach for OSS - QCD or MKID and coupling scheme based on results obtained in 2022. Selection criteria: achieve noise performance over median of pixels with coupled efficiency $>50\%$ in prototype arrays. Preference will be given to a detector technology that shows performance at higher operating temperature.

5. Task 5.1 (Years 2023 and 2024): Design and build arrays based on the results from task 4 that have multiplexing scalable to the requirements of *Origins*, 2000 pixels per 4 GHz of readout band. Effort focused on designing, fabricating and packaging arrays for long wavelength band (300-600 μm) with pixel operability of $>80\%$, defined as ($>50\%$ optical efficiency and optical NEP $<3 \times 10^{-20} \text{ W/Hz}^{-1/2}$ tested in a cryostat with a cryogenic blackbody source.

Task 5.2 (Year 2024): Perform environmental vibration, aging and packaging reliability testing with prototype arrays.

6. Task 6.1: Develop new cryostat or adapt cryostat used for dark testing and with cryogenic blackbody source to allow coupling to exterior source for full spectral and beam shape characterization.
- Task 6.2: Design and build arrays based on the results from task 4 that have multiplexing scalable to the requirements of *Origins*, 2000 pixels per 4 GHz of readout band. Effort focused on designing, fabricating and packaging arrays for short wavelength band (25-30 μm) with pixel operability of $>80\%$, defined as $>50\%$ optical efficiency and optical NEP $<5 \times 10^{-20} \text{ W/Hz}^{-1/2}$ tested in cryostat with cryogenic blackbody source.

7. Task 7.1 (Years 2024 and 2025): Complete beam characterization of long and short wavelength band arrays using cryostat from task 6.1.
- Task 7.2 (Year 2025) Complete radiation testing of at least one packaged and operating array with a local alpha source and with >30MeV protons at a beamline facility.

3.4 Quantum Capacitance Detector

MKID arrays have been demonstrated at the sensitivity level required for FIP, but a working MKID array with performance required by OSS has not been demonstrated. The required sensitivity for OSS, and even photon counting ability, has been demonstrated using the Quantum Capacitance Detector (QCD) (Echternach *et al.*, 2018) with a lens-coupled pixel optical efficiency of ~90%. (Figure 26). In the QCD, incident photons break Cooper pairs in a metalized mesh absorber coupled by a tunnel junction to a Single Cooper Pair Box (SCB). The SCB island formed by the tunnel junction and a gate capacitor embedded in a microwave feedline is readout identically as is an MKID. However, in the QCD, the absorbed photon(s) cause modulation of the SBC gate capacitance. This modulation is high enough that noise contributions such as the TLS are negligible. Since publication (Echternach *et al.*, 2018), QCD arrays in $5 \times 5 = 25$ pixel and $21 \times 21 = 441$ pixel format have been tested (Figure 26a). Further, a readout scheme using commercial digitization electronics and Graphics Processing Units (GPU) with open source software has been developed and successfully used with both MKIDs (<https://ieeexplore.ieee.org/document/8703439>) and the 441-element QCDs array showing detector-limited noise performance. Tests of the QCD with these electronics show good optical response and 10^{-20} W $\text{Hz}^{-1/2}$ NEP with simultaneous pixel readout show that the QCD is an excellent candidate technology for OSS. Further modeling and testing is required to demonstrate the dynamic range of the QCD at higher photon flux and photon energies specified for OSS and FIP

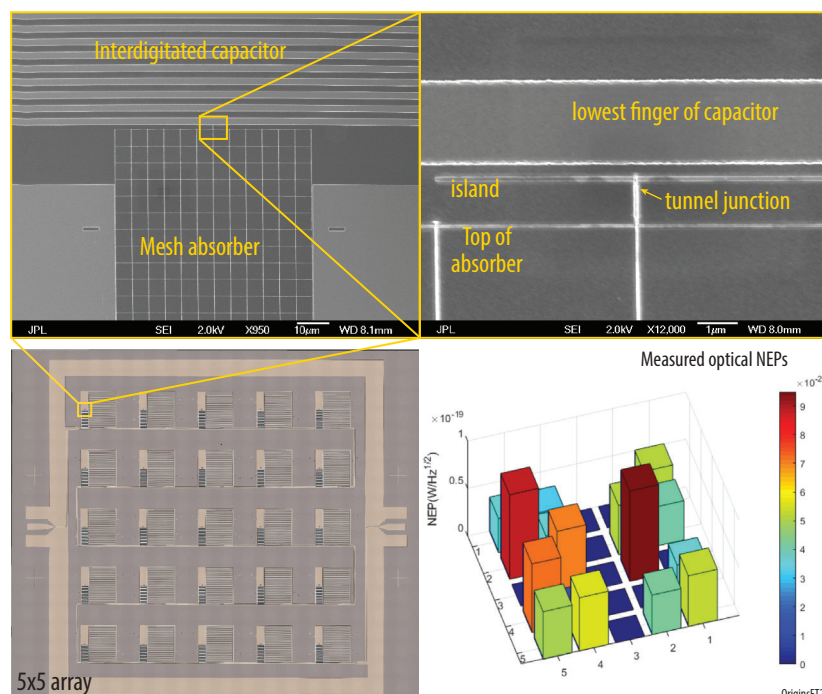


Figure 26: Quantum Capacitance Detector (QCD) 25 pixel demonstrator. Most of each pixel's area is for the meandered inductor and interdigitated capacitor which form the resonator. Resonant frequencies lie between 613 and 644 MHz and they are all coupled to the feedline circulating through the array. Radiation couples from the back side through a Fresnel lens array into the 60 micron x 60 micron mesh absorber shown in the upper left. Photo-produced quasiparticles tunnel into and out of the island shifting the frequency of the resonator, readily detected in the warm electronics. Of these devices in this prototype, 16/25 (64%) are optically active. The optical NEPs have been measured in a carefully characterized low-background test bed with a tunable blackbody viewed through small hole and set of filters. In this prototype 28% meet the OSS sensitivity requirement of 3×10^{-20} W $\text{Hz}^{-1/2}$. Fabrication process to improve pixel yield is in progress. Though not shown here, these detectors are fast enough to count individual far-IR photons.

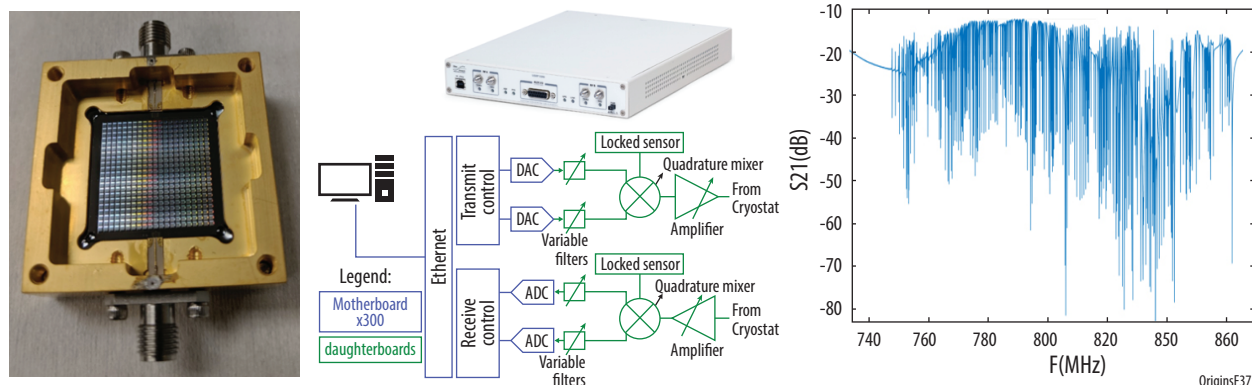


Figure 26a: (Left) 441-element QCD array packaged for test without lenslet array. (Center top) Multiplexed readout X300 USRP – Ettus research signal digitizer and analog digitizer (center bottom) Schematic of microwave readout electronics including the GPU/PC tone FFT and resonance feedback. (Right) Measured resonances for the 441 QCD array.

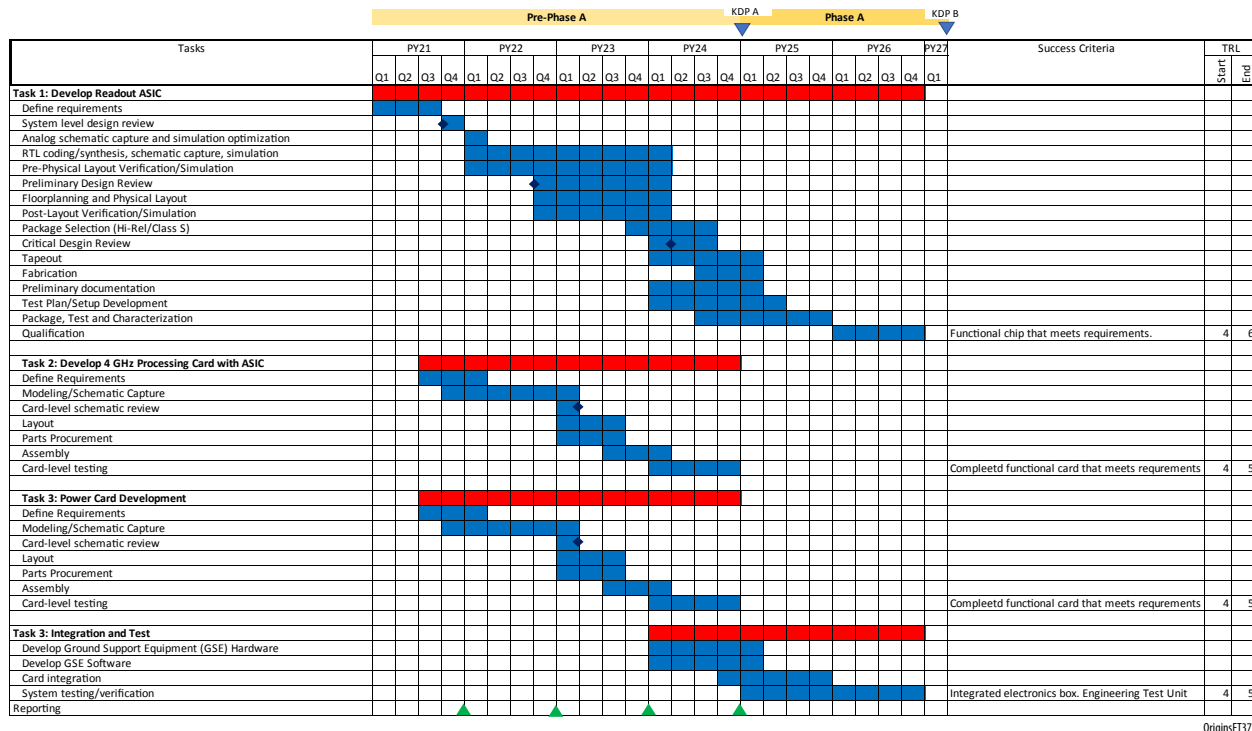
3.5 Warm Readout Electronics

All of the detector systems under consideration employ some form of frequency-domain multiplexing in the RF. The warm electronics generates a comb of frequencies, typically one per pixel, this comb interacts with the array and returns to the warm electronics. Each tone incurs a frequency or amplitude shift as it interacts with its corresponding detector pixel. The comb signal returning to the warm side is then digitized and demodulated to extract each frequency's information. No fundamentally new algorithms or approaches are required, it is just a question of total bandwidth and power.

In all three potential detector configurations, information bandwidth, B , is the most important parameter because it governs the warm electronics architecture. For direct microwave multiplexing of the FIP instrument detectors, the information bandwidth is $B=20$ GHz, since the detector signals are split into five 4 GHz HEMT channels. For the TDM/CDM hybridized detectors and associated readout methodology, bandwidth is reduced to $B=4$ GHz for every grouping of 64,000 TES resonators if using a 32-element TES array with a 2000-channel microwave mux for all arrays.

The detector readout electronics philosophy for both the FIP and OSS instruments is to use a scalable linear system approach to break down the overall information bandwidth to smaller segments for digital signal processing. This approach offers the advantages of graceful degradation, multi-purpose cross-cutting electronics application beyond just this observatory, and facilitation of integration and test capability once this observatory is built. At the present time, there are new, emergent radio-frequency (RF) chip technologies that are capable of acquiring, processing, and generating detector-related signals at increments of 4 GHz. The detector electronics concept demonstrated by a partnership between NASA Goddard Space Flight Center's Digital Signal Processing Technology Group, and Arizona State University, in November 2018 showed TRL-4 lab feasibility of a system that can process up to 16 GHz of detector bandwidth by a single processor integrated circuit (IC) chip. To advance from TRL-4 to TRL-6, similar single-IC's need to not only be demonstrated functionally in the lab, but also perform over space environment temperature test extremes, vacuum, and within a radiation-tolerant specification for the observatory. Currently, there is no technology that meets all of these requirements in a single IC, but this is likely within the next 18 months since several private companies are making the key investments today (Omnisys, Alphacore, Pacific Microchip, Xilinx) to advance the readout electronics technology. A technology development schedule with individual tasks to result in a TRL 6 readout system for the *Origins* Far IR detectors is shown in Figure 26b.

It is important to note that the readout electronics described herein can be applied in equal measure to the three types of detector technologies that are under consideration for the FIP and OSS instruments,



OriginsFT37

Figure 26b: The far IR warm readout system can easily reach TRL5 before the start of *Origins* Phase A, and TRL6 before PDR.

namely Microwave Kinetic Inductance Detectors (MKIDs), Transition Edge Sensor Bolometers (TES), and Quantum Capacitance Detectors (QCDs). From the perspective of the readout system, all 3 detector types produce a set of RF signals that are band-limited by the HEMT amplifier, and all are processed similarly. Only the TES detector array needs additional signals and electronics to facilitate readout.

3.5.1 Power vs. TRL

In 2018, the TRL 6 electronics approach would be to use a combination of RF-Sampling data converters (DACs, ADCs) in tandem with the densest radiation-tolerant Field-Programmable Gate Arrays (FPGAs) to handle signal acquisition and processing. The rule of thumb for selecting a data converter is 1 Watt per GHz of bandwidth I/O per converter and 15–30 Watts per monolithic FPGA. Assuming an ambitious 20 W per FPGA and two FPGAs per 4 GHz Nyquist processing bandwidth, FIP would need an electronics system that used 80 W for the data converters (20 W for bandwidth x2 Nyquist, x2 ADC and DAC) and 40 W total for the two FPGA required in the system. Assuming 70% power efficiency, the total power budget for the FIP warm electronics (not including RF interfacing electronics between HEMT amplifiers and DSP electronics) would be ~172 Watts. To achieve this power dissipation, current radiation-tolerant versions of commercially available FPGAs would not be viable. Only Xilinx, which makes the multiprocessor system-on-chip (MPSoC), has a device that can interface a large number of data converters. This suggests that an architecture that includes MPSoC devices as its main processing element for readout currently can perform no better than a TRL-4 Earth-based lab experiment. These devices are neither immune nor tolerant to radiation effects – specifically degradation via Total Ionizing Dose (TID) and single event functional upsets (SEU).

The optimal power solution would be realized using a new chip architecture: RF System-on-Chip (RFSoc). RFSoc is a new type of FPGA that integrates RF-data converters into the same chip die, as well as multi-core microprocessors (Figure 27). Xilinx has announced a family of these groundbreaking new devices (Feb 2017 Whitepaper). Xilinx RFSocs have been under evaluation since October 2017

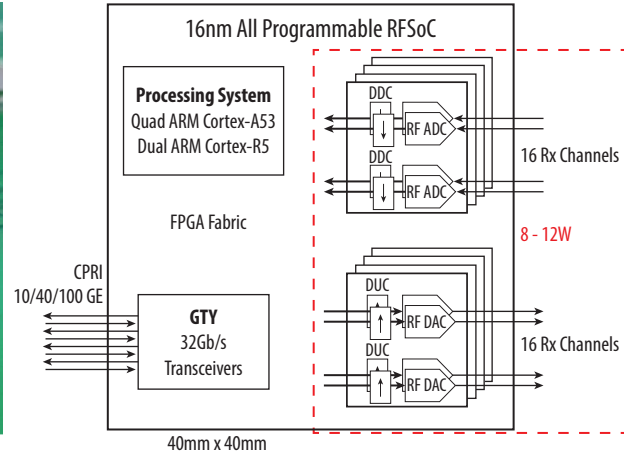
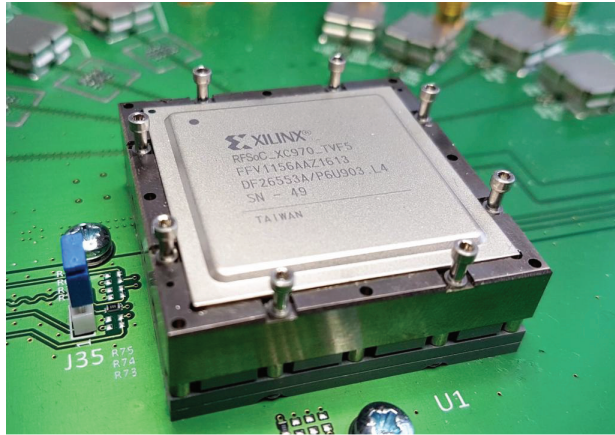


Figure 27: Xilinx RF System-on-Chip (RFSoc)

and show a power performance of ~30 W total, to be compared with 172 Watts of a conventional TRL 6 system with discrete data converters and multiple FPGAs. One RFSoc can handle 16 GHz of information bandwidth; two RFSocs can handle all processing required for FIP in the direct microwave multiplexing configuration.

In November 2018, a team from NASA GSFC (D. Bradley, T. Jamison-Hooks, L. Miles, T. Brown-ing) conducted a joint lab experiment to evaluate the new RFSoc system from Xilinx for the first time, for reading out MKID detectors. In this experiment, we showed the feasibility of using the RFSoc as a processor that could accommodate 16 GHz bandwidth worth of detector signal, as well as generate the detector tone signals required for detector readout. As a result, TRL-4 maturity of the OST detector readout concept has been demonstrated as mature to TRL-4, or lab-experiment grade. This is applicable to both the OSS and FIP instruments.

To advance the TRL past level 4 and through to 6, the OST detector readout and signal processing electronics must pass environmental test screening – including survivability over space temperature, vacuum, as well as radiation hardness. To date, The RFSoc does not demonstrate these characteristics, though there are current research efforts to evaluate the chip for these conditions. Further investment must be made in advanced electronics that use the RFSoc as a functional starting point. Similar chip design approaches utilizing RF-CMOS approaches combined with QML chip design processes will yield a specialized ASIC that can perform functionally as well as the RFSoc, but also meet the TRL-6 criteria of thermal-vac and radiation survivability. The idea, proposed by D. Bradley on the *Origins* study, consists of a new RF-Spectrometer chip, combined with a supervisory processor that coordinates all other board functions besides detector signal processing. This DSP board, in Figure 28, is an

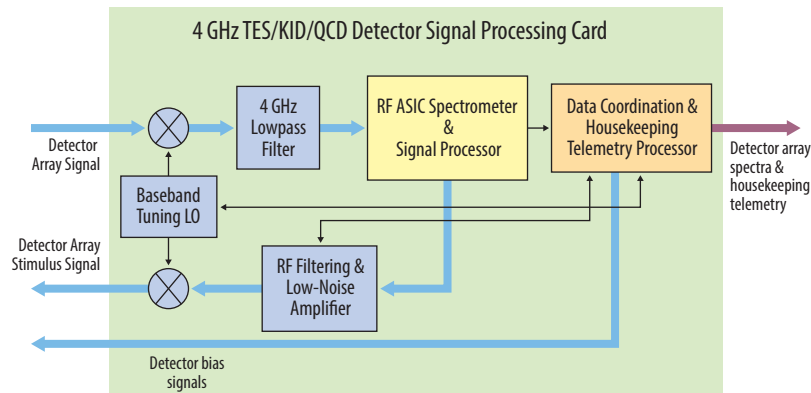


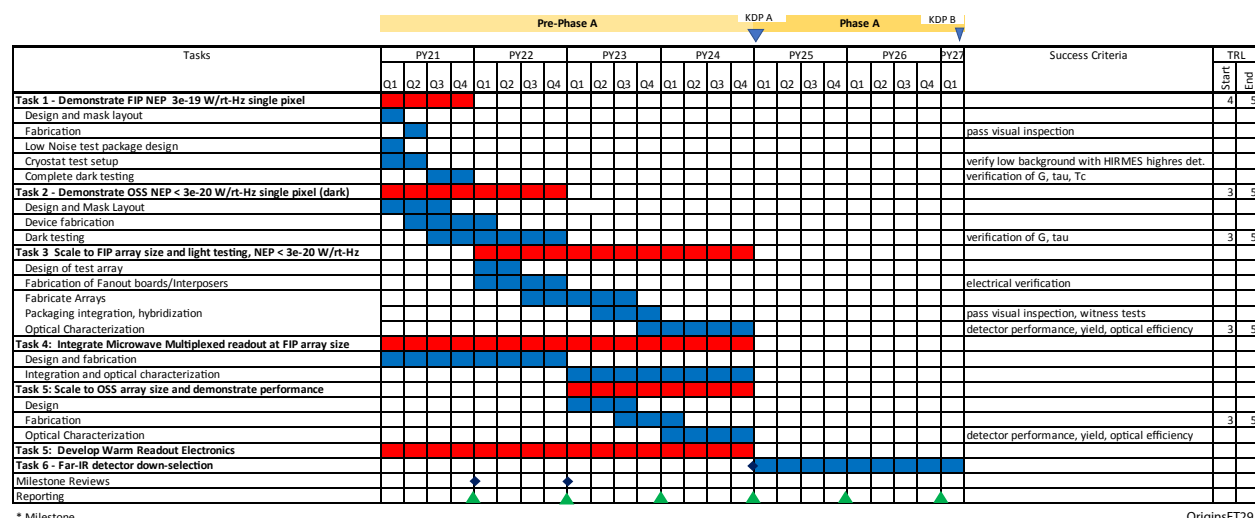
Figure 28: Scalable Detector Signal Processing Card

electronics card assembly that can be made into an area approximately 20 cm x 30 cm (or smaller in the next decade), and perform all of the necessary processing for 4 GHz detector readout. The current state-of-the-art processor designs are being invested in by private industry, and initial offerings will be made available by 2021 approximately. NASA is currently investing in and plans to invest in SBIR and ROSES-SAT technology that targets similar developments.

This card architecture is inherently scalable, meaning that the addition of duplicates of this card will process additional 4 GHz segments of spectra, and hence more detector pixels. Figure 28 shows only one of these cards. Once one card is proven functional, it is a straightforward electronics exercise to manufacture duplicates, using the same test equipment to evaluate each one. A card like this would consume less than 4W of power in operation extrapolating current technology trends in RFC-MOS processes.

3.6 Schedule for FIR Array Development, Down Select Strategy, and Cost Estimate

Monitoring development of the TES and KID technologies to reach the required specifications for OSS and FIP will be rigorous, with regular reporting to motivate progress and provide assistance to resolve issues. The *Origins* team envisions a manager to oversee progress and a standing review board of experts to provide useful oversight. The technology program will draft a technology enhancement milestone and performance criteria which will be the basis for assessing continued development. A down-select to a single detector technology is scheduled in FY2025, the beginning of mission Phase A (Figures 29 and 30).



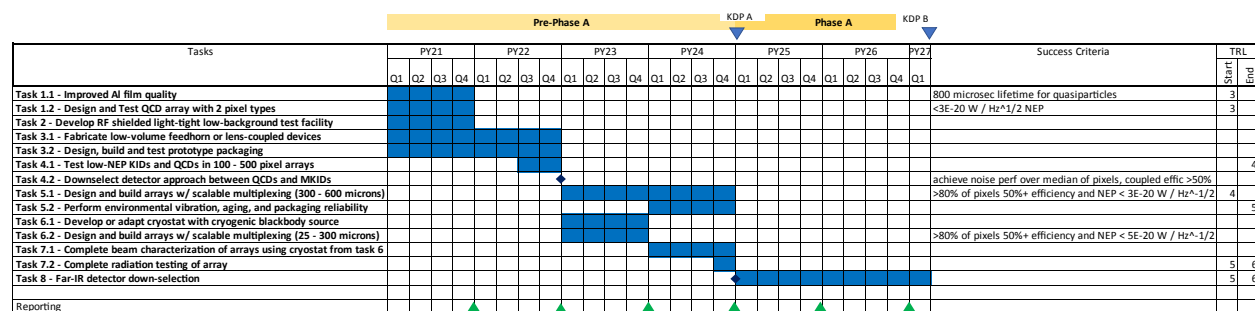
* Milestone

Note: Task 1 and Task 3 are building off of current ROSES/APRA work Stagnun (through 2020) and Rostem (through 2019)

Microwave Multiplexed Readout requires separate development from NIST or PTB.

OriginsFT29

Figure 29: TES development schedule



OriginsFT30

Figure 30: KID and QCD development schedule

Detailed detector development labor plans and budgets are presented for TES and MKID detectors in Appendices A and B, respectively. QCDs are also discussed in Appendix B.

4 - MID-INFRARED ARRAYS

4.1 Mid-IR Array Requirements

Transit spectroscopy has proven to be an essential tool for characterizing the atmospheres of exoplanets. The key performance metric for these observations is stability of the response of the instrument during the transit, secondary eclipse, or planetary orbit phase curve (typically on the time scale of hours to days). JWST/MIRI uses the same detectors as *Spitzer*/IRAC (Figure 31), which has been able to achieve ~60 ppm precision on timescales of several hours, including the phenomenological calibration of on-orbit drifts. Systematic errors for transit observations expected with JWST based on previous observation are described in Beichman *et al.* (2014).

Studying the atmospheres of potentially habitable planets orbiting M-dwarf stars is a key science goal for *Origins*. The bio-signature case for *Origins* requires a mid-IR detector stability of down to ~5 ppm, depending on the wavelength, over several hours (Table 6; Figure 32). This stability requirement in performance is on the order of one magnitude beyond the state-of-the-art that has been achieved on-orbit and may require new development for existing technology.

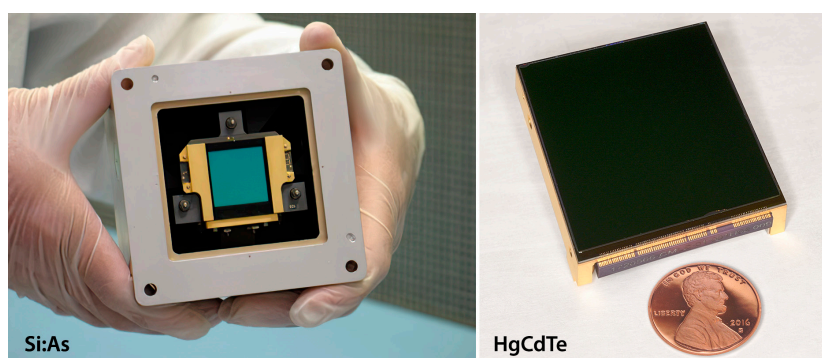


Figure 31: State of the art mid-infrared detectors: Left: Si:As detector array used in JWST/MIRI. Right: HgCdTe long wavelength detector to be used in NEOCam.

Table 6: Detector characteristics for *Origins* mid-infrared instrument

Inst.	Temp (K)	λ_{\min} (μm)	λ_{\max} (μm)	$R=\lambda/\Delta\lambda$	N_{pix}	Sensitivity	Saturation Limits	Notes
MISC-T	50 mK 30 K	2.8	20	Up to 295	10^4 or 4×10^6	NEP= 3×10^{-18} (W/Hz ^{1/2}) 5 ppm stability over a few hours	K~3.0 mag 30 Jy @ 3.3 μm	Detector stability limiting (5 ppm aimed for the short and mid wavelength band)

4.2 Mid-IR Detector Technology State-of-the-Art

There have been remarkable current achievements in stability with IR detectors. Knutson *et al.* (2009) obtained 65 ppm noise with Si:As arrays (similar to those on JWST) with *Spitzer* (Figure 33). The InSb arrays on *Spitzer* have achieved 50-150 ppm stability, depending on the algorithm used to remove correlated noise (Knutson *et al.* 2009; Ingalls *et al.*, 2016; Demory *et al.*, 2012). The HST WFC3 1.7 μm H1RG HgCdTe arrays have achieved 23 ppm in two exoplanet transits (Knutson *et al.*, 2014). JWST expects to achieve ~50 ppm stability with the H2RG 5 μm arrays (Beichman *et al.*, 2014; Clanton *et al.*, 2012). JWST, NEOCam, ARIEL, and TESS will produce an extensive set of image processing and analysis algorithms, which can be used by *Origins*. In particular, JWST will observe transiting exoplanets, which will require processing at levels even beyond what has been done for Kepler, HST, and *Spitzer*. The read noise of the Si:As detectors has not dramatically improved from the *Spitzer*/IRAC to JWST/MIRI (McMurtry *et al.*, 2005, Figure 14 and Lum *et al.*, 1993, Figure 11, where the conversion

Origins Transit Stability Components (in ppm unless otherwise noted) for a 9.8 K magnitude M-star, 85 transits of 4 hours duration each

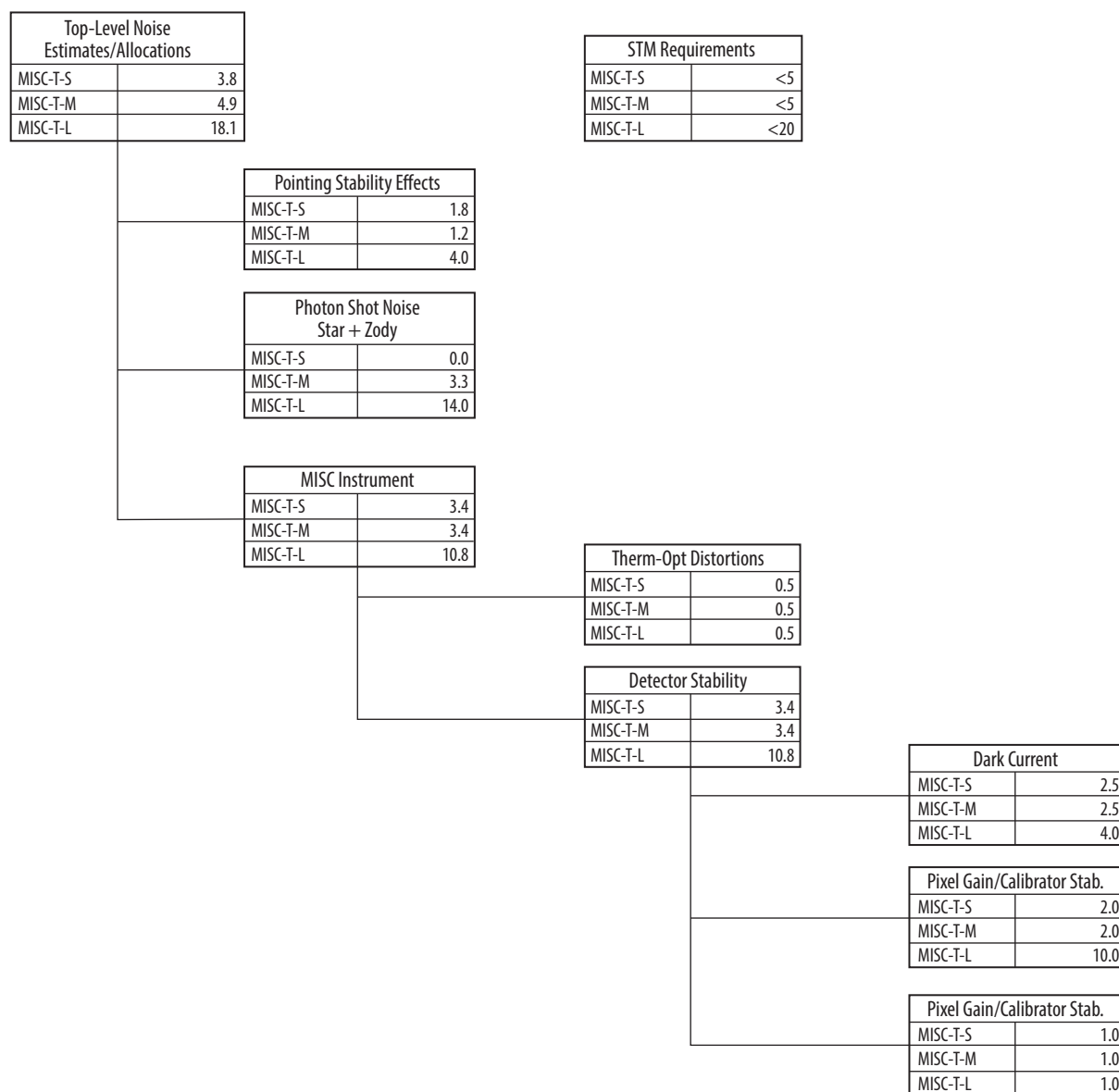


Figure 32: Tentative allocation budget for the MISC-T Spectral accuracy for exoplanet transit spectroscopy.

factor is $\sim 9 \times 10^{-12}$ between the two graphs). With the Read Out Integrated Circuits (ROICs) used in *Spitzer*, the noise was largely unchanged as the temperature decreased below 40 K. However, for JWST/MIRI ROICs, the noise increased as the temperature decreased (McMurtry *et al.*, 2005; Rieke *et al.*, 2015). Many researchers are currently working to improve stability through image processing, but that is an ex post facto solution. However, much can be done to improve the stability while the data are being taken (*i.e.*, improve the technology as well as the image processing software).

Spitzer/IRAC Si:As detectors have demonstrated ~ 60 ppm precision in transit observations of several hours. JWST/MIRI is expected to achieve similar or slightly better stability (*e.g.*, Love *et al.*, 2005; Greene, 2016). Limiting factors in stability are currently unidentified. Once on orbit, the MIRI detectors are expected to establish the state-of-the-art for transit spectroscopy in the mid-IR band.

MIRI uses the same arsenic-doped silicon impurity band conductor (IBC) detector technology as *Spitzer*/IRAC and a hybridized readout that improves their stability. Improvements can definitely be made - current laboratory testing of an engineering JWST Si:As array has shown that with careful attention to the readout electronics stabilities can be achieved that are over a factor of four better than achieved with the *Spitzer* IRAC detectors (T.Matsuo, *et al.*, 2019, submitted).

4.3 Mid-IR Array Challenges

The biggest challenge to reaching *Origins*' mid-IR requirements involves the stability requirement for the Transit Spectrometer instrument. It is likely there are a number of factors (*e.g.*, pointing jitter, control electronics, etc.) limiting the stability of the *Spitzer* and JWST observations. Unfortunately, laboratory test systems do not currently provide the required stability to measure at levels needed to simulate even *Spitzer* or JWST observations. A few teams (Staguhn, Greene & Matsuo) are currently working to improve the laboratory systems to improve ground testing capabilities.

Because high-stability detectors are critical to the success of the MISC transit channel, we envision a dedicated detector program to identify a detector that meets the stability requirements. We expect that once such a detector is identified, that an appropriate instrument would be designed based on the detector. Sections 4.4 and 4.6 outline the steps needed to progress HgCdTe and TES detectors to meet *Origins* requirements (Tables 6 & 7). Section 4.5 discusses how to re-institute Si:As detectors. In Section 4.7 we describe the strategy for Mid-IR array development and down-select strategy.

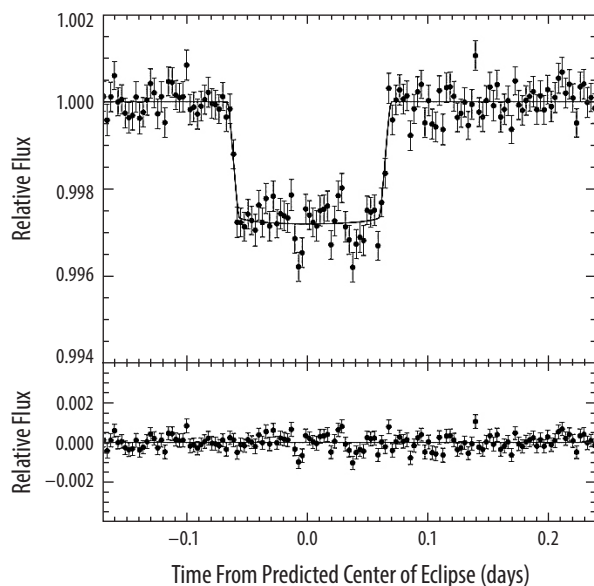


Figure 33: Noise characteristics of exoplanet observations with *Spitzer*/IRAC by Knutson et al. (2009) shows the noise (scatter in the points) does not decrease past a certain amount of time and reaches a noise floor of 65 ppm.

Table 7: *Origins* requirements for $\lambda < 11 \mu\text{m}$ vs. state of the art

Parameter	<i>Origins</i> Needs/Requirements	HgCdTe State-of-the-Art
Format	2K x 2K	2K x 2K (2040 x 2040 active)
Pixel Size	$\sim 18 \mu\text{m}$ (subject to trade study)	$18 \mu\text{m}$
Wavelength Coverage	$2.8\text{--}11 \mu\text{m}$	$1\text{--}16 \mu\text{m}$
Readout Rate	10 sec full frame	1.3 sec full frame (32 outputs)
Detective QE	$>50\%$ at all wavelengths in range above	$>55\%$ at all wavelengths without AR coating (higher with AR coat)
Dark Current	$<0.3 \text{ e}^-/\text{s}$	$<0.3 \text{ e}^-/\text{s}$
Read Noise	10 e^-	$12\text{--}18 \text{ e}^-$ (correlated double sample), lower with multiple sampling!
Full Well	250 Ke^-	$70\text{--}90 \text{ Ke}^-$
Operability	$>95\%$ (TBD)	$>95\%$
Operating Temperature	$<30 \text{ K}$	$24\text{--}30 \text{ K}$
Other: Img/Cor/Spec	Window guide mode	Yes in HAWAII-2RG
Other: Transit Spec	$<3 \text{ ppm}$ stability over 10 hr	$35\text{--}50 \text{ ppm}$

4.4 HgCdTe Detector Array Technology Development

The *Origins* team has assessed that the mid-IR HgCdTe detector arrays, developed with Teledyne Imaging Sensors (TIS) under several NASA grants to the University of Rochester (UR), are a better alternative than Si:As IBC arrays for sensitive exoplanet characterization missions requiring stabilities

of 5 ppm. In fact, mid-IR detector stability was recently added to the NASA Science Missions Directorate Astrophysics Division “Technology Gap List” in recognition of the importance of exoplanet characterization and the power of the mid-IR to trace important molecules in the atmospheres of exoplanets discovered through transit observations (<https://exoplanets.nasa.gov/exep/technology/gap-lists/>). The 3-11 μm range is better covered by HgCdTe than Si:As, since at short wavelengths Si:As is known to be virtually transparent. As Pipher *et al.* (2004) and Rieke *et al.* (2015) have shown, Si:As detector arrays are quite transparent below 10 μm . Photons that are not absorbed in the detector material can either 1) produce a diffraction pattern in reflection off of the metal pads (Babinet’s principle – Rieke, private communication) or 2) enter and bounce around in the epoxy layer between the detector and ROIC material and before being reflected back into Si:As detector, hence producing a wavelength dependence to these features which corresponds to absorption by the epoxy. In addition, HgCdTe photodiodes do not exhibit gain variation with bias, whereas Si:As IBCs do. HgCdTe photodiodes operate at a higher temperature and exhibit a quantum efficiency (QE) 2x higher than Si:As. These reasons point to better performance at lower mission cost with HgCdTe arrays.

If JWST/MIRI or NIRSpec perform at the 5 ppm level, those techniques and software can be implemented on *Origins*. In the intervening years before *Origins* is built and launched, *Origins* will improve the detector technology, read-out integrated circuits (ROIC), and control electronics. Furthermore, the *Origins* transit spectrometer will employ a densified pupil optical design, which, although limited in use for a wide range of astronomical investigations, is optimized for the removal of systematic instabilities in the detector arrays as well as due to pointing jitter. Taken together, all signs point to the likelihood that *Origins* will significantly outperform JWST at characterization of habitable, life-bearing exoplanets.

4.4.1 HgCdTe Detector Development Plan

To make HgCdTe viable for use on *Origins* will require ROIC stability improvements, including major development programs that address decreasing read noise, alleviating non-linearity effects, reducing pixel-to-pixel variations, and resetting anomalies. For the Image/Cor/Spec instrument, the remaining challenges are to: 1) increase the full well, which may require a selectable capacitor/pixel addition to the ROIC, which is fairly straight forward; and 2) redesign ROIC to decrease read noise and change pixel size while not increasing dark current or adversely affecting the image quality (MTF or PSF). The second challenge is more involved, but not impossible (*i.e.*, it requires multiple iterations of silicon foundry runs with extensive testing after each run).

HgCdTe has benefitted from existing development work for JWST (5 μm cutoff), NEOCam (10 μm cutoff; PI: Amy Mainzer, JPL) and University of Rochester’s (UR) 15- μm cutoff development aimed at supporting spectroscopic detection of biosignatures via space missions, such as *Origins*. The Ariel mission will require similar detectors to those on NEOCam. For the past three years, UR has been extending this technology (under NASA grant; Forrest, PI) to longer wavelength cutoffs. To begin the process of extending to 15+ μm , the UR team took the first step by moving to a 13 μm cutoff wavelength. First results have been reported (Forrest *et al.*, 2016; McMurtry *et al.*, 2016), and the team is completing characterization (Cabrera *et al.*, 2019, in preparation; Figure 34). The team started the next phase in 2017, working to extend the wavelength to the final goal. The new HgCdTe detector arrays with cutoff wavelength >16 μm have been grown, hybridized, and packaged, and were delivered in early September 2018. Testing is underway, and results will be presented in August 2019 at SPIE in San Diego, CA.

The growth of HgCdTe detectors is often fraught with difficulties, *e.g.* low well depth and high dark current due to tunneling currents, softer material at longer wavelengths, which makes hybridization more difficult, cluster defects such as those from Hg precipitates, thinning of substrates, and targeting the cutoff wavelength. While each of these issues may be understood in principle, it is difficult to fully

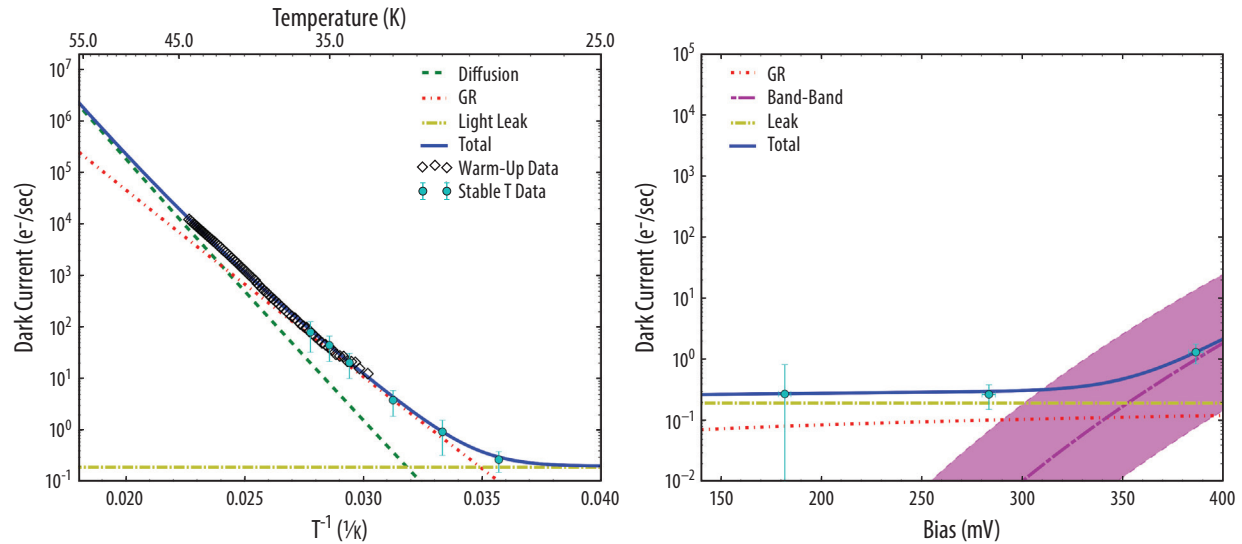


Figure 34: (a) Dark current vs. temperature (applied bias of 250 mV) and (b) dark current vs. bias (at 28 K) averaged data of 50 operable pixels in H1RG-18509 which has a cutoff wavelength of 12.6 microns. In (a), the mean actual bias of 283.5 mV, corresponding to the 28 K stable data point, was used to fit the dark current models. (from Cabrera et al., 2019)

constrain all of them in practice, which results in lower yield of detectors, which in-turn results in higher costs to produce the flight detectors for any given program. Thus, we will take what is learned during both JWST's and NEOCam's production runs of flight detector arrays (heritage reduces cost and risk) and apply all possible solutions to improve the yield of detectors.

HgCdTe arrays are susceptible to damage from cosmic rays. The current 10-micron cutoff HgCdTe arrays have been qualified to TRL 6 for the NEOCam mission after proton irradiation experiments where <1% of the pixels were degraded (increased dark current) after 1.5× and 2.0× lifetime TID for the L1 environment proposed (Dorn *et al.*, 2016). The HAWAII-2RG HgCdTe arrays have been qualified to >TRL 6 for JWST (OCO-2, HST, ECHO).

The next steps are to address the remaining requirements for *Origins*: stability, read noise, and well capacity. One possibility (Figure 33) is that dark current stability can be reached by operating at a sufficiently high temperature (28 K) so the detector is thermally dark current limited (G-R) instead of bias dependent dark current limited (trap-assisted tunneling), while still meeting the 0.3 e-/s dark current requirement for *Origins*. Teledyne HxRG ROICs, generally used for low background space astronomy, are source follower per detector (SFD) pixel and the lowest noise and low power choice. Although a CTIA ROIC could provide constant bias, which might initially seem the most stable choice, other reasons (*e.g.*, high power – typically Watts rather than milliwatts - and glow) make this ROIC an unsuitable choice for space exoplanet missions, at least as it is currently envisioned. The high power occurs because all pixels are powered during the read of each pixel. Some detector groups have discussed turning off the power to all but the pixel being read out; however, then turning on the power to each pixel would be unstable, and still more powerful than a few milliwatts. Extra closed cycle cryo-refrigerators would be required, adding cost and weight to the mission. The high current leads to ROIC glow, which affects the background flux levels in an unstable way. First efforts will be directed toward improving the HxRG ROICs before considering a completely new cryogenic ROIC design.

Redesigning the ROIC, by definition, will decrease the complete detector array's TRL to 4. Once the design is complete and tested in a lab environment, it will be back at TRL 5. With sufficient funding, this process will take ~4-5 years. The redesigned ROIC will then need to pass proton radiation testing, thermal cycling, and shake/vibration testing to once again reach TRL 6 (HgCdTe is currently TRL 6).

4.4.2 HgCdTe Detector Manufacturing

Our primary objective is to improve the overall radiometric stability of the HgCdTe detector arrays. This requires several tasks, as detailed below. In collaboration with Teledyne, the University of Rochester (UR) group proposes to develop test circuits (chips) with smaller arrays of pixels that mimic what is used in full, large format array ROICs. This path was selected as a cost savings compared to attempting multiple iterations of a fully redesigned ROIC, which would cost 20 to 50 times the small array option. Each foundry run will produce several test chips with variations (lot splits) on the foundry process or the circuit architecture to evaluate which are the best performing devices. The plan has seven Tasks:

Task 1: The most important objective is to decrease the noise, both the long term (between images over 1 day) $1/f$ noise component and the short term (single image) read noise.

The $1/f$ noise component directly impacts the long-term radiometric stability since it adds uncertainty to the measurement, which cannot be removed via repeated sampling to reduce the noise. Popcorn noise is another form of both traditional read noise and $1/f$ noise that follows a power law distribution in both frequency of transitions and voltage of transitions (Bacon *et al.* 2005). The lowest frequency popcorn noise has the largest voltage transition. There are a few methods to reduce $1/f$ noise. First, the use of buried channel MOSFETs can reduce the $1/f$ and popcorn (random telegraph) noises. Second, switching to an all PMOS process (i.e. not fully CMOS) can reduce the number of defects introduced during processing, i.e. less dopants and thus less contaminants enter the silicon. Finally, if one had enough funding ($> \$500M$ which is clearly cost-prohibitive) to purchase dedicated equipment, conduct engineering improvements, and pay staff at a foundry, then the process itself could be cleaned to the point of removing the contaminant responsible for the popcorn noise.

Although most exo-planet transit observations will be photon shot noise limited due to bright host stars in the raw data, the read noise of the ROIC is still important because the extracted signal from the exo-planet's atmosphere will be very small ($1-100 e^-$) and thus comparable to the read noise. Therefore improvements to the read noise will translate to lower number of repeat observations needed to extract the small signal of the planet's atmosphere. For the most recent detector arrays, the read noise must be improved (decreased) from $\sim 12 e^-$ to below $10 e^-$, or ideally below $4 e^-$. A major effort is required to achieve this goal. The main issue with improving the read noise is the lack of true cryogenic foundries. In the past, Teledyne, DRS and Raytheon Vision Systems have all worked with the silicon foundries to change their standard process to improve ROIC performance. While not impossible, this will be an extra cost to the program.

The source-follower FET has a thermal shot noise component due to the current that flows in the FET. That thermal noise is white across frequencies and thus may be reduced by decreasing the bandwidth of the FET. The reduction of the bandwidth is achievable via increasing the number of ROIC outputs while decreasing the speed with which each pixel is read, i.e. 20 ms/pixel instead of 10. This option increases the power consumption per array due to the increased number of outputs, however that is still within our budget of 100mW per array.

Both the dopant and concentration of the dopant (actual not provided since that is proprietary) in the silicon wafer can be adjusted to improve the cryogenic performance of the ROIC (McMurtry *et al.* 2003, McMurtry *et al.* 2005). In addition, it is possible to improve the foundry process to make each layer more planar, i.e. place more oxide between FETs and traces such that the overlying oxide on those traces is flat and plane parallel with the starting silicon wafer. Without such a process improvement, the oxide becomes thinner at the corners of the traces (as seen in cross-section) and leads to micro shorts between crossing traces or the substrate (Alan Hoffman, private communication, 2003). Adjustments to the combined parameters of the insulating oxide thickness, its planarization, the dopant and its concentration will help to reduce micro-shorts within the ROIC which in turn will reduce currents in the substrate, reduce clock feed-through and thus lower the read noise.

Task 2: We will implement design improvements to improve the stability of clocks and biases, which in turn will improve the overall detector stability. This is primarily a strict analysis of the design used to reduce stray capacitances and any potential shorts or cross-talk between adjacent circuits, *e.g.* move shift registers away from sensitive bias lines and output amplifiers (source follower FETs), adding more metal layers for shielding, employing lower voltages for switches and dual polarity (differential) switches. The designs will also need to minimize the resistance of long lines for voltage supplies to decrease the voltage drop that occurs from one side of the ROIC to the other. The increase in pixel size will provide the ability to reduce resistances on long supply lines (reset voltage, drain voltage, etc.) by using larger width traces, while also spacing those traces better to decrease the amount of stray capacitances. We will also utilize the improvements that were introduced into the HAWAII-4RG ROIC design to minimize clock feedthrough.

Task 3: Improve the pixel-to-pixel uniformity. The increase in pixel size (see Objective 5) will allow for better pixel-to-pixel uniformity since the team will be producing FETs well above the design rule limits for the chosen foundry, and thus inherent foundry process variations in the FET dimensions will be a smaller fraction of the area of the FET. Having better pixel-to-pixel uniformity will reduce the variation of the measured source signal from one observation to the next due to telescope pointing fluctuations (*i.e.* spot position on the detector array).

Task 4: Change the pixel pitch from 18 microns to an optimized value derived by the final optical design of the MISC-T instrument. The existing HAWAII-2RG 2Kx2K pixel ROICs used for HgCdTe arrays have 18 micron pixel pitches, which may not be optimum - for example pitches that are approximately wavelength-sized do not produce good image quality (*e.g.* MTF, Boreman 2001). Further, changing the size of the pixel pitch will allow more room within each pixel to accommodate changes made to satisfy the other tasks, both above and below.

Increasing the pixel pitch is not without its disadvantages. The final ROIC, produced after *Origins* selects its optimal design, will be large in physical area and therefore require stitching of reticles during the foundry process in order to create the full array. The optics for any future telescope will be more difficult to design given that the array extends over a larger area of the focal plane, thus putting more strain on the optical designer to deliver a flat focus over that larger area. Further the size of the actual detector die will cover a larger portion of the HgCdTe wafers, which results in greater risk of non-uniformity of the detector and thus impacts the yield. With a larger detector die to be hybridized to the ROIC comes a larger force needed to bond all the pixels. This will require a short development period in order to be able to reproducibly hybridize the larger HgCdTe die to the larger ROIC die.

A pixel pitch increase would normally increase the dark current, *i.e.* larger p-n junctions for larger pixels. However, we will not be changing the size of the p-n junction, hence dark current will not change. Despite having smaller p-n junctions relative to the pixel area, a pixel pitch increase will not adversely affect the lateral charge collection by a large amount due to Teledyne's proprietary techniques in growing the HgCdTe.

The interpixel capacitance (IPC) will also be affected by the change in pixel size. However, an increase in pitch will result in a decrease in IPC, which is a beneficial outcome. And an increase in the pixel pitch would allow more room to accommodate an increase in the capacitance allowing a commensurate increase in well depth as described in Task 5 below.

All of these advantages and disadvantages will need to be properly weighed during a trade study on the pixel size. While the current goal is to produce 15 micron pixels (as given by the optics team to the detector team), it is likely that *Origins* will decide to use pixels that are larger than that.

Task 5: We will add internal capacitance to each unit cell (pixel) to increase the well capacity and reduce the bias dependence of DQE and dark current by effectively reducing the contribution of the detector to the total capacitance. This unfortunately also will increase the effective read noise since

the read noise is actually a voltage noise despite always being quoted in electrons. The increased read noise must be traded against the gain in well capacity in order to find the optimal value for the added internal capacitors.

Task 6: Once a final ROIC design is made, we can begin to qualify the ROIC to TRL-6. Part of that qualification process involves proton radiation testing. This will be conducted on bare ROICs.

Task 7: The final objective is to produce hybridized LWIR (11 μm) HgCdTe detector arrays utilizing the best ROIC design. These arrays will then be tested against the *Origins* requirements. A small number of these arrays will be subjected again to radiation testing, thermal cycling and vibe/shake testing to complete the qualification to TRL-6 for the SCA.

4.5 Si:As Detector Development Plan

The Si:As detectors that are currently baselined in the design of the MISC-T instrument long wavelength channel will operate over 11-20 μm , where this detector material has high quantum efficiency. The cooling requirements are very modest as these detectors will operate quite happily at the temperature of the *Origins* optics and their power dissipation is low enough that simple heat straps will be sufficient to cool the detectors. Most importantly, the stability requirements are considerably relaxed compared to the shorter wavelengths – the biogenic spectral features of interest are much more pronounced at these longer wavelengths. As a result, there is little additional development that is needed to meet these requirements. The detector format (2k x 2k) is twice as large as the 1k x 1k Si:As detectors used in the JWST MIRI instrument, but increasing the pixel count is expected to be straightforward. These detectors are therefore already at a TRL 6 level for their stability, and at TRL 4 considering the need to increase the pixel count.

The biggest issue is the question of detector availability. The industrial detector fabricators (Raytheon and DRS) that have built these detectors in the past for such missions as *Spitzer*, WISE, and JWST, have dropped their fabrication efforts in this wavelength range. The past developments were largely funded by interest from the Department of Defense, which is no longer interested in this wavelength range. As a result the industrial fabrication facilities and institutional experience have declined significantly. Rebuilding this capability will be straightforward, but costly. We therefore estimate that three years and roughly \$10M would be needed to bring the fabrication facilities up to date and increase the pixel count.

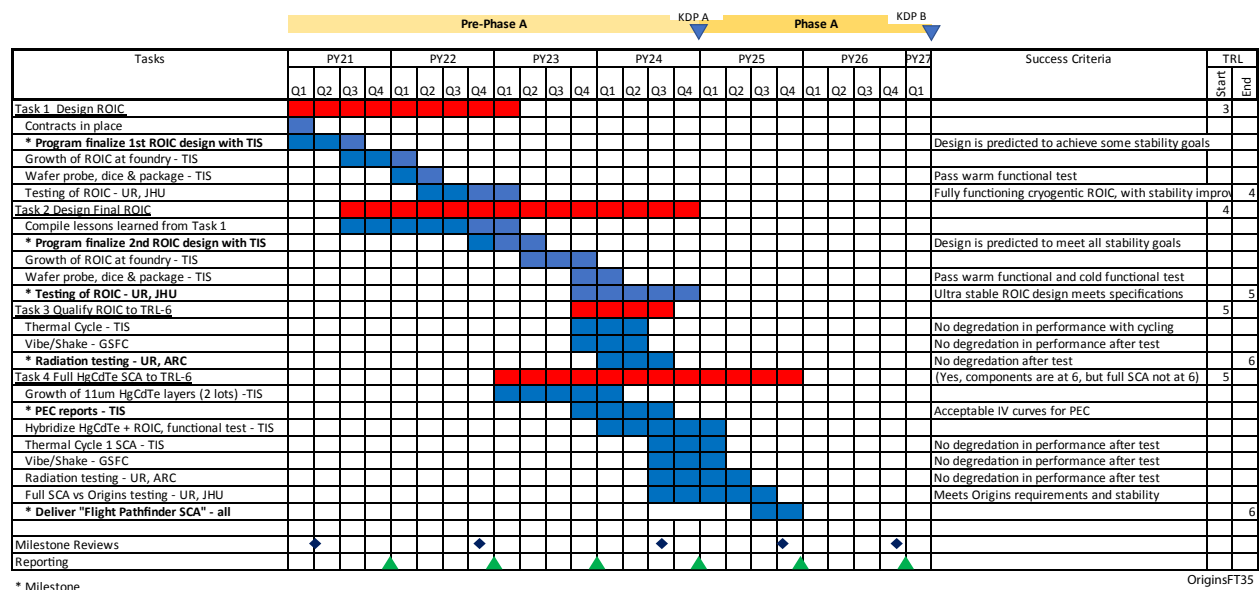


Figure 35: Development schedule for the Mid-IR HgCdTe detectors. The Si:As detectors follow a similar schedule.

4.6 HgCdTe Detector Testing

NASA ARC and the University of Rochester have been conducting tests of mid-IR array detectors for many years and have supported detector testing of a number of earlier and current space missions, including *Spitzer*, WISE, NEOCam, and JWST. The ARC facilities are currently in use to test the stability and performance of the densified pupil spectrometer design (Matsuo *et al.*, 2016) being considered for *Origins*. The UR facilities are currently in use to test the pre-flight production of HgCdTe arrays for NEOCam. To fully test the detector/spectrometer designs, both the ARC and UR facilities must be upgraded to measure the extremely low (few ppm over 10 hours) pixel-to-pixel photometric stabilities necessary to meet *Origins* transit science requirements. These facilities must be capable of testing the Si:As and HgCdTe detector technologies currently baselined for the Origin mid-IR instrument, which in practice means separate cryogenic dewars will be required for each detector type.

The scope of these test facility improvements fits the need to demonstrate TRL 5 by 2025 and TRL 6 detector technologies by *Origins* PDR, currently anticipated to occur in 2027. An estimated budget and schedule is provided in Figure 35. This budget and schedule is broken into two separate, but concurrent facets: 1) the test facilities and 2) the cost of the detectors and readout development program.

Test Facilities

Year 1: Procure and manufacture two dedicated cryogenic dewars for each facility (4 dewars total), including cryocooler heads and compressors, internal optics, high-stability internal calibration source: ~\$1250k. Procure detector drive electronics from Astronomical Research Cameras (aka Leach), Gen-IV ultra-stable version: \$104k (quantity 4 at \$26k each).

Labor: 5 FTE/WYE (1 scientist + 3 engineers + 2 graduate students). The scientist will oversee the engineers and students, while providing guidance to ensure the proper design of the dewars to meet the low background space telescope like environment. The engineers will produce the designs for the dewars, optics, sources and drive electronics. The engineers and graduate students will assemble the systems. Overhead and lab fees: \$100k. Travel: \$20k.

Year 2: Commission the test system. Procure data system hardware and software (not including detector drive electronics): ~\$175k. Labor: 3 FTE/WYE (2 engineers + 2 graduate students). Overhead and lab fees: \$100k. Travel: \$20k.

HgCdTe Detector and ROIC Development Program

Prior development costs (circa 2002) for ROICs were \$1-2M per iteration based upon an existing design. Scaling those to the scope of this development, which is two iterations that are on the more costly end of that range, and allowing for inflation (factor of 2), we estimate that the 2.5 year development will cost \$8M. Production runs of HgCdTe detector arrays at Teledyne are \$800k per run, with 4 runs needed, for a total of \$3.2M.

Schedule: 5 year development and test period. Labor for testing at ARC and UR: 5 FTE/WYE (2 scientists + 2 engineers + 2 graduate students) per year for 5 years. The scientists will work with Teledyne to produce the ROIC designs and foundry run lot splits that will meet the *Origins* Space Telescope's requirements. The scientists will also evaluate the success of the ROICs and HgCdTe detector arrays after delivery and testing is complete. The engineers and the graduate students will conduct the testing of the ROICs, full detector arrays and radiation testing. Travel \$40k/year. Overhead and fees: \$100k/year. Radiation testing at UC Davis: \$100k.

Si:As Detector and ROIC Development Program

Cost of Si: As detector arrays to test. Based on informal conversations with Raytheon over a year ago we estimate a total of \$10M for the first production run of ~10 Si:As detectors. It is expected that

this would be spent over a 3-year development and test period. A second detector run should be baselined so that the design can be refined. This second run should be less expensive since the fabrication facilities will now be back up and running – with an estimate of \$3M for this run.

4.7 TES Development Plan

The *Origins* team is also studying Transition Edge Sensors (TES) as an alternative option for the Transit Spectrometer (Section 3.1). This alternative option for the mid-infrared detectors will leverage the TES development effort that is being undertaken for the *Origins* OSS and FIP instruments. To provide a detector array with the required stability while reducing development efforts, the team selected an extremely stable and linear superconducting detector, TES, in combination with a calibration system. There are two disadvantages of this technology compared to the large-format Hg-CdTe and Si:As detectors: 1) as their array sizes are smaller than the 2k x 2k sizes used in the MISC-T densified pupil optical design, using TES detectors would necessitate a completely different optical design, and 2) they would require additional cryocoolers within the MISC-T instrument in order to reach their sub-Kelvin operating temperatures. However, in spite of these disadvantages we feel that pursuing this alternative technology development path is an important risk-reduction approach to achieving the very high detector stability requirements. Given the impact on the MISC optical and mechanical designs and the additional cryogenic requirements for the TES detectors, the selection of which detector technology to use will have to be made before the *Origins* System Requirements Review.

Very stable, large format, high efficiency, low noise TES-based bolometer arrays operating in the millimeter through far-infrared wavelength regimes have already been developed (*e.g.*, Benford *et al.*, 2010). Such arrays have been successfully integrated into bolometer cameras (*e.g.*, GISMO, HAWC+); additional applications are planned for GISMO-2, PIPER, and HIRMES. The detectors for these instruments were produced at GSFC. These detectors have very low 1/f noise with 1/f knees of close to 0.01 Hz, as shown in a lab current noise density measurement of a PIPER array (Figure 36). The ADR was running open loop during the measurements; with feedback, the device will be even more stable.

The PIPER and HIRMES detectors have sufficient sensitivity and dynamic range for mid-IR spectroscopic applications with a NEP of a few 10^{18} W/ $\sqrt{\text{Hz}}$ and a saturation power of ~ 2 pW. Since TES are used as bolometers (resistance changes with temperature), they can also be used as near and mid-IR detectors. The only required development for this application is a suitable mid-infrared absorber to deposit the radiation energy into the detector membrane. The required absorbers can be optimized independently of other detector parameters such that a high quantum efficiency can be achieved. Quarter wave resonators will not be incorporated into the detector arrays for this demonstration.

To extend stability of the mid-IR arrays to the required time scales (*i.e.*, hours), the team introduced a calibration system with a high precision reference load and real time load temperature monitoring (Staguhn *et al.*, accepted by IEEE). The load temperature is modulated, so detector response to the load signal can be monitored. This system approach has recently been awarded as an APRA program.

The calibration scheme is independent from the detector used (even though it will only provide a sufficient SNR for calibrating individual time intervals of several minutes, so the detector needs to be stable within a fraction of that, which was demonstrated for TES). Should better detectors become available in the future, using this calibration scheme to improve their long-term stability would also be straightforward.

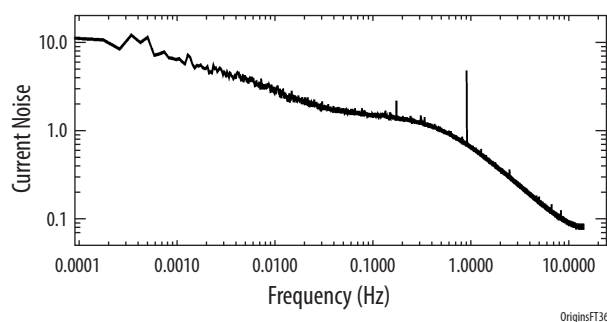


Figure 36: Long duration laboratory measurement of the average noise spectrum of a GSFC TES Detector array (in units of normalized current noise density).

4.8 Schedule for MIR array development and Down Select Strategy

A dedicated mid-infrared detector program for *Origins*' MISC-T instruments will provide a strategic NASA investment outside of the grants program. This program will focus on development of a high-stability mid-infrared transit spectrometer. In sections 4.4 to 4.6 we outlined the efforts needed to advance HgCdTe arrays, Si:As arrays and TES bolometers. By the start of this program (2021), JWST will be taking data and we will have better data to evaluate the performance of the HgCdTe and Si:As arrays and their applicability to *Origins* transit spectrometer. Hence, within the first year, we will assess the best path to take. For example, we could pursue all three options or HgCdTe and Si:As or TES bolometers.

If we pursue all three options, our strategy will focus on maximizing resource by implementing review and progress assessment program, so that a technology that meets and shows performance needed for *Origins* will be chosen as early as possible. For example, if during the initial phases of the program, TES bolometers meet the 5 ppm stability requirement, it will be chosen for *Origins* and developed to meet TRL requirements. The *Origins* team envisions any mid-IR detector development as a collaboration between industry, NASA centers, and universities.

Appendix C presents a detailed labor plan and budget for the HgCdTe and mid-IR TES bolometer development efforts.

5 - COST SUMMARY

Table 8 summarizes the estimated cost to mature all *Origins* mission-enabling technology to TRL 6 by mission PDR. All costs reported here are grass-roots estimates from relevant subject matter experts, including several members of the *Origins* Science and Technology Definition Team, *Origins* Study Office engineers, and a number of external experts. The technology maturation costs in PY26 and PY27 are included in the Phase A mission cost, which is reported elsewhere. The total Pre-Phase A cost (PY21 – PY24) to mature *Origins* technology is \$156M (in Real Year dollars).

Table 8: Estimated Cost to mature all *Origins* mission-enabling technology to TRL 6 by mission PDR

Technology Investment Area	Year					
	PY21	PY22	PY23	PY24	PY25	PY26
Technology management	\$480,000	\$494,400	\$509,232	\$524,509	\$540,244	\$556,452
4.5 K Cryocooler	\$9,900,000	\$9,900,000	\$11,100,000	\$11,200,000	\$5,000,000	\$5,000,000
Sub-K Cryocooler	\$2,243,003	\$2,394,153	\$2,483,010	\$2,247,416		
Far-IR Detectors						
TES Bolometers	\$5,707,629	\$4,349,812	\$3,981,624	\$4,082,304	\$2,500,000	\$2,500,000
MKIDs	\$3,074,000	\$2,882,000	\$2,884,000	\$3,057,000	\$2,931,000	\$2,500,000
Detector Readout Electronics	\$4,020,744	\$3,306,460	\$3,276,678	\$3,159,631	\$4,633,412	\$4,676,977
Far-IR detector subtotal	\$12,802,373	\$10,538,272	\$10,142,302	\$10,298,935	\$10,064,412	\$9,676,977
Mid-IR Detectors						
HgCdTe and TES Bolometers	\$7,669,583	\$6,216,053	\$1,876,295	\$1,688,491	\$894,302	
Si:As	\$1,000,000	\$3,000,000	\$3,000,000	\$3,000,000		
Mid-IR detector subtotal	\$8,669,583	\$9,216,053	\$4,876,295	\$4,688,491	\$894,302	\$0
Total without reserve	\$34,094,959	\$32,542,878	\$29,110,839	\$28,959,351	\$16,498,958	\$15,233,429
Manager's reserve (25%)	\$8,523,740	\$8,135,720	\$7,277,710	\$7,239,838	\$4,124,740	\$3,808,357
Total, including reserve	\$42,618,699	\$40,678,598	\$36,388,549	\$36,199,189	\$20,623,698	\$19,041,786

Acronyms and Definitions

Acronym	Definition
ACE	Advanced Composition Explorer
ACEIT	Automated Cost Estimating Integrated Tools
AC-Modulated	Alternating-Current Modulated
ACS	Attitude Control System
ACTDP	Advanced Cryocooler Technology Development Program
ADC	Analog digital Converter
ADR	Adiabatic Demagnetization Refrigerator
ADRC	Adiabatic Demagnetization Refrigerator Controller
AGN	Active Galactic Nucleus or Nuclei
ALMA	Atacama Large Millimeter/submillimeter Array
AO	Adaptive Optics
AO	Announcement of Opportunity
AOS	Aft Optics Structure
APD	Astrophysics Division
ARC	AMES Research Center
ARIEL	Atmospheric Remote-sensing Infrared Exoplanet Large-survey
ASIC	Application-Specific Integrated Circuits
ASIST	Advance Spacecraft Integration and System Test
ATP	Authority/Authorization to Proceed
AU	Astronomical Unit
B	Billion
BIB	blocked impurity band
BIRB	Ball infrared Black
BFR	Big Falcon Rocket
BHAR	Black-Hole Accretion Rate
BHARD	Black-Hole Accretion-Rate Density
BLASTPol	Balloon-borne LargeAperture Submillimeter Telescope for Polarimetry
BOL	Beginning of Life
BW	Bandwidth
BY	Base Year (is defined equivalent to Fiscal Year (FY))
C	Cooper Pair
CADR	Continuous Adiabatic Demagnetization Refrigerator
CBE	Current Best Estimate
CCA	Cryocooler Assembly
CCHP	Constant Conduction Heat Pipes
CDF	Cummulative Density Function
C&DH	Command and Data Handling
CDM	Code Division Multiplexing
CDR	Critical Design Review
CEA	French Alternative Energies and Atomic Energy Commis-sion
CEMA	Cost Estimating and Modeling Analysis
cFE	core Flight Executive
CFRP	Carbon Fiber Reinforced Polymer
cFS	core Flight Software
CGH	computer-generated hologram
CGM	Circumgalactic Medium
CIDC	interdigitated capacitor
CL	confidence levels
CMB	Cosmic Microwave Background

Acronym	Definition
CMM	Coordinate Measuring Machine
CMMI	Capability Maturity Model Integration
CNES	Centre National d'Études Spatiales (National Center for Space Studies)
CM&O	Center Management and Operations
CMOS	Complementary metal oxide semi-conductor
COBE	Cosmic Background Explorer
COTS	Commercial off the shelf
CPA	chrome-potassium-alum
CPI	Cloud Particle Imager
CPM	Cryogenic Payload Module
CPT	Comprehensive Performance Test
CPU	Computer Programmable Unit
CRM	Continuous Risk Management
CRTBP	Circular Restricted Three Body Problem
CSO	Chief Safety Officer
CTE	Coefficient of Thermal Expansion
CTIA	capacitive trans-impedance amplifier
CVZ	Continuous Viewing Zone
DAC	Distributed Monte Carlo Method Analysis Code
DAK	Double Aluminized Kapton
DC	Direct Current
DDL	Detector Development Lab
DES	Dark Energy Survey
DET	Direct Energy Transfer
DIT	Differential Impedance Transducer
DIT	Dublin Institute of Technology
DM	Deformable Mirror
DR	dilution refrigerator
DRO	Distant Retrograde Orbit
DSCOVR	Deep Space Climate Observatory
DSN	Deep Space Network
DSOC	Deep Space Optical Comm
DTU	Data Transfer Unit
DTN	Delay/Disruption Tolerant Network
EAR	Export Administration Regulations
EDRS	European Data Relay System
EDU	Engineering Demonstration Unit
EGSE	Electrical Ground Support Equipment
ELT	Extremely Large Telescope
EM	Electromagnetic
EM	Engineering Model
EMC	Electromagnetic Compatibility
EMI	Electro-Magnetic Interference
EOL	End-of-Life
EoR	Epoch of Reionization
EPS	Electrical Power System
ESA	European Space Agency
ETU	Engineering Test Unit
EQW	Equivalent Width
F&A	Facilities and Administrative
Far-IR SIG	Far-IR Science Interest Group

Acronym	Definition
FDM	frequency-division-multiplexed
FIP	Far-infrared Imager Polarimeter
FIR	Far-Infrared (~30–300 μ m)
FM	Flight Model
FM	Fold Mirror
FOG	Fiber Optic Gyro
FoR	Field of Regard
FOR	Flight Operations Review
FOV	Field of View
FPA	Focal Plane Array
FPGA	Field Programmable Gate Array
FPI	Fabry-Perot interferometer
FRR	Flight Readiness Review
FS	Fine Structure
FSM	Field Steering Mirror
FSR	Final Systems Review
FSW	Flight Software
FTE	full-time-equivalent
FTS	Fourier Transform Spectrometer
FUN CAIs	Calcium-aluminium-rich inclusions with isotopic mass fractionation effects and unidentified nuclear isotopic anomalies
FWHM	Spectral Line Full Width at Half-Maximum
GCC	Goddard Composite Coating
GI	Guest Investigator
GLF	gadolinium-lithium-fluoride
GMT	Giant Magellan Telescope
GNC	Guidance Navigation and Control
GO	General Observer
GOES	Geostationary Operational Environmental Satellite
GOLD	Goddard Open Learning Design
GRC	Glenn Research Center
GSE	Ground Support Equipment
GSFC	Goddard Space Flight Center
GW	gravitational wave
HAWC+	High-resolution Airborne Wideband Camera-plus
HEB	Hot Electron Bolometer mixer
HEMT	High-electron-mobility transistor
HERO	HEterodyne Receiver for Origins
HFI	Planck High Frequency Instrument
HGA	High Gain Antenna
HIFI	Heterodyne Instrument for the Far-Infrared
HIRMES	High Resolution Mid-infrared Spectrometer
HQ	NASA Headquarters
HST	Hubble Space Telescope
HWP	Half-wave Plate
IBC	impurity band conductor
IC	integrated circuit
IDE	Integrated Development Environment
IDL	Instrument Design lab
IF	Intermediate Frequency
IFU	Integral Field Unit
IGM	Intergalactic Medium
IMF	Initial Mass Function

Acronym	Definition
IMP	Instrument Mounting Plate
IMS	Integrated Master Schedule
IMS	Inner Mirror Segments
IMU	Inertial Measurement Unit
IPT	In-Plant Transporter
IPAC	Infrared Processing and Analysis Center
IPC	interpixel capacitance
IR	InfraRed
IRAC	InfraRed Array Camera
IRAS	InfraRed Astronomy Satellite
IRS	InfraRed Spectrometer (on Spitzer)
IRSA	IPAC Infrared Science Archive
IS	Image Surface
ISE	Instrument Systems Engineer
ISM	Interstellar Medium
ISO	Infrared Space Observatory
I&T	Integration and Test
ITAR	International Traffic in Arms Regulations
ITOS	Integrated Test and Operations System
JAXA	Japan Aerospace and eXploration Agency
JCMT	James Clerk Maxwell Telescope
JHU	Johns Hopkins University
JPL	Jet Propulsion Laboratory
JSC	Johnson Space Center
JWST	James Web Space Telescope
KB	Kuiper-belt
KDP	Key Decision Point
KIDs	Kinetic Inductance Detectors
L	inductor
LCRD	Laser Communication Relay Demonstration
LEMNOS	Laser-Enhanced Mission Communications Navigation and Operational Services
LEO	Low Earth Orbit
LEV	SEL2 Earth-Vehicle
LIGO	Laser Interferometer Gravitational Wave Observatory
LIR	Infrared Luminosity
LIRG	Luminous Infrared Galaxies
LISA	Laser Interferometer Space Antenna
LM	Lockheed Martin
LO	Local Oscillator
LOFAR	Low Frequency Array
LOI	Libration Orbit Insertion
LOS	Line Of Sight
LRS	Low-Resolution Spectrometry
LSST	Large Synoptic Survey Telescope
LTE	Local Thermal Equilibrium
LV	Launch Vehicle
LWS	Long Wavelength Spectrometer (on infrared space observatory)
M	Million
MAST	Mikulski Archive for Space Telescopes
MAM	Mission Assurance Manager
MCC	Mid-Course Correction
MDL	microdevices lab

Acronym	Definition
MDL	Mission Design Lab
MEB	Main Electronics Box
MEL	Master Equipment List
MEMS	Micro-Electro-Mechanical Systems
MEV	Maximum Expected Value
MHD	magneto-hydrodynamical
MIR	Mid-Infrared (~3-30 μ m)
MIRI	Mid InfraRed Instrument
MIRI-IFU	Mid InfraRed Instrument Integral Field Unit
MISC	Mid-Infrared Spectrometer and Camera
MISC-T	Mid-Infrared Spectrometer and Camera Transit Spectrometer Module
MKID	Microwave Kinetic Inductance Device
MLI	Multi-Layer Insulation
MOC	Mission Operations Center
MOR	Mission Operations Readiness Review
MPC	Minor Planet Center
MPMF	Mass Properties Measurement Facility
MPSoC	multiprocessor system-on-chip
MPV	Maximum Possible Value
MSE	Mission Systems Engineer
MSFC	Marshall Space Flight Center
MSX	Mid-course Space eXperiment
NASA	National Aeronautics and Space Administration
NEA	Noise Equivalent Angle
NEN	Near Earth Network
NEOCam	Near-Earth Object Camera mission
NEP	Noise Equivalent Power
NIRCam	Near-Infrared Camera
NIRSpec	Near InfraRed Spectrograph
NOEMA	Northern Extended Millimeter Array
NRHO	Near Rectilinear Halo Orbit
OFCO	Office of the Chief Financial Office
OFSW	Origins Flight SoftWare
OMS	Outer Mirror Segments
OPD	Optical Path Difference
Origins	Origins Space Telescope
ORR	Operations Readiness Review
OSS	Origins Survey Spectrometer
OTIS	Optical Telescope Element and Integrated Science Instrument Module
PACE	Plankton, Aerosol, Cloud, ocean Ecosystem
PACS	Photodetector Array Camera and Spectrometer
PAF	Payload Adaptor Fitting
PAH	Polycyclic Aromatic Hydrocarbon
PAH-SFR	PAH Star Formation Rate
PCA	Pressure Control Assembly
PDR	Preliminary Design Review
PDR	Photon-Dominated Region or Photo-Dissociation Region
PEEK	PolyEthylEtherKetone
PER	Pre-Environmental Review
PES	PRICE Estimating Suite
PHOENIX	A radiative-transfer atmosphere code (not an acronym)
PM	Primary Mirror

Acronym	Definition
PMBSS	Primary Mirror Backplane Support Structure
PMSA	Primary Mirror Segment Assembly
PIA	Propellant Isolation Assembly
PIR	PAF Interface Ring
POM	Pick-off-Mirror
PM	Primary Mirror
PMD	Propellant Management Device
PPM	Pulse Position Modulation
PS	Propulsion System
PSE	Power Supply Electronics
PSF	Point Spread Function
PSI	Pounds per Square Inch
PSR	Pre-Ship Review
QCDs	Quantum Capacitance Detectors
QE	quantum efficiency
QML	Quality Management Plan
QSO	Quasi-Stellar Object
R	Resolving Power
RA	Resource Analyst
RAO	Resource Analysis Office
RF	Radio Frequency
RFSoc	RF-system on chip
RLP	Rotating Libration Point
RM	Risk Manager
RMS	Root Mean Squared
RMSWE	Root Mean Square Wavefront Error
ROICs	Read Out Integrated Circuits
RV	Radial Velocity
RXTE	Rossi X-ray Timing Explorer
RY	Real Year
S/A	Solar Array
SAFARI	Spica FAR-infrared Instrument
SAM	System Assurance Manager – check this... “Safety”
SAMPEX	Solar, Anomalous, and Magnetospheric Particle Explorer
SAT	Strategic Astrophysics Technology
SB	Spectroscopic Binary
SBC	Single Board Computer
SBIR	Small Business Innovation Research
SBM	Spacecraft Bus Module
SC	Spacecraft
SCPPM	Serially Concatenated Pulse Position Modulation
SC TILT	Spacecraft Top-Level Integration and Test
SDO	Scattered-Disk Object
SDO	Solar Dynamics Observatory
SDSS	Sloan Digital Sky Survey
SECCHI	Sun Earth Connection Coronal and Heliospheric Investigation
SEC01	Second Engine Cut-Off 1
SED	Spectral Energy Distribution
SED	Sciences and Exploration Directorate
SEL1	Sun-Earth Libration Point 1
SEL2	Sun-Earth Libration Point 2
SEM	Scanning Electron Microscope

Acronym	Definition
SES	Space Environment Simulator
SEU	single event functional upsets
SF	Star Formation
SFD	source follower per detector
SFR	Star Formation Rate
SFRD	Star Formation Rate Density
SHI	Sumitomo Heavy Industries
SiC	Silicon Carbide
SIR	System Integration Review
SIS	Superconducting Insulating Superconducting mixer
SKA	Square Kilometre Array
SLS	Space Launch System
SM	Secondary Mirror
SM3	Servicing Mission 3
SMA	Secondary Mirror Assembly
SMA	Safety and Mission Assurance
SMBH	Supermassive Black Hole
SMSS	Secondary Mirror Support Structure
S/N	See SNR (if we're using both, we should pick one!)
SNe	Supernovae
SNR	Signal-to-Noise Ratio
SNR	Supernova remnants
SOA	state-of-the-art
SOC	Science Operations Center
SOFIA	Stratospheric Observatory for Infrared Astronomy
SPECULOOS	Search for habitable Planets Eclipsing ULtra-cOOl Stars
SPF	Space Power Facility
SPICA	SPace Infrared telescope for Cosmology and Astrophysics
SPIFI	South Pole Imaging Fabry-Perot Interferometer
SPIRE	Spectral and Photometric Imaging Receiver
SQUIDS	Superconducting Quantum-Interference Devices
SRR	System Requirement Review
SSDIF	Spacecraft Systems Development and Integration Facility
SSPD	Satellite Servicing Projects Division
SSR	Solid State Recorder
SRON	Netherlands Institute for Space Research
SS	Study Scientist
SSA	Sun Shield Assembly
STDT	Science and technology Definition Team
STM	Science Traceability Matrix
STScI	Space Telescope Science Institute
STTARS	Space Telescope Transportation Air, Road and Sea
SV	Servicing Vehicle
SWAS	Submillimeter Wave Astronomy Satellite
SWS	Short Wave Spectrometer (on Infrared Space Observatory)
T	Transit Spectrometer
TAA	Technical Assistance Agreements
TAC	Time Allocation Committee
TAI	International Atomic Time
TBD	To Be Determined
TDM	Time-Frequency Division Multiplexing
TDRSS	Tracking and Data Relay Satellite System
TES	Transition-edged Sensors

Acronym	Definition
TESS	Transiting Exoplanet Survey Satellite
TFSM	Telescope Fine Steering Mirror
TID	Total Ionizing Dose
TIM	Technical Interchange Meeting
TIP	Transfer to Insertion Point
TIS	Teledyne Imaging Sensors
T-L	MISC Transit Spectrometer Long Wavelength Channel
TLS	two-level-system (fluctuators)
TM	Tertiary Mirror
T-M	MISC Transit Spectrometer Mid Wavelength Channel
TMA	Triple Mirror Assembly
TMA	Three Mirror Anastigmat
TMT	Thirty Meter Telescope
TNO	Trans Neptunian Object
TOO	Targets of Opportunity
TRAPPIST	Transiting Planets and Planetesimals Small Telescope
TRL	Technology Readiness Level
TRMM	Tropical Rainfall Mapping Mission
T-S	MISC Transit Spectrometer Short Wavelength Channel
TTM	Tip-Tilt Mirror
TTS	MISC Tip-Tilt Sensor
ULE	Ultra Low Expansion
ULIRG	Ultra-Luminous Infrared Galaxy
upGREAT	upgraded German REceiver at Terahertz
UR	University of Rochester
VDA	Vapor Deposited Aluminum
VELLOs	Very Low Luminosity Objects
VNA	Vector Network Analyzer
VSMOW	Vienna Standard Mean Ocean Water (standard used for D/H)
WBS	Work Breakdown Structure
WFI	MISC Wide Field Imager Module
WFIRST	Wide Field InfraRed Survey Telescope
WFIRST/HLS	WFIRST High Latitude Survey
WISE	Wide-Field Infrared Explorer
WMAP	Wilkinson Microwave Anisotropy Probe
WSC	White Sands Complex
XRCF	X-Ray Calibration Facility
XUV	X-ray and Ultraviolet
YSO	Young Stellar Object
ZEUS	redshift (Z) and Early Universe Spectrometer

References

- Adam, R., Adane, A., Ade, P. A. R., Andre, P., Andrianasolo, A., Aussel, H., Beelen, A., Benoît, A., Bideaud, A., Billot, N., Bourrion, O., Bracco, A., Calvo, M., Catalano, A., Coiffard, G., Comis, B., De Petris, M., Desert, F. X., Doyle, S., Driessen, E. F. C., Evans, R., Goupy, J., Kramer, C., Lagache, G., Leclercq, S., Leggeri, J. P., Lestrade, J. F., Macias-Perez, J. F., Mauskopf, P., Mayet, F., Maury, A., Monfardini, A., Navarro, S., Pascale, E., Perotto, L., Pisano, G., Ponthieu, N., Reveret, V., Rigby, A., Ritacco, A., Romero, C., Roussel, H., Ruppén, F., Schuster, K., Sievers, A., Trique-neaux, S., Tucker, C., and Zylka, R., 2018, “The NIKA2 large-field-of-view millimetre continuum camera for the 30 m IRAM telescope,” *A&A* 609, A115.
- Adelberger, K.L., Steidel, C.C., Shapley, A.E., and Pettini, M., 2003. “Galaxies and Intergalactic Matter at $z \sim 3$: Overview”, *The Astrophysical Journal*, 584, 45.
- Agol, E., Cowan, N. B., Knutson, H. A., Deming, D., Steffen, J. H., Henry, G. W., Charbonneau, D., 2010. “The climate of HD 189733b from Fourteen Transits and Eclipses Measured by Spitzer” *The Astrophysical Journal*, 721, 1861.
- Aguirre, James, and STARFIRE Collaboration. 2018. “STARFIRE: The Spectroscopic Terahertz Airborne Receiver for Far-InfraRed Exploration.” American Astronomical Society Meeting Abstracts.
- Aird, J., et al. 2013. “PRIMUS: An Observationally Motivated Model to Connect the Evolution of the Active Galactic Nucleus and Galaxy Populations out to $z \sim 1$ ”, *The Astrophysical Journal*, 775, 41.
- Albertsson, T., et al. 2014. Chemodynamical Deuterium Fractionation in the Early Solar Nebula: The Origin of Water on Earth and in Asteroids and Comets. *The Astrophysical Journal*. 784, 39.
- Alexander, D.M., Chary, R.-R., Pope, A., Bauer, F.E., Brandt, W.N., Daddi, E., Dickinson, M., Elbaz, D., Reddy, N.A., 2008, “Reliable Identification of Compton-thick Quasars at $z=2$: Spitzer Mid-Infrared Spectroscopy of HDF-oMD49.” *The Astrophysical Journal*, 687, 835
- Allard, F., Homeier, D., Freytag, B., 2011. “Model Atmospheres From Very Low Mass Stars to Brown Dwarfs,” *Astronomical Society of the Pacific Conference Series*, 448, 91.
- ALMA Partnership et al. 2015, The 2014 ALMA Long Baseline Campaign: First Results from High Angular Resolution Observations toward the HL Tau Region, *The Astrophysical Journal*, 808, 3
- Alonso, R., 2018. “Characterization of Exoplanets: Secondary Eclipses,” *Handbook of Exoplanets*, 1441.
- Altwegg, K., et al. 2015. 67P/Churyumov-Gerasimenko, a Jupiter family comet with a high D/H ratio. *Science*. 347, 1261952.
- Amaro-Seoane et al., 2017, Laser Interferometer Space Antenna, arXiv:1702.00786.
- Andersson, B.-G., et al., 2015, Interstellar Dust Grain Alignment, *Annual Review of Astronomy and Astrophysics*, 53, 501
- Andrews, Sean M. and Williams, Jonathan P. 2007. High-Resolution Submillimeter Constraints on Circumstellar Disk Structure. *The Astrophysical Journal*. 659, 705.
- Andrews, Sean M. et al. 2018. The Disk Substructures at High Angular Resolution Project (DSHARP). I. Motivation, Sample, Calibration, and Overview, *The Astrophysical Journal*. 869, L41
- Angerhausen, D., Sapers, H., Citron, R., Bergantini, A., Lutz, S., Queiroz, L. L., Alexandre, M., Araujo, A. C. V., 2013. “HABEBEE: Habitability of Eyeball-Exo-Earths.” *Astrobiology*, 13.

- Antonellini, S., et al. 2016. Mid-IR spectra of pre-main sequence Herbig stars: An explanation for the non-detections of water lines. *Astronomy and Astrophysics*. 585, A61.
- Appleton, P. N., et al. 2017. “Powerful H₂ Line Cooling in Stephan’s Quintet. II. Group-wide Gas and Shock Modeling of the Warm H₂ and a Comparison with [C II] 157.7 μ m Emission and Kinematics”, *The Astrophysical Journal*, 836, 76.
- Appleton, P. N., et al. 2006. “Powerful High-Velocity Dispersion Molecular Hydrogen Associated with an Intergalactic Shock Wave in Stephan’s Quintet”, *The Astrophysical Journal* 639, L51.
- Arenberg, J.W., et al. 2019, “Origins Space Telescope: Alternate Architecture”, in preparation for submission to JATIS 2019.
- Armitage, P.J. 2015, Physical processes in protoplanetary disks, ARXIV:1509.06382
- Armus, L., et al. 2004. “Observations of Ultraluminous Infrared Galaxies with the Infrared Spectrograph (IRS) on the Spitzer Space Telescope: Early Results on Markarian 1014, Markarian 463, and UGC 5101”, *The Astrophysical Journal Supplement Series*, 154, 178.
- Armus, L., et al. 1990. “The optical emission-line nebulae of powerful far-infrared galaxies”, *The Astrophysical Journal*, 364, 471.
- Armus, L., et al. 2006. “Detection of the Buried Active Galactic Nucleus in NGC 6240 with the Infrared Spectrograph on the Spitzer Space Telescope”, *The Astrophysical Journal*, 640, 204.
- Armus, L., et al. 2007. “Observations of Ultraluminous Infrared Galaxies with the Infrared Spectrograph on the Spitzer Space Telescope. II. The IRAS Bright Galaxy Sample”, *The Astrophysical Journal*, 656, 148.
- Aronstein, D. L. and Smith, J. S. “Phase-retrieval uncertainty estimation and algorithm comparison for the JWST-ISIM test campaign,” 2016 IEEE Aerospace Conference, Big Sky, MT, 2016, pp. 1-10. doi: 10.1109/AERO.2016.7500786
- Audard, M. et al. 2014, Episodic Accretion in Young Stars, Protostars and Planets VI, 387
- Audley, M.D., de Lange, G., Gao, J-R, et al. 2018, “The SAFARI detector system,” *Proceedings of SPIE*, 10708, 0
- Austermann, J. E., Beall, J. A., Bryan, S. A., Dober, B., Gao, J., Hilton, G., Hubmayr, J., Mauskopf, P., McKenney, C. M., Simon, S. M., Ullom, J. N., Vissers, M. R., and Wilson, G. W., 2018, “Millimeter-Wave Polarimeters Using Kinetic Inductance Detectors for TolTEC and Beyond,” *Journal of Low Temperature Physics*.
- Bacon R., et al. 2010. “The MUSE second-generation VLT instrument,” *Proc. SPIE*, 773508.
- Bacon R., Piqueras L., Conseil S., Richard J., and Shepherd M. 2016. “MPDAF: MUSE Python Data Analysis Framework,” *Astrophysics Source Code Library*, record ascl:1611.003.
- Banzatti, A., et al. 2017. The Depletion of Water During Dispersal of Planet-forming Disk Regions. *The Astrophysical Journal*. 834, 152.
- Baraffe, I. & Chabrier, G. 2010, Effect of episodic accretion on the structure and the lithium depletion of low-mass stars and planet-hosting stars, *Astronomy & Astrophysics*, 521, 44
- Baraffe, I. et al. 2017, Self-consistent evolution of accreting low-mass stars and brown dwarfs, *Astronomy & Astrophysics*, 597, 19

- Barclay, T., Pepper, J., Quintana, E. V., 2018. “A Revised Exoplanet Yield from the Transiting Exoplanet Survey Satellite (TESS).” *The Astrophysical Journal Supplement Series*, 239, 2.
- Bardeen, J. M. 1973 “Timelike and Null Geodesics in the Kerr Metric”. In: *Black Holes (Les Astres Occlus)*. Ed. by C. Dewitt and B. S. Dewitt. Gordon and Breach Scientific Publishers, p. 215.
- Barends, R., Daalman, W.K.-G., Endo, A., et al. 2009, “Frequency and quality factor of NbTiN/Au bilayer superconducting resonators,” *The Thirteenth International Workshop on Low Temperature Detectors-LTD13*, AIP Conference Proceedings, 1185, 152
- Bartlett, J. , Rostem, K. , Wollack, E. J. *Robust modeling of acoustic phonon transmission in nano-mechanical structures*, Appl. Phys. Lett., Submitted (2019), arXiv:1812.02695
- Barlis, Alyssa, Steven Hailey-Dunsheath, James E Aguirre, Charles M Bradford, Joseph G Redford, Tashalee S Billings, Henry G LeDuc, Christopher M McKenney, and Matthew I Hollister. 2018. “Development of aluminum LEKIDs for balloon-borne far-infrared spectroscopy (Conference Presentation).” *Millimeter, Submillimeter, and Far-Infrared Detectors and Instrumentation for Astronomy IX*.
- Barstow, J. K., Aigrain, S., Irwin, P. G. J., Kendrew, S., Fletcher, L. N., 2015. “Transit spectroscopy with James Webb Space Telescope: systematics, starspots, and stitching,” *Monthly Notices of the Royal Astronomical Society*, 448, 2546.
- Barstow, J. K., Irwin, P. G. J., 2016. “Habitable worlds with JWST: transit spectroscopy of the TRAPPIST-1 system?” *Monthly Notices of the Royal Astronomical Society: Letters*, 461, L92.
- Baselmans, J. J. A., Bueno, J., Yates, S. J. C., Yurduseven, O., Llombart, N., Karatsu, K., Baryshev, A. M., Ferrari, L., Endo, A., Thoen, D. J., de Visser, P. J., Janssen, R. M. J., Murugesan, V., Driessen, E. F. C., Coiffard, G., Martin-Pintado, J., Hargrave, P., and Gri n, M., 2017, “A kilo-pixel imaging system for future space based far-infrared observatories using microwave kinetic inductance detectors,” *A&A* 601, A89.
- Bast, J. E., et al. 2013. Exploring organic chemistry in planet-forming zones. *Astronomy and Astrophysics*. 551, A118.
- Bastien, F. A., Stassun, K., Basri, G. S., Pepper, J., 2016. “A Light Curve Probe of Stellar Surface Convection and MEasure of Stellar Surface Gravity,” *American Astronomical Society, AAS Meeting #227*.
- Bastien, F. A., Stassun, K., Pepper, J., Wright, J., 2013. “Are the Photometrically Quietest Stars the Best Radial-Velocity Planet Search candidates?” *American Astronomical Society, AAS Meeting #221*.
- Batalha, N. E., Lewis, N. K., Line, M. R., Valenti, J., Stevenson, K., 2018. “Strategies for Constraining the Atmospheres of Temerate Terrestrial Planets with JWST,” *The Astrophysical Journal Letters*, 856, L34.
- Beck, R. 2015, Magnetic fields in spiral galaxies, *AAPR*, 24, 4
- Beichman, C., Benneke, B., Knutson, H., Smith, R., Lagage, P.-O., Dressing, C., et al. (2014). Observations of Transiting Exoplanets with the James Webb Space Telescope (JWST). *Publications of the Astronomical Society of the Pacific*, 126(946), 1134–1173.
- Beirao, P., et al. 2015. “Spatially resolved Spitzer-IRS spectral maps of the superwind in M82”, *Monthly Notices of the Royal Astronomical Society*, 451, 2640.
- Benford, D.J., et al., 2010, *SPIE*, 7741, 77411

- Benneke, B., Seager, S., 2012. "Atmospheric Retrieval for Super-Earths: Uniquely Constraining the Atmospheric Composition with Transmission Spectroscopy," *The Astrophysical Journal*, 753,100.
- Bennett, C.L., Halpern, M., Hinshaw, G., et al. 2003, "First-Year Wilkinson Microwave Anisotropy Probe (WMAP) Observations: Preliminary Maps and Basic Results" *The Astrophysical Journal Supplement Series*, 148, 1
- Bergin, Edwin A., et al. 2013. An old disk still capable of forming a planetary system. *Nature*. 493, 644.
- Bergin, Edwin A., et al. 2015. Tracing the ingredients for a habitable earth from interstellar space through planet formation. *Proceedings of the National Academy of Science*. 112, 8965.
- Bergin, Edwin A., et al. 2016. Hydrocarbon Emission Rings in Protoplanetary Disks Induced by Dust Evolution. *The Astrophysical Journal*. 831, 101.
- Bergner, Jennifer B., et al. 2018. A Survey of CH₃CN and HC₃N in Protoplanetary Disks. *The Astrophysical Journal*. 857, 69.
- Bernard-Salas, J., Pottasch, S.R., Beintema, D.A., and Wesselius, P.R. 2001. "The ISO-SWS spectrum of planetary nebula NGC 7027", *Astronomy & Astrophysics*, 367, 949.
- Berta, Z. K., Charbonneau, D., Bean, J., Irwin, J., Burke, C. J., Désert, J.-M., Nutzman, P., Falco, E. E., 2011. "The GJ1214 Super-Earth System: Stellar Variability, New Transits, and a Search for Additional Planets," *The Astrophysical Journal*, 736,12.
- Bertin E., and Arnouts S. 1996. "SExtractor: Software for source extraction," *A&AS*, 117, 393.
- Bethermin, M., Wu, H-Y, Lagache, G., Davidzon, I., Ponthieu, N., Cousin, M.Wang, L., Dore, O., Daddi, E., Lapi, A., 2017, "The impact of Clustering and angular resolution on far-infrared and millimeter continuum observations," *Astronomy and Astrophysics*, 607, 89
- Beust, H., et al. 1990. The beta Pictoris circumstellar disk. X. Numerical simulations of infalling evaporating bodies. *Astronomy and Astrophysics*. 236, 202.
- Beyer, A. D., Kenyon, M. E., Echternach, P. M., Chui, T., Eom, B.-H., Day, P. K., Bock, J. J., Holmes, W. A., and Bradford, C. M., 2011, "Ultra-sensitive Transition-Edge Sensors for the Background Limited Infrared/Sub-mm Spectrograph (BLISS)," *Journal of Low Temperature Physics* , 143.
- Beyer, A. D., Echternach, P. M., Kenyon, M. E., Runyan, M. C., Bumble, B., Bradford, C. M., Bock, J. J., and Holmes, W. A., 2013, "Effect of mo/cu superconducting bilayer geometry on ultra-sensitive transition-edge sensor performance," *IEEE Transactions on Applied Superconductivity* 23, 2100104–2100104 (June 2013).
- Birkmann, S.M., Eberle, K., Grözing, U., Lemke, D., Schreiber, J., Barl, L., Katterloher, R., Poglitsch, A., Schubert, J. and Richter, H., 2004. Characterization of high-and low-stressed Ge: Ga array cameras for Herschel's PACS instrument. *Optical, Infrared, and Millimeter Space Telescopes*, 5487(1), pp.437-447.
- Blevins, Sandra M., et al. 2016. Measurements of Water Surface Snow Lines in Classical Protoplanetary Disks. *The Astrophysical Journal*. 818, 22.
- Blum, J. and Wurm, G. 2008. The growth mechanisms of macroscopic bodies in protoplanetary disks.. *Annual Review of Astronomy and Astrophysics*. 46, 21.
- Bockelée-Morvan, D., et al. 2012. Herschel measurements of the D/H and ¹⁶O/¹⁸O ratios in water in the Oort-cloud comet C/2009 P1 (Garradd). *Astronomy and Astrophysics*. 544, L15.

- Bonato, M., et al. 2019. “Origins Space Telescope: Predictions for far-IR spectroscopic surveys,” *Publ. Astron. Soc. Aust.* 36, e017.
- Boogert, A. C. A., Gerakines, P. A., Whittet, D. C. B., 2015. “Observations of the icy universe,” *Annual Review of Astronomy and Astrophysics*. 53, 541.
- Booth, Mark, et al. 2009. The history of the Solar system’s debris disc: observable properties of the Kuiper belt. *Monthly Notices of the Royal Astronomical Society*. 399, 385.
- Boreman, Glenn D. 2001, “User’s guide to IR detectors,” *Proceedings of the SPIE*, 4420, 79
- Borgonie, G., Linage-Alvarez, B., Ojo, A. O., Mundle, S. O. C., Freese, L. B., Van Rooyen, C., et al. (2015). “Eukaryotic opportunists dominate the deep-subsurface biosphere in South Africa.” *Nature communications*, 6, 8952.
- Botke, William F. and Norman, Marc D. 2017. The Late Heavy Bombardment. *Annual Review of Earth and Planetary Sciences*. 45, 619.
- Boutle, I. A., Mayne, N. J., Drummond, B., Manners, J., Goyal, J., Hugo Lambert, F., Acreman, D. M., Earnshaw, P. D., 2017. “Exploring the climate of Proxima B with the Met Office Unified Model.” *Astronomy & Astrophysics*, 601, A120.
- Bradford, C. Matt; Stacey, Gordon J.; Swain, Mark R.; Nikola, Thomas; Bolatto, Alberto D.; Jackson, James M.; Savage, Maureen L.; Davidson, Jacqueline A.; Ade, Peter A. R. 2002. SPIFI: a direct-detection imaging spectrometer for submillimeter wavelengths. *Applied Optics*, 41, 2561.
- Bradford, C. M.; Nikola, T.; Stacey, G. J.; Bolatto, A. D.; Jackson, J. M.; Savage, M. L.; Davidson, J. A.; Higdon, S. J. 2003. CO (J=7-6) Observations of NGC 253: Cosmic-Ray-heated Warm Molecular Gas, *The Astrophysical Journal*, 586, 891.
- Bradford, C. M.; Aguirre, J. E.; Aikin, R.; Bock, J. J.; Earle, L.; Glenn, J.; Inami, H.; Maloney, P. R.; Matsuhara, H.; Naylor, B. J.; Nguyen, H. T.; Zmuidzinas, J. 2009. The Warm Molecular Gas around the Cloverleaf Quasar, *The Astrophysical Journal*, 705, 112.
- Bradford, C. M., Hailey-Dunsheath, S., Shiroko, E., Hollister, M., McKenney, C. M., LeDuc, H. G., Reck, T., Chapman, S. C., Tikhomirov, A., Nikola, T., and Zmuidzinas, J., 2014, “X-Spec: a multi-object trans- millimeter-wave spectrometer for CCAT,” in [Millimeter, Submillimeter, and Far-Infrared Detectors and Instrumentation for Astronomy VII], *Proc. of the SPIE* 9153, 91531Y.
- Brandeker, A., et al. 2016. Herschel detects oxygen in the β Pictoris debris disk. *Astronomy and Astrophysics*. 591, A27.
- Brandl, B.R., et al. 2006. “The Mid-Infrared Properties of Starburst Galaxies from Spitzer-IRS Spectroscopy”, *The Astrophysical Journal*, 653, 1129
- Breedlove, J. et al, 2014, “Testing of a two-stage 10 k turbo-brayton cryocooler for space applications,” *Cryocoolers* **18**, 445–452.
- Broderick, A. E. et al. “Testing the No-hair Theorem with Event Horizon Telescope Observations of Sagittarius A*.” In: *ApJ*, 784, 7 (Mar. 2014), p. 7. doi: 10.1088/0004-637X/784/1/7. arXiv: 1311.5564.
- Brogi, M., Line, M. R., 2019. “Retrieving Temperatures and Abundances of Exoplanet Atmospheres with High-resolution Cross-correlation Spectroscopy.” *The Astronomical Journal*, 157, 114.
- Burrows, A., 2014. “Highlights in the study of exoplanet atmospheres.” *Nature*, 513.
- Busemann, Henner, et al. 2006. Interstellar Chemistry Recorded in Organic Matter from Primitive Meteorites. *Science*. 312, 727.

- Cabrera, M.S., et al. 2019, in preparation
- Carone, L., Keppens, R., Decin, L., Henning, T., 2018. “Stratosphere circulation on tidally locked ExoEarths,” *Monthly Notices of the Royal Astronomical Society*, 473.
- Carr, John S. and Najita, Joan R. 2011. Organic Molecules and Water in the Inner Disks of T Tauri Stars. *The Astrophysical Journal*. 733, 102.
- Carter, J. A., Winn, J. N., Holman, M. J., Fabrycky, D., Berta, Z. K., Burke, C. J., Nutzman, P., 2011. “The Transit Light Curve Project. XIII. Sixteen Transits of the Super-Earth GJ 1214b,” *The Astrophysical Journal*, 730, 82.
- Caselli, Paola and Ceccarelli, Cecilia 2012. Our astrochemical heritage. *Astronomy and Astrophysics Review*. 20, 56.
- Caselli, P. et al., 2012. “First Detection of Water Vapor in a Pre-stellar Core,” *The Astrophysical Journal Letters*, 759, 2, L37.
- Casey, C.M., et al. 2018. “The Brightest Galaxies in the Dark Ages: Galaxies’ Dust Continuum Emission during the Reionization Era”, *The Astrophysical Journal*, 862, 77C.
- Catalano, A., Adam, R., Ade, P.A.R. et al., “The NIKA2 Instrument at 30-m IRAM Telescope: Performance and Results,” *Journal of Low Temperature Physics*, 193, 916
- Cataldi, Gianni, et al. 2018. ALMA Resolves C I Emission from the β Pictoris Debris Disk. *The Astrophysical Journal*. 861, 72.
- Catling, D. C., Krissansen-Totton, J., Kiang, N. Y., Crisp, D., Robinson, T. D., DasSarma, S., Rushby, A. J., Del Genio, A., Bains, W., Domagal-Goldman, S., 2018. “Exoplanet Biosignatures: A Framework for Their Assessment,” *Astrobiology*, 18, 709.
- Ceccarelli, C. et al. 2014. Deuterium Fractionation: The Ariadne’s Thread from the Precollapse Phase to Meteorites and Comets Today. In *Protostars and Planets VI*, Henrik Beuther, Ralf S. Klessen, Cornelis P. Dullemond, and Thomas Henning (eds.), University of Arizona Press, Tucson, 914 pp., p.859-882.
- Chamandy, L., Shukurov, A., Subramanian, K. 2015, Magnetic spiral arms and galactic outflows. *MNRAS*, 446, 6
- Chambers, J. E. 2013. Late-stage planetary accretion including hit-and-run collisions and fragmentation. *Icarus*. 224, 43.
- Chandrasekhar S., Fermi E., 1953, Magnetic fields in spiral arms. *The Astrophysical Journal*, 118, 113
- Charbonneau, D., Allen, L. E., Megeath, S. T., Torres, G., Alonso, R., Brown, T. M., Gilliland, R. L., Latham, D. W., Mandushev, G., O’Donovan, F. T., Sozzetti, A., 2005. “Detection of Thermal Emission from an Extrasolar Planet,” *The Astrophysical Journal*, 626, 523.
- Charbonneau, D., Brown, T. M, Latham, D. W, Mayor, M., 2000. “Detection of Planetary Transits Across a Sun-like Star,” *The Astrophysical Journal*, 529, L45.
- Chervenak, J.A., Irwin, K.D., Grossman, E.N., Martinis, J.M., Reintsema, C.D., & Huber, M.E. 1999, *Applied Physics Letters* 74 (26), pp.4043-4045, “Superconducting Multiplexer for Arrays of Transition Edge Sensors”
- Cherednichenko, S. et al, 2008, “Hot-electron bolometer terahertz mixers for the Herschel Space Observatory,” *Rev. Sci. Instr.*, vol. **79**, art ID 034501.

- Chiavassa, A., Caldas, A., Selsis, F., Leconte, J., Von Paris, P., Bordé, P., Magic, Z., Collet, R., Asplund, M., 2017. “Measuring stellar granulation during planet transits,” *Astronomy & Astrophysics*, 597, A94.
- Chokshi, Arati, Tielens, A. G. G. M., Hollenbach, D., 1993. “Coagulation, Interplanetary Dust, Interplanetary Medium, Planetary Evolution, Solar System, Grain Size, Molecular Clouds, Silicones, Stellar Envelopes, Surface Roughness,” *The Astrophysical Journal*. 407, 806.
- Chopra, A. & Lineweaver, C. H. 2010. Sun → Earth → Crust → Life: Quantifying the Elemental Fractionations that Led to Life on Earth. LPICo. 1538, 5547
- Chyba, Christopher F., et al. 1990. Cometary Delivery of Organic Molecules to the Early Earth. *Science*. 249, 366.
- Cicone, C., Maiolino, R., Sturm, E., Gracia-Carpio, J., Feruglio, C., Neri, R., et al. 2014, “Massive molecular outflows and evidence for AGN feedback from CO observations,” *Astronomy & Astrophysics*, 562, 21
- Ciesla, Fred J. and Cuzzi, Jeffrey N. 2006. The evolution of the water distribution in a viscous protoplanetary disk. *Icarus*. 181, 178.
- Clanton, C., Beichman, C., Vasisht, G., Smith, R., Gaudi, B.S., 2012, “Precision Near-Infrared Photometry for Exoplanet Transit Observations. I. Ensemble Spot Photometry for an All-Sky Survey,” *Publications of the Astronomical Society of the Pacific*, 124, 917
- Cleeves, L. I., et al. 2014. “The ancient heritage of water ice in the solar system.” *Science*, 345, 1590.
- Cleeves, L. Ilse, et al. 2018. Constraining Gas-phase Carbon, Oxygen, and Nitrogen in the IM Lup Protoplanetary Disk. *The Astrophysical Journal*. 865, 155.
- Cluver, M. E., Appleton, P. N., Boulanger, F., et al. 2010, *The Astrophysical Journal*, 710, 248
- Collaudin, B., Passvogel, T., 1999, “The FIRST and Planck ‘Carrier’ missions. Description of the cryogenic systems.” *Cryogenics*, 39, 157-165
- Connelly, James N., et al. 2012. The Absolute Chronology and Thermal Processing of Solids in the Solar Protoplanetary Disk. *Science*. 338, 651.
- Cormier, D., Abel, N.P., Hony, S., Lebouteiller, V., Madden, S.C., Polles, F.L., Galliano, F., De Looze, I., Galametz, M., Lambert-Huyghe, A., et al. 2019, “The Herschel Dwarf Galaxy Survey. II. Physical conditions, origin of [CII] emission, and porosity of the multiphase low-metallicity ISM,” *A&A*, 626, 23
- Cowan, N. B., Greene, T., Angerhausen, D., Batalha, N. E., Clampin, M., Colón, K., Crossfield, I. J. M., Fortney, J. J., Gaudi, B. S., Harrington, J., Iro, N., Lillie, C. F., Linsky, J. L., Lopez-Morales, M., Mandell, A. M., Stevenson, K. B., 2015. “Characterizing Transiting Planet Atmospheres through 2025,” *Publications of the Astronomical Society of the Pacific*, 127.
- Crossfield, I. J. M., 2015. “Observations of Exoplanet Atmospheres.” *Publications of the Astronomical Society of the Pacific*, 127.
- Crossfield, I. J. M., Hansen, B. M. S., Harrington, J., Cho, J. Y.-K., Deming, D., Menou, K., Seager, S., 2010. “A New 24 μ m Phase Curve for υ Andromedae b.” *The Astrophysical Journal*, 723.

- Croton, D.J., et al. 2006. “The many lives of active galactic nuclei: cooling flows, black holes and the luminosities and colours of galaxies”, *Monthly Notices of the Royal Astronomical Society*, 365, 11.
- Crutcher, R. M., 2012, *Magnetic Fields in Molecular Clouds*, *Annual Review of Astronomy and Astrophysics*, 50, 29
- Czesla, S., Huber, K. F., Wolter, U., Schröter, S., Schmitt, J. H. M. M., 2009. “How stellar activity affects the size estimates of extrasolar planets,” *Astronomy & Astrophysics*, 505, 1277.
- D’Alessio, Paola, et al. 1999. On the Thermal Stability of Irradiation-dominated Pre-Main-Sequence Disks. *The Astrophysical Journal*. 511, 896.
- Dasyra, K.M., Ho, L.C., Armus, L., Ogle, P., Helou, G., Peterson, B.M., Lutz, D., Netzer, H., Sturm, E. 2008, “High-Ionization Mid-Infrared Lines as Black Hole Mass and Bolometric Luminosity Indicators in Active Galactic Nuclei”, *The Astrophysical Journal*, 674, L9
- Daukant, P. “Optical Innovations in the James Webb Space Telescope.” https://www.osa-opn.org/home/articles/volume_22/issue_11/features/optical_innovations_in_the_james_webb_space_telescope
- Dawson, Rebekah I. and Johnson, John Asher 2018. *Origins of Hot Jupiters*. *Annual Review of Astronomy and Astrophysics*. 56, 175.
- Day, P. K., LeDuc, H. G., Mazin, B. A., Vayonakis, A., and Zmuidzinas, J., 2003, “A broadband superconducting detector suitable for use in large arrays,” *Nature* 425, 817–821.
- Dave, Romeel, Finlator, K., Oppenheimer, B.D. 2011, “Galaxy evolution in cosmological simulations with outflows – II. Metallicities and gas fractions” *Monthly Notices of the Royal Astronomical Society*, 416, 1354
- de Graauw, Th. *et al.*, 2009, “The Herschel-Heterodyne Instrument for the Far-Infrared (HIFI),” *ESA Publication Series*, vol. **34**, pp. 3-20.
- de Wit, J., Wakeford, H. R., Gillon, M., Lewis, N. K., Valenti, J. A., Demory, B.-O., Burgasser, A. J., Burdanov, A., Delrez, L., Jehin, E., Lederer, S. M., Queloz, D., Triaud, A. H. M. J., Van Grootel, V., 2016. “A combined transmission spectrum of the Earth-sized exoplanets TRAPPIST-1 b and c,” *Nature*, 537, 69.
- de Wit, J., Gillon, M., Demory, B.-O., Seager, S., 2012. “Towards consistent mapping of distant worlds: secondary-eclipse scanning of the exoplanet HD 189733b,” *Astronomy & Astrophysics*, 548, A128.
- de Wit, J., Wakeford, H. R., Lewis, N. K., Delrez, L., Gillon, M., Selsis, F., Leconte, J., Demory, B.-O., Bolmont, E., Bourrier, V., Burgasser, A. J., Grimm, S., Jehin, E., Lederer, S. M., Owen, J. E., Stamenković, V., Triaud, A. H. M. J., 2018. “Atmospheric reconnaissance of the habitable-zone Earth-sized planets orbiting TRAPPIST-1,” *Nature Astronomy*, 2, 214.
- Delrez, L., Gillon, M., Queloz, D., Demory, B.-O., Almléay, Y., de Wit, J., Jehin, E., Triaud, A. H. M. J., Barkaoui, K., Burdanov, A., Burgasser, A. J., Ducrot, E., McCormac, J., Murray, C., Silva Fernandes, C., Sohy, S., Thompson, S. J., Van Grootel, V., Alonso, R., Benkhaldoun, Z., Rebolo, R., 2018. “SPECULOOS: a network of robotic telescopes to hunt for terrestrial planets around the nearest ultracool dwarfs,” *Proceedings of the SPIE*, 10700, 107001I.
- Deming, D., Seager, S., 2009. “Light and shadow from distant worlds,” *Nature*, 462, 301.
- Deming, D., Seager, S., 2017, “Illusion and reality in the atmospheres of exoplanets,” *Journal of Geophysical Research: Planets*, 122, 53-57

- Deming, D., Louie, D., & Sheets, H., 2019. “How to Characterize the Atmosphere of a Transiting Exoplanet,” *Publications of the Astronomical Society of the Pacific*, 131, 013001
- Deming, D., Seager, S., Richardson, L. J., Harrington, J., 2005. “Infrared radiation from an extra-solar planet,” *Nature*, 434, 740.
- Demory, B-O, Gillon, M., Seager, S., et al. 2012, ”Detection of Thermal Emission from a Super-Earth,” *The Astrophysical Journal*, 751, 28
- Dent, W. R. F., et al. 2013. GASPS—A Herschel Survey of Gas and Dust in Protoplanetary Disks: Summary and Initial Statistics. *Publications of the Astronomical Society of the Pacific*. 125, 477.
- Desch, S. J. 2007. Mass Distribution and Planet Formation in the Solar Nebula. *The Astrophysical Journal*. 671, 878.
- Désert, J.-M., Charbonneau, D., et al., 2011. “The Hot-Jupiter Kepler-17b: Discovery, Obliquity from Stroboscopic Starspots, and Atmospheric Characterization,” *The Astrophysical Journal Supplement*, 197, 14.
- Devost, D. 2007. “From Dwarfs To Giants; Ionization Properties of BCD, Starburst Galaxies And AGN”, *Bulletin of the American Astronomical Society*, 39, 237.
- Diaz-Santos, T., et al. 2017. “A Herschel/PACS Far-infrared Line Emission Survey of Local Luminous Infrared Galaxies”, *The Astrophysical Journal*, 846, 32.
- Dittmann, J. A., Irwin, J. M., Charbonneau, D., Berta-Thompson, Z. K., Newton, E. R., Latham, D. W., Latham, C. A., Esquerdo, G., Berlind, P., Calkins, M. L., 2017. “Discovery and Precise Characterization by the MEarth Project of LP 661-13, an Eclipsing Binary Consisting of Two Fully Convective Low-mass Stars,” *The Astrophysical Journal*, 836, 124.
- Dobbs, C., Baba, J. 2014, Dawes Review 4: Spiral structures in disc galaxies. *PASA*, 31, 35
- Dodson-Robinson, S. E. et al., 2009. Ice lines, planetesimal composition and solid surface density in the solar nebula. *Icarus*, 200, 672.
- Domagal-Goldman, S. D., Meadows, V. S., Claire, M. W., Kasting, J. F., 2011. “Using Biogenic Sulfur Gases as Remotely Detectable Biosignatures on Anoxic Planets.” *Astrobiology*, 11.
- Dones, L., Brasser, R., Kaib, N., & Rickman, H. 2015, *SSRv*, 197, 191
- Dong, C., Jin, M., Lingam, M., Airapetian, V. S., Ma, Y., van der Holst, B., 2017. “Atmospheric escape from the TRAPPIST-1 planets and implications for habitability,” *Proceedings of the National Academy of Sciences*, 115,260.
- Dorn, M. L., Pipher, J.L., McMurtry, C., Hartman, S., Mainzer, A., McKelvey, M., McMurray, R., Chevara, D., Rosser, J., 2016, “Proto irradiation results for long-wave HgCdTe infrared detector arrays for Near-Earth Object Camera,” *Journal of Astronomical Telescopes, Instruments, and Systems*, 2, 6002.
- Dotti, M., Salvaterra, R., Sesana, A., Colpi, M., Haardt, F., 2006, “On the search of electromagnetic cosmological counterparts to coalescences of massive black hole binaries,” *Monthly Notices of the Royal Astronomical Society*, 372, 869.
- Draine, B., & Woods, D.T. 1990. “On the H₂ line emission from NGC 6240 and other starburst galaxies”, *The Astrophysical Journal*, 363, 464.
- Drazkowska, J. & Alibert, Y. 2017. Planetesimal formation starts at the snow line. *Astronomy & Astrophysics*, 608, A92.

- Dressing, C. D., Charbonneau, D., 2015. “The Occurrence of Potentially Habitable Planets Orbiting M Dwarfs Estimated from the Full Kepler Dataset and an Empirical Measurement of the Detection Sensitivity.” *The Astrophysical Journal*, 807, 45.
- Driscoll, P. E., Barnes, R., 2015. “Tidal Heating of Earth-like Exoplanets around M Stars: Thermal, Magnetic, and Orbital Evolutions.” *Astrobiology*, 15.
- Du, Fujun and Bergin, Edwin A. 2014. Water Vapor Distribution in Protoplanetary Disks. *The Astrophysical Journal*. 792, 2.
- Du, Fujun, et al. 2017. Survey of Cold Water Lines in Protoplanetary Disks: Indications of Systematic Volatile Depletion. *The Astrophysical Journal*. 842, 98.
- Dullemond, C. P. and Dominik, C. 2005. Dust coagulation in protoplanetary disks: A rapid depletion of small grains. *Astronomy and Astrophysics*. 434, 971.
- Dullemond, C. P., Hollenbach, D., Kamp, I., D’Alessio, P., 2007. Models of the Structure and Evolution of Protoplanetary Disks. *Protostars and Planets V*, 555.
- Dunham, M. M., et al., 2008. Identifying the Low-Luminosity Population of Embedded Protostars in the c2d Observations of Clouds and Cores, *The Astrophysical Journal Supplement Series*, Volume 179, Issue 1, pp. 249-282
- Dunham, M.M. et al. 2010, Evolutionary Signatures in the Formation of Low-Mass Protostars. II. Toward Reconciling Models and Observations, *The Astrophysical Journal*, 710, 470
- Dunham, Michael M., et al. 2015. Young Stellar Objects in the Gould Belt. *The Astrophysical Journal Supplement Series*. 220, 11.
- Echternach, P. M., Stone, K. J., Bradford, C. M., Day, P. K., Wilson, D. W., Megerian, K. G., Llobart, N., and Bueno, J., 2013 “Photon shot noise limited detection of terahertz radiation using a quantum capacitance detector,” *Applied Physics Letters* 103, 053510.
- Echternach, P. M., Pepper, B. J., Reck, T., and Bradford, C. M., 2018, “Single photon detection of 1.5 THz radiation with the quantum capacitance detector,” *Nature Astronomy* 2, 90–97.
- Edinger, Derek J., and Alison A. Nordt. “Selection of I-220H Beryllium for NIRCам Optical Bench.” *Optical Materials and Structures Technologies II*, 2005
- Elbaz, D., et al. 2010. “Herschel unveils a puzzling uniformity of distant dusty galaxies”, *Astronomy & Astrophysics*, 518, 29.
- Elbaz, D., Leiton, R., Nagar, N., Okumura, K., Franco, M., Schrieber, C., Pannella, M., Wang, T., Dickinson, M., Diaz-Santo, T., Ciesla, L., Daddi, E., Bournaud, F., Magdix, G., Zhou, L., Rujopakarn, W. 2018, “Starburst in and out of the star-formation main sequence” *Astronomy and Astrophysics*, 616, 110
- “Enduring Quests, Daring Visions: NASA Astrophysics in the Next Three Decades,” NASA 2013 Science Roadmap Team (Kouveliotou, C., Chair), <https://science.nasa.gov/astrophysics/documents>.
- Engelbracht, C.W., et al. 2005. “Metallicity Effects on Mid-Infrared Colors and the 8 μ m PAH Emission in Galaxies”, *The Astrophysical Journal*, 628, 29L.
- Erb, D.K. 2015. “Feedback in low-mass galaxies in the early Universe”, *Nature*, 523, 169.
- Evans, Neal J., II, et al. 2009. The Spitzer c2d Legacy Results: Star-Formation Rates and Efficiencies; Evolution and Lifetimes. *The Astrophysical Journal Supplement Series*. 181, 321.

- Evans, T. M., Sing, D. K., Goyal, J. M., Nikolov, N., Marley, M. S., Zahnle, K., Henry, G. W., Barstow, J. K., Alam, M. K., Sanz-Forcada, J., Kataria, T., Lewis, N. K., Lavvas, P., Ballester, G. E., Ben-Jaffel, L., Blumenthal, S. D., Bourrier, V., Drummond, B., García Muñoz, A., López-Morales, M., Tremblin, P., Ehrenreich, D., Wakeford, H. R., Buchhave, L. A., Lecavelier des Etangs, A., Hébrard, É., Williamson, M. H., 2018. “An Optical Transmission Spectrum for the Ultra-hot Jupiter WASP-121b Measured with the Hubble Space Telescope,” *The Astronomical Journal*, 156, 283.
- Event Horizon Telescope Collaboration et al. 2019a, “First M87 Event Horizon Telescope Results. I. The Shadow of the Supermassive Black Hole”. In: *ApJ* 875.1, L1 (Apr. 2019), p. L1. doi: 10.3847/2041-8213/ab0ec7.
- Event Horizon Telescope Collaboration et al. 2019b, “First M87 Event Horizon Telescope Results. III. Data Processing and Calibration”. In: *ApJ* 875.1, L3 (Apr. 2019), p. L3. doi: 10.3847/2041-8213/ab0c57.
- Event Horizon Telescope Collaboration et al. 2019c, “First M87 Event Horizon Telescope Results. IV. Imaging the Central Supermassive Black Hole”. In: *ApJ* 875.1, L4 (Apr. 2019), p. L4. doi: 10.3847/2041-8213/ab0e85.
- Fang, M., et al. 2009. Star and protoplanetary disk properties in Orion’s suburbs. *Astronomy and Astrophysics*. 504, 461.
- Fang, J., Zhang, L., & Bazylinski, D. A. (2010). “Deep-sea piezosphere and piezophiles: geomicrobiology and biogeochemistry.” *Trends in microbiology*, 18(9), 413-422.
- Farley, B., Erdmann, C., Vaz, B., McGrath, J., Cullen, E., Verbruggen, B., Pelliconi, R., Breathnach, D., Lim, P., Bourmaalif, A., Lynch, P., Mesadri, C., Melinn, D., Yap, K.P., Madden, L., 2017, IEEE Asian Solid-State Circuits Conference (A-SSCC), DOI: 10.1109/ASSCC.2017.8240201
- Farrah, D., et al. 2007. “High-Resolution Mid-Infrared Spectroscopy of Ultraluminous Infrared Galaxies”, *The Astrophysical Journal*, 667, 149.
- Farrah, D., et al. 2017. Far-Infrared Instrumentation and Technology Development for the Next Decade. *arXiv preprint arXiv:1709.02389*.
- Favre, Cécile, et al. 2013. A Significantly Low CO Abundance toward the TW Hya Protoplanetary Disk: A Path to Active Carbon Chemistry?. *The Astrophysical Journal*. 776, L38.
- Fedele, D., et al. 2011. Water Depletion in the Disk Atmosphere of Herbig AeBe Stars. *The Astrophysical Journal*. 732, 106.
- Fedele, D., et al. 2013. DIGIT survey of far-infrared lines from protoplanetary disks. I. [O I], [C II], OH, H₂O, and CH⁺. *Astronomy and Astrophysics*. 559, A77.
- Ferkinhoff, C., Nikola, T., Parshley, S., Stacey, G. J., Irwin, K.D., Cho, H-M, Niemack, M., Halpern, M., Hasselfield, M., Amiri, M. 2012, “Design and first-light performance of TES bolometer arrays for submillimeter spectroscopy with ZEUS-2” , *Millimeter, Submillimeter, and Far-Infrared Detectors and Instrumentation for Astronomy VI. Proceedings of the SPIE*, Volume 8452, article id. 845207, 12 pp
- Fernandez-Ontiveros, J.A., Spinoglio, L., Pereira-Santaella, M., Malkan, M.A., Andreani, P., Dasyra, K.M., 2016, “Far-infrared Line Spectra of Active Galaxies from the Herschel/PACS Spectrometer: The Complete Database” *The Astrophysical Journal Supplement Series*, 226, 19

- Feroz, F., Hobson, M. P., 2008. “Multimodal nested sampling: an efficient and robust alternative to Markov Chain Monte Carlo methods for astronomical data analyses,” *Monthly Notices of the Royal Astronomical Society*, 384, 449.
- Feruglio, C., et al. 2010. “Quasar feedback revealed by giant molecular outflows”, *Astronomy & Astrophysics*, 518, 155.
- Fischer, D., et al. 2015: “Exoplanet Detection Techniques,” eprint arXiv: 1505.06869
- Fischer, C., Beckmann, S., Bryant, A., Colditz, S., Fumi, F., Geis, N., Hamidouche, M., Henning, T., Honle, R., Iserlohe, C., Klein, R., Krabbe, A., Looney, L., Poglitsch, A., Raab, W., Rebollado, F., Rosenthal, D., Savage, M., Schweitzer, M., Trinh, C., Vacca, W., 2018, “FIFI-LS: The Field-Imaging Far-Infrared Line Spectrometer on SOFIA,” *Journal of Astronomical Instrumentation*, 7, 1840003-556
- Fischer, J., et al. 2010. “Herschel-PACS spectroscopic diagnostics of local ULIRGs: Conditions and kinematics in Markarian 231”, *Astronomy & Astrophysics*, 518, L41.
- Fissel, L. M., et al., 2016, Balloon-Borne Submillimeter Polarimetry of the Vela C Molecular Cloud: Systematic Dependence of Polarization Fraction on Column Density and Local Polarization-Angle Dispersion, *Astrophysical Journal*, 824, 134
- Fletcher, A., 2011, Magnetic fields and spiral arms in the galaxy M51 *MNRAS*, 412, 2396
- Flock, M., et al. 2015. Gaps, rings, and non-axisymmetric structures in protoplanetary disks. From simulations to ALMA observations. *Astronomy and Astrophysics*. 574, A68.
- Forrest, W.J., McMurtry, C.W., Dorn, M., Pipher, J., Cabrera, M.S., 2016, “Development of megapixel HgCdTe detector arrays with 15 micron cutoff,” *AAS Meeting #228*, 216.18
- Fortney, J. J., Lodders, K., Marley, M. S., Freedman, R. S., 2008. “A Unified Theory for the Atmospheres of the Hot and Very Hot Jupiters: Two classes of Irradiated Atmospheres,” *The Astrophysical Journal*, 678, 1419.
- Fortney, J. J., 2018. “Modeling Exoplanetary Atmospheres: An Overview,” eprint arXiv:1804.08149
- Fraine, J. D., Deming, D., Gillon, M., Jehin, E., Demory, B.-O., Benneke, B., Seager, S., Lewis, N. K., Knutson, H., Désert, J.-M., 2013. “Spitzer Transits of the Super-Earth GJ1214b and Implications for its Atmosphere,” *The Astrophysical Journal*, 765, 127.
- Fraine, J., Deming, D., Benneke, B., Knutson, H., Jordán, A., Espinoza, N., Madhusudhan, N., Wilkins, A., Todorov, K., 2014. “Water vapour absorption in the clear atmosphere of a Neptune-sized exoplanet,” *Nature*, 513, 526.
- France, K., Froning, C. S., Linsky, J. L., Roberge, A., Stocke, J. T., Tian, F., Bushinsky, R., Désert, J.-M., Mauas, P., Vieytes, M., Walkowicz, L. M., 2013. “The Ultraviolet Radiation Environment around M dwarf Exoplanet Host Stars,” *The Astrophysical Journal*, 763, 149.
- Fujimoto, R., Takei, Y., Mitsuda, K., et al. 2018, ”Performance of the helium dewar and the cry-coolers of the Hitomi soft x-ray spectrometer,” *Journal of Astronomical Telescopes, Instruments, and Systems*, Vol. 4, 1208
- Fulton, B. J., Petigura, E. A., Howard, A. W., Isaacson, H., Marcy, G. W., Cargile, P. A., Hebb, L., Weiss, L. M., Johnson, J. A., Morton, T. D., Sinukoff, E., Crossfield, I. J. M., Hirsch, L. A., 2017. “The California-Kepler Survey. III. A Gap in the Radius Distribution of Small Planets,” *The Astronomical Journal*, 154, 109.

- Fulton, B. J., Petigura, E. A., 2018. "The California-Kepler Survey. VII. Precise Planet Radii Leveraging Gaia DR2 Reveal the Stellar Mass Dependence of the Planet Radius Gap," *The Astrophysical Journal*, 156, 264.
- Gautier, N. 1986. "Observations of Infrared Cirrus," in *Light on Dark Matter*, ed. F.P. Israel, D. Reidel Publishing Company, p. 49.
- Genda, H., et al. 2015. Warm Debris Disks Produced by Giant Impacts during Terrestrial Planet Formation. *The Astrophysical Journal*. 810, 136.
- Genzel, R., et al. 1998. "What Powers Ultraluminous IRAS Galaxies?," *The Astrophysical Journal*, 498, 579.
- Gerin, M., Neufeld, D. A., & Goicoechea, J. R. 2016. Interstellar hydrides. *Annual Review of Astronomy and Astrophysics*, 54, 181
- Gerin, M., Neufeld, D. A., Goicoechea, J. R., 2016. Interstellar Hydrides. *Annual Reviews of Astronomy and Astrophysics*. 54, 181
- Gillon, M., Jehin, E., Lederer, S. M., Delrez, L., de Wit, J., Burdanov, A., Van Grootel, V., Burgasser, A. J., Triaud, A. H. M. J., Opitom, C., Demory, B.-O., Sahu, D. K., Bardalez Gagliuffi, D., Magain, P., Queloz, D., 2016. "Temperate Earth-sized planets transiting a nearby ultracool dwarf star," *Nature*, 533, 221.
- Gillon, M. 2018, "Searching for red worlds", *Nature Astronomy*, Vol. 2, p. 344
- Gladman, B., Marsden, B. G., & Vanlaerhoven, C. 2008, "Nomenclature in the Outer Solar System," in *The Solar System beyond Neptune*, 592, 43 ed. M. A. Barucci, H. Boehnhardt, D. P. Cruikshank, and A. Morbidelli, University of Arizona Press, Tucson.
- Glaister, D.S., Gully, W., Ross, R.G., Jr., et al., 2007, "Ball Aerospace 4-6 K Space Cryocooler," *Cryocoolers 14*, ICC Press, Boulder, CO, pp. 41-48.
- Glasse, A., Rieke, G.H., Bauwens, E., Garia-Marin, M., Ressler, M.E., Rost, S., Tikkanen, T.V., Vandenbussche, B., Wright, G.S., 2015, *Publications of the Astronomical Society of the Pacific*, 127, 686.
- Glassgold, Alfred E., et al. 2004. Heating Protoplanetary Disk Atmospheres. *The Astrophysical Journal*. 615, 972.
- Glenn, J., Bradford, C.M., Amini, R., et al. 2018, "The Galaxy Evolution Probe: a concept for a mid and far-infrared space observatory," *Proceedings of the SPIE*, 10698, 0
- Glover, S. C. O and Clark, P. C., 2012. Is molecular gas necessary for star formation? *Monthly Notices of the Royal Astronomical Society*, 421, 9.
- Goldsmith, P. F., et al. 2012. Collisional Excitation of the [C II] Fine Structure Transition in Interstellar Clouds. *The Astrophysical Journal Supplement*. 203, 13.
- Gong, Y. Cooray, A., Santos, M. G. 2013, "Probing the Pre-reionization Epoch with Molecular Hydrogen Intensity Mapping," *The Astrophysical Journal*, 768, 130.
- Gonzalez-Alfonso, E., et al. 2017. "Molecular Outflows in Local ULIRGs: Energetics from Multi-transition OH Analysis", *The Astrophysical Journal*, 836, 11.
- Gonzalez-Alfonso, E., et al. 2014. "The Mrk 231 molecular outflow as seen in OH", *Astronomy & Astrophysics*, 561, 27.

- Goulding, A.D., & Alexander, D.M., 2009. "Towards a complete census of AGN in nearby Galaxies: a large population of optically unidentified AGN", *Monthly Notices of the Royal Astronomical Society*, 398, 1165.
- Governato, F., et al. 2007. "Forming disc galaxies in Λ CDM simulations", *Monthly Notices of the Royal Astronomical Society*, 374, 1479.
- Gowardhan, A., et al. 2018. "The Dual Role of Starbursts and Active Galactic Nuclei in Driving Extreme Molecular Outflows", *The Astrophysical Journal*, 859, 35.
- Green, J. D., et al., 2013. Embedded Protostars in the Dust, Ice, and Gas In Time (DIGIT) Herschel Key Program: Continuum SEDs, and an Inventory of Characteristic Far-infrared Lines from PACS Spectroscopy, *The Astrophysical Journal*, Volume 770, Issue 2, article id. 123, 45
- Greene, T. P., Line, M. R., Montero, C., Fortney, J. J., Lustig-Yaeger, J., Luther, K., 2016. "Characterizing Transiting Exoplanet Atmospheres with JWST," *The Astrophysical Journal*, 817, 17.
- Grenfell, J. L., 2017. "A review of exoplanetary biosignatures," *Physics reports*, 713, 1.
- Grenier, I. A., Black, J. H., Strong, A. W., 2015. The Nine Lives of Cosmic Rays in Galaxies. *Annual Reviews of Astronomy and Astrophysics*. 53, 199
- Griffin, M. J., Abergel, A., Abreu, A., Ade, P. A. R., Andre, P., Augeres, J., Babbedge, T., Bae, Y., Bailie, T., Baluteau, J., Barlow, M. J., Bendo, G., Benielli, D., Bock, J. J., Bonhomme, P., Brisbin, D., Brockley-Blatt, C., Caldwell, M., Cara, C., Castro-Rodriguez, N., Cerulli, R., Chaniel, P., Chen, S., Clark, E., Clements, D. L., Clerc, L., Coker, J., Communal, D., Conversi, L., Cox, P., Crumb, D., Cunningham, C., Daly, F., Davis, G. R., de Antoni, P., Delderfield, J., Devin, N., di Giorgio, A., Didschuns, I., Dohlen, K., Donati, M., Dowell, A., Dowell, C. D., Duband, L., Dumaye, L., Emery, R. J., Ferlet, M., Ferrand, D., Fontignie, J., Fox, M., Franceschini, A., Frerking, M., Fulton, T., Garcia, J., Gastaud, R., Gear, W. K., Glenn, J., Goizel, A., Griffin, D. K., Grundy, T., Guest, S., Guillemet, L., Hargrave, P. C., Harwit, M., Hastings, P., Hatziminaoglou, E., Herman, M., Hinde, B., Hristov, V., Huang, M., Imhof, P., Isaak, K. J., Israelsson, U., Ivison, R. J., Jennings, D., Kiernan, B., King, K. J., Lange, A. E., Latter, W., Laurent, G., Laurent, P., Leeks, S. J., Lellouch, E., Levenson, L., Li, B., Li, J., Lilienthal, J., Lim, T., Liu, S. J., Lu, N., Madden, S., Mainetti, G., Marliani, P., McKay, D., Mercier, K., Molinari, S., Morris, H., Moseley, H., Mulder, J., Mur, M., Naylor, D. A., Nguyen, H., O'Halloran, B., Oliver, S., Olofsson, G., Olofsson, H., Orfei, R., Page, M. J., Pain, I., Panuzzo, P., Papageorgiou, A., Parks, G., Parr-Burman, P., Pearce, A., Pearson, C., Perez-Fournon, I., Pinsard, F., Pisano, G., Podosek, J., Pohlen, M., Polehampton, E. T., Pouliquen, D., Rigopoulou, D., Rizzo, D., Roseboom, I. G., Roussel, H., Rowan-Robinson, M., Rownd, B., Saraceno, P., Sauvage, M., Savage, R., Savini, G., Sawyer, E., Scharnberg, C., Schmitt, D., Schneider, N., Schulz, B., Schwartz, A., Shafer, R., Shupe, D. L., Sibthorpe, B., Sidher, S., Smith, A., Smith, A. J., Smith, D., Spencer, L., Stobie, B., Sudiwala, R., Sukhatme, K., Surace, C., Stevens, J. A., Swinyard, B. M., Trichas, M., Tourette, T., Triou, H., Tseng, S., Tucker, C., Turner, A., Vaccari, M., Valtchanov, I., Vigroux, L., Virique, E., Voellmer, G., Walker, H., Ward, R., Waskett, T., Weilert, M., Wesson, R., White, G. J., Whitehouse, N., Wilson, C. D., Winter, B., Woodcraft, A. L., Wright, G. S., Xu, C. K., Zavagno, A., Zemcov, M., Zhang, L., and Zonca, E., 2010, "The Herschel-SPIRE instrument and its in-flight performance," *A&A* 518, L3+.
- Griffiths A., and Conselice C. J. 2018. "AUTOSPEC: Fast Automated Spectral Extraction Software for IFU Data Cubes," *The Astrophysical Journal*, 869, 68.
- Grigorieva, A., et al. 2007. Survival of icy grains in debris discs. The role of photosputtering. *Astronomy and Astrophysics*. 475, 755.

- Grimm, S. L., Demory, B.-O., Gillon, M., Dorn, C., Agol, E., Burdanov, A., Delrez, L., Sestovic, M., Triaud, A. H. M. J., Turbet, M., Bolmont, É., Caldas, A., de Wit, J., Jehin, E., Leconte, J., Raymond, S. N., Van Grootel, V., Burgasser, A. J., Carey, S., Fabrycky, D., Heng, K., Hernandez, D. M., Ingalls, J. G., Lederer, S., Selsis, F., Queloz, D., 2018. "The nature of the TRAPPIST-1 exoplanets," *Astronomy & Astrophysics*, 613, A68.
- Gruppioni, C., et al. 2016. "Tracing black hole accretion with SED decomposition and IR lines: from local galaxies to the high-z Universe", *Monthly Notices of the Royal Astronomical Society*, 458, 4297.
- Guillard, P., Boulanger, F., Pineau Des Forêts, G., & Appleton, P. N. 2009, *A&A*, 502, 515
- Guillard, P., et al. 2012. "Strong Molecular Hydrogen Emission and Kinematics of the Multiphase Gas in Radio Galaxies with Fast Jet-driven Outflows", *The Astrophysical Journal*, 747, 95.
- Gundlach, B. and Blum, J. 2015. The Stickiness of Micrometer-sized Water-ice Particles. *The Astrophysical Journal*. 798, 34.
- Günther, Maximilian N., Zhan, Zhuchang, Seager, Sara, Rimmer, Paul B., Ranjan, Sukrit, Stassun, Keivan G., Oelkers, Ryan J., Daylan, Tansu, Newton, Elisabeth, Gillen, Edward, Rappaport, Saul, Ricker, George R., Latham, David W., Winn, Joshua N., Jenkins, Jon M., Glidden, Ana, Fausnaugh, Michael, Levine, Alan M., Dittmann, Jason A., Quinn, Samuel N., Krishnamurthy, Akshata, Ting, Eric B., 2019. "Stellar Flares from the First TESS Data Release: Exploring a New Sample of M-dwarfs." eprint arXiv:1901.00443
- Hailey-Dunsheath, S., Barlis, A. C. M., Aguirre, J. E., Bradford, C. M., Redford, J. G., Billings, T. S., LeDuc, H. G., McKenney, C. M., and Hollister, M. I., 2018, "Development of Aluminum LEKIDs for Balloon-Borne Far-IR Spectroscopy," *Journal of Low Temperature Physics*.
- Haiman, Z., Kocsis, B., Menou, K., Lippai, Z., Frei, Z., 2009, "Identifying decaying supermassive black hole binaries from their variable electromagnetic emission," *Classical and Quantum Gravity*, 26, 4032.
- Haisch, Karl E., Jr., et al. 2001. Disk Frequencies and Lifetimes in Young Clusters. *The Astrophysical Journal*. 553, L153.
- Hallis, L. J. 2017. D/H ratios of the inner Solar System. *Philosophical Transactions of the Royal Society of London Series A*. 375, 20150390.
- Haqq-Misra, J., Wolf, E. T., Joshi, M., Zhang, Xi, Kopparapu, R. K., 2018. "Demarcating Circulation Regimes of Synchronously Rotating Terrestrial planets within the Habitable Zone," *The Astrophysical Journal*, 852, 67.
- Harrington, J., Hansen, B. M., Luszcz, S. H., Seager, S., Deming, D., Menou, K., Cho, J. Y.-K., Richardson, L. J., 2006. "The Phase-Dependent Infrared Brightness of the Extrasolar Planet υ Andromedae b," *Science*, 314, 623.
- Harsono, D., et al. 2015. Volatile snowlines in embedded disks around low-mass protostars. *Astronomy and Astrophysics*. 582, A41.
- Hartmann, L., Cassen, P., & Kenyon, S.J. 1997, Disk Accretion and the Stellar Birthline, *The Astrophysical Journal*, 475, 770.
- Hartmann, L., Herczeg, G., & Calvet, N. 2016, Accretion onto Pre-Main Sequence Stars, *Annual Review of Astronomy and Astrophysics*, 54, 135

- Hartogh, Paul, et al. 2011. Ocean-like water in the Jupiter-family comet 103P/Hartley 2. *Nature*, 478, 218.
- Harper, D.A., Runyan, M.C., Dowell, C.D., Wirth, C. J., Armato, M., Ames, T., et al. 2018, “HAWC+, the Far-Infrared Camera and Polarimeter for SOFIA,” *Journal of Astronomical Instrumentation*, 7, 8.
- Hashimoto, T., et al. 2018. “The onset of star formation 250 million years after the Big Bang”, *Nature*, 557, 392.
- Hayward, C.C. & Hopkins, P.F., et al. 2017. “How stellar feedback simultaneously regulates star formation and drives outflows”, *Monthly Notices of the Royal Astronomical Society*, 465, 1682.
- Heckman, T.M., Armus, L., Miley, G.K. 1987, “Evidence for Large-Scale Winds from Starburst Galaxies. II. An Optical Investigation of Powerful Far-Infrared Galaxies,” *The Astronomical Journal*, 93, 276
- Heckman, T.M., Armus, L., Miley, G.K. 1990, “On the Nature and Implications of Starburst-driven Galactic Superwinds,” *The Astrophysical Journal Supplement*, 74, 833
- Heckman, T.M., Lehnert, M.D., Stickland, D.K., Armus, L. 2000, “Absorption-Line Probes of Gas and Dust in Galactic Superwinds,” *The Astrophysical Journal Supplement Series*, 129, 493
- Heng, K., Showman, A. P., 2015. “Atmospheric Dynamics of Hot Exoplanets,” *Annual Review of Earth and Planetary Sciences*, 43.
- Henriques, B.M.B., et al. 2015. “Galaxy formation in the Planck cosmology - I. Matching the observed evolution of star formation rates, colours and stellar masses”, *Monthly Notices of the Royal Astronomical Society*, 451, 2663.
- Henriques, B.M.B., et al. 2018. “Galaxy formation in the Planck cosmology - IV. Mass and environmental quenching, conformity and clustering”, *Monthly Notices of the Royal Astronomical Society*, 469, 2626.
- Herbig, G.H. 1977, Eruptive phenomena in early stellar evolution, *The Astrophysical Journal*, 217, 693
- Herbig, G.H. 2008, History and Spectroscopy of EXor Candidates, *The Astronomical Journal*, 135, 637
- Herczeg G.J. et al. 2017, How Do Stars Gain Their Mass? A JCMT/SCUBA-2 Transient Survey of Protostars in Nearby Star-forming Regions, *The Astrophysical Journal*, 849, 43
- Herczeg, G. J., et al. 2012. Water in star-forming regions with Herschel: highly excited molecular emission from the NGC 1333 IRAS 4B outflow. *Astronomy and Astrophysics*. 540, A84.
- Herenz E. C., and Wisotzki L. 2017. “LSDCat: Detection and cataloguing of emission-line sources in integral-field spectroscopy datacubes,” *A&AS*, 602, A111.
- Hickox & Alexander 2018, “Obscured Active Galactic Nuclei,” *Annual Review of Astronomy and Astrophysics*, 65, 625
- Hillenbrand, Lynne A. 1997. On the Stellar Population and Star-Forming History of the Orion Nebula Cluster. *The Astronomical Journal*. 113, 1733.
- Hijmering, R.A., den Hartog, R., Ridder, M., et al. 2016, “Readout of a 176 pixel FDM system for SAFARI TES arrays,” *Proceedings of SPIE* 9914, 1

- Ho, L.C. & Keto, E., 2007. “The Mid-Infrared Fine-Structure Lines of Neon as an Indicator of Star Formation Rate in Galaxies”, *The Astrophysical Journal*, 658, 314.
- Hogerheijde, Michiel R., et al. 2011. Detection of the Water Reservoir in a Forming Planetary System. *Science*. 334, 338.
- Holland, Wayne S., et al. 2017. SONS: The JCMT legacy survey of debris discs in the submillimetre. *Monthly Notices of the Royal Astronomical Society*. 470, 3606.
- Holland, W. S., Bintley, D., Chapin, E. L., Chrysostomou, A., Davis, G. R., Dempsey, J. T., Duncan, W. D., Fich, M., Friberg, P., Halpern, M., Irwin, K. D., Jenness, T., Kelly, B. D., MacIntosh, M. J., Robson, E. I., Scott, D., Ade, P. A. R., Atad-Ettdgui, E., Berry, D. S., Craig, S. C., Gao, X., Gibb, A. G., Hilton, G. C., Hollister, M. I., Kycia, J. B., Lunney, D. W., McGregor, H., Montgomery, D., Parkes, W., Tilanus, R. P. J., Ullom, J. N., Walther, C. A., Walton, A. J., Woodcraft, A. L., Amiri, M., Atkinson, D., Burger, B., Chuter, T., Coulson, I. M., Doriese, W. B., Dunare, C., Economou, F., Niemack, M. D., Parsons, H. A. L., Reintsema, C. D., Sibthorpe, B., Smail, I., Sudiwala, R., and Thomas, H. S., 2013, “SCUBA-2: the 10 000 pixel bolometer camera on the James Clerk Maxwell Telescope,” *MNRAS* 430, 2513–2533.
- Hopkins, P.F., 2014. “Galaxies on FIRE (Feedback In Realistic Environments): stellar feedback explains cosmologically inefficient star formation”, *Monthly Notices of the Royal Astronomical Society*, 445, 581.
- Hopkins, P.F., et al. 2013. “Star formation in galaxy mergers with realistic models of stellar feedback and the interstellar medium”, *Monthly Notices of the Royal Astronomical Society*, 430, 1901.
- Houck, J. R., Roellig, T. L., Van Cleve, J., Forrest, W. J., Herter, T. L., Lawrence, C. R., Matthews, K., Reitsema, H. J., Soifer, B. T., Watson, D. M., Weedman, D., Huisjen, M., Troeltzsch, J. R., Barry, D. J., Bernard-Salas, J., Blacken, C., Brandl, B. R., Charmandaris, V., Devost, D., Gull, G. E., Hall, P., Henderson, C. P., Higdon, S. J. U., Pirger, B. E., Schoenwald, J., Sloan, G. C., Uchida, K. I., Appleton, P. N., Armus, L., Burgdorf, M. J., Fajardo-Acosta, S. B., Grillmair, C. J., Ingalls, J. G., Morris, P. W., and Teplitz, H. I., 2004, “The infrared spectrograph on the Spitzer Space Telescope,” in [Optical, Infrared, and Millimeter Space Telescopes], Mather, J. C., ed., *Proc. of the SPIE* 5487, 62–76.
- Houck, J., et al. 2005. “Spectroscopic Redshifts to $z > 2$ for Optically Obscured Sources Discovered with the Spitzer Space Telescope”, *The Astrophysical Journal*, 622, L105.
- Houde, M., et al., 2009, Dispersion of Magnetic Fields in Molecular Clouds. II., *Astrophysical Journal*, 706, 1504
- Howard J M, Hayden B, Keski-Kuha R, and Feinberg, L.. “Optical Modeling of the Alignment and Test of the NASA James Webb Space Telescope”. 2007 IEEE Aerospace Conference. Big Sky, MT, USA: IEEE, 2007.
- Hsiao, F., Tang, A., Kim, Y., Drouin, B., Chattopadhyay, G., and Chang, M. C. F., 2015, “A 2.2 gs/s 188mw spectrometer processor in 65nm cmos for supporting low-power thz planetary instruments,” in [2015 IEEE Custom Integrated Circuits Conference (CICC)], 1–3.
- Huang, J.-S., et al. 2007. “AEGIS: Infrared Spectroscopy of an Infrared-luminous Lyman Break Galaxy at $z=3.01$ ”, *The Astrophysical Journal*, 660, L69.
- Hughes, A. Meredith, et al. 2018. Debris Disks: Structure, Composition, and Variability. *Annual Review of Astronomy and Astrophysics*. 56, 541.

- Huisman, R. et al., 2011 “Cryogenic mechatronic design of the HIFI Focal Plane Chopper,” *Mechatronics*, 21(8), 1259-1271.
- Hunter, D., et al., 2012. Little Things. *The Astronomical Journal*. 144, 134.
- Hurley P. D., et al. 2017. “HELP: XID+, the probabilistic de-blender for Herschel SPIRE maps,” *MNRAS*, 464, 885.
- Husser, T.-O., Wende-von Berg, S., Dreizler, S., Homeier, D., Reiners, A., Barman, T., Hauschildt, P. H., 2013. “A new extensive library of PHOENIX stellar atmospheres and synthetic spectra,” *Astronomy & Astrophysics*, 553, A6.
- Ida, S. and Lin, D. N. C. 2004. Toward a Deterministic Model of Planetary Formation. I. A Desert in the Mass and Semimajor Axis Distributions of Extrasolar Planets. *The Astrophysical Journal*. 604, 388.
- Inami, H., et al. 2013. “Mid-infrared Atomic Fine-structure Emission-line Spectra of Luminous Infrared Galaxies: Spitzer/IRS Spectra of the GOALS Sample”, *The Astrophysical Journal*, 777, 156.
- Ingalls, J.G., Krick, J.E., Carey, S.J. et al. 2016, “Repeatability and Accuracy of Exoplanet Eclipse Depths Measured with Post-cryogenic Spitzer,” *The Astronomical Journal*, 152, 44
- Irwin, K.D. 1995, *Applied Physics Letters* 66 (15), pp. 1998-2000, “An application of electrothermal feedback for high resolution cryogenic particle detection”
- Irwin, K.D. and Hilton, G.C., 2005. Transition-edge sensors. *Cryogenic particle detection*, pp.81-97.
- Irwin, K. D.; Beall, J. A.; Doriese, W. B.; Duncan, W. D.; Hilton, G. C.; Mates, J. A. B.; Reintsema, C. D.; Schmidt, D. R.; Ullom, J. N.; Vale, L. R.; Zink, B. L.; Lehnert, K. W., 2006, *NIMPA*, 559, 802I
- Jameson, K.E., Bolatto, A.D., Wolfire, M., Warren, S.R. et al. 2018, “First Results from the Herschel and ALMA Spectroscopic Surveys of the SMC: The Relationship between [CII]-bright Gas and CO-bright Gas at Low Metallicity,” *The Astrophysical Journal*, 853, 111
- Johannsen, T. and Psaltis, D. “Testing the No-hair Theorem with Observations in the Electromagnetic Spectrum. II. Black Hole Images”. In: *ApJ*, 718 (July 2010), pp. 446-454. doi: 10.1088/0004-637X/718/1/446. arXiv: 1005.1931.
- Johnson, M. D. et al. “Universal Interferometric Signatures of the M87 Photon Ring”. In preparation (2019).
- Johnstone, D. et al. 2013, Continuum Variability of Deeply Embedded Protostars as a Probe of Envelope Structure, *The Astrophysical Journal*, 765, 133
- Johnstone, D. et al. 2018, The JCMT Transient Survey: Stochastic and Secular Variability of Protostars and Disks In the Submillimeter Region Observed over 18 Months, *The Astrophysical Journal*, 854, 31
- Jones, T.J., Dowell, C.D., Lopez-Rodriguez, E., et al. 2019, “SOFIA Far-infrared Imaging Polarimetry of M82 and NGC 253: Exploring the Supergalactic Wind,” *The Astrophysical Journal*, 870, 9
- Joshi, M., 2003. “Climate Model Studies of Synchronously Rotating Planets,” *Astrobiology*, 3, 415.
- Joshi, M., Haberle, R., 1996. “The Atmospheres of Synchronously Rotating Planets,” *Bulletin of the American Astronomical Society*, 28, 1114.
- Joshi, M., Haberle, R., Reynolds, R. T., 1997. “Simulations of the Atmospheres of Synchronously Rotating Terrestrial Planets Orbiting M Dwarfs: Conditions for Atmospheric Collapse and the Implications for Habitability,” *Icarus*, 129, 450.

- Kaltenegger, L., 2017. "How to characterize Habitable Worlds and Signs of Life," Annual Review of Astronomy and Astrophysics, 55, 433.
- Kama, M., et al. 2016. Volatile-carbon locking and release in protoplanetary disks. A study of TW Hya and HD 100546. Astronomy and Astrophysics. 592, A83.
- Kamp, I., et al. 2003. Line emission from circumstellar disks around A stars. Astronomy and Astrophysics. 397, 1129.
- Kamp, I., et al. 2018. Diagnostic value of far-IR water ice features in T Tauri disks. Astronomy and Astrophysics. 617, A1.
- Kardashev, N. S. et al. "RadioAstron - A telescope with a size of 300 000 km: Main parameters and first observational results". In: Astronomy Reports 57 (Mar. 2013), pp. 153-194. doi: 10.1134/S1063772913030025. arXiv: 1303.5013.
- Kashlinsky, A., 1998, "Reconstructing the Spectru, of the Pregalactic Density Field from Astronomical Data", The Astrophysical Journal, 492, 1
- Kasliwal M. M., et al., 2017. SPIRITS:Uncovering Unusual Infrared Transients with *Spitzer*. The Astrophysical Journal. 829, 2.
- Kasting, J. F., Whitmire, D. P., Reynolds, R. T., 1993. "Habitable Zones around Main Sequence Stars," Icarus 101, 108.
- Kataria, T., Sing, D. K., Lewis, N. K., Visscher, C., Showman, A. P., Fortney, J. J., Marley, M. S., 2016. "The Atmospheric Circulation of a Nine-hot-Jupiter Sample: Probing Circulation and Chemistry over a Wide Phase Space," The Astrophysical Journal, 821, 9.
- Kellermann, K. I. and Pauliny-Toth, I. I. K. "The Spectra of Opaque Radio Sources". In: ApJ 155 (Feb. 1969), p. L71. doi: 10.1086/180305.
- Kelsall, T., et al. 1998. "The COBE Diffuse Infrared Background Experiment Search for the Cosmic Infrared Background. II. Model of the Interplanetary Dust Cloud," The Astrophysical Journal, 508, 44.
- Kennicutt et al. 1998. "The Hubble Space Telescope Key Project on the Extragalactic Distance Scale. XIII. The Metallicity Dependence of the Cepheid Distance Scale", The Astrophysical Journal, 498, 181.
- Kenyon, S.J. et al. 1990, An IRAS survey of the Taurus-Auriga molecular cloud, The Astronomical Journal, 99, 869
- Kenyon, Scott J. and Bromley, Benjamin C. 2008. Variations on Debris Disks: Icy Planet Formation at 30-150 AU for 1-3 M_{\odot} Main-Sequence Stars. The Astrophysical Journal Supplement Series. 179, 451.
- Kerr, A. R. et al, 2015, "The genesis of SIS mixers - the legacy of John Tucker in radioastronomy," 2015 IEEE MTT-S International Microwave Symposium, Phoenix, AZ.
- Keto, Eric, et al. 2014. Chemistry and radiative transfer of water in cold, dense clouds. Monthly Notices of the Royal Astronomical Society. 440, 2616.
- Keto, E., Rawlings, J., Caselli, P., 2015. "The dynamics of collapsing cores and star formation," Monthly Notices of the Royal Astronomical Society, 446, 4, 3731.

- Keski-Kuha, R. A., Bowers, C. W. Manuel, Quijada, A., Heaney, J. B., Gallagher, B., McKay, A., Stevenson, I. 2012, “James Webb Space Telescope optical telescope element mirror coatings,” Proc. SPIE 8442, Space Telescopes and Instrumentation 2012: Optical, Infrared, and Millimeter Wave, 84422J
- Kewley, L.J. and Ellison, S.L. 2008, “Metallicity Calibrations and the Mass-Metallicity Relation for Star-forming Galaxies,” *The Astrophysical Journal*, 681, 1183
- Khosropanah, P., Suzuki, T., Ridder, M. L., Hijmering, R. A., Akamatsu, H., Gottardi, L., van der Kuur, J., Gao, J. R., and Jackson, B. D., 2016, “Ultra-low noise TES bolometer arrays for SAFARI instrument on SPICA”. Proc. SPIE 9914, Millimeter, Submillimeter, and Far-Infrared Detectors and Instrumentation for Astronomy VIII, 99140B (19 July 2016); <https://doi.org/10.1117/12.2233472>
- Kim, M.-R., et al. 2016, A Search for Very Low-luminosity Objects in Gould Belt Clouds, *The Astrophysical Journal Supplement Series*, Volume 225, Issue 2, article id. 26, 17
- Kirkpatrick, A., et al. 2015. “The Role of Star Formation and an AGN in Dust Heating of $z = 0.3\text{--}2.8$ Galaxies. I. Evolution with Redshift and Luminosity”, *The Astrophysical Journal*, 814, 9.
- Kiss, Cs., Abraham, P., Klaas, U., Lemke, D., Heraudeau, Ph., del Burgo, C., and Herbstmeier, U. 2003. “Small-scale structure of the galactic cirrus emission,” *A&A*, 399, 177.
- Kim, Y., Zhang, Y., Tang, A., Reck, T., and Chang, M.-C. F, 2018, “A 1.5W 3 GHz Back-end Processor in 65 m CMOS for Sub-millimeter-wave Heterodyne Receiver Arrays,” *International Symposium for Space Terahertz Technology*.
- Knutson, H. A., Charbonneau, D., Allen, L. E., Fortney, J. J., Agol, E., Cowan, N. B., Showman, A. P., Cooper, C. S., Megeath, S. T., 2007. “A map of the day-night contrast of the extrasolar planet HD 189733b,” *Nature* 447, 183.
- Knutson, H.A., Charbonneau, D., Cowan, N.B, Fortney, J., Showman, A.P., Agol, E., Henry, G.W., 2009, “The 8 micron Phase Variation of the Hot Saturn HD 149026b”, *The Astrophysical Journal*, 703, 769-784
- Knutson, H.A., Dragomir, D., Kreidberg, L., et al. 2014, “Hubble Space Telescope Near-IR Transmission Spectroscopy of the Super-Earth HD 97658b,” *The Astrophysical Journal*, 794, 155
- Konopacky, Quinn M., et al. 2013. Detection of Carbon Monoxide and Water Absorption Lines in an Exoplanet Atmosphere. *Science*. 339, 1398.
- Kopparapu, R. K., Ramirez, R. M., SchottelKotte, J., Kasting, J. E., Domagal-Goldman, S., Eymet, V., 2014. “Habitable Zones around Main-sequence Stars: Dependence on Planetary Mass,” *The Astrophysical Journal Letters*, 787, L29.
- Kopparapu, R. K., Wolf, E. T., Arney, G., Batalha, N. E., Haqq-Misra, J., Grimm, S. L., Heng, K., 2017. “Habitable Moist Atmospheres on Terrestrial Planets near the Inner Edge of the Habitable Zone around M Dwarfs,” *The Astrophysical Journal*, 845, 5.
- Kopparapu, R. K., Wolf, E. T., Haqq-Misra, J., Yang, J., Kasting, J. F., Meadows, V., Terrien, R., Mahadevan, S., 2016. “The Inner Edge of the Habitable Zone for Synchronously Rotating Planets around Low-mass Stars Using General Circulation Models,” *The Astrophysical Journal*, 819, 84.
- Kornei, K.A., et al. 2012. “The Properties and Prevalence of Galactic Outflows at $z \sim 1$ in the Extended Groth Strip”, *The Astrophysical Journal*, 758, 135.
- Kovacs, A., 2008, “Scanning strategies for imaging arrays,” *Millimeter and Submillimeter Detectors and Instrumentation for Astronomy IV*, SPIE, 7020, 07.

- Kral, Q., et al. 2016. A self-consistent model for the evolution of the gas produced in the debris disc of β Pictoris. *Monthly Notices of the Royal Astronomical Society*. 461, 845.
- Kral, Quentin, et al. 2017. Predictions for the secondary CO, C and O gas content of debris discs from the destruction of volatile-rich planetesimals. *Monthly Notices of the Royal Astronomical Society*. 469, 521.
- Kreidberg, L., Line, M. R., Bean, J. L., Stevenson, K. B., Désert, J.-M., Madhusudhan, N., Fortney, J. J., Barstow, J. K., Henry, G. W., Williamson, M. H., Showman, A. P., 2015. “A Detection of Water in the Transmission Spectrum of the Hot Jupiter WASP-12b and Implications for Its Atmospheric Composition,” *The Astrophysical Journal*, 814, 66.
- Kreidberg, L., 2018. “Exoplanet Atmosphere Measurements from Transmission Spectroscopy and Other Planet Star Combined Light Observations,” *Handbook of Exoplanets*, 100
- Krissansen-Totton, J., Garland, R., Irwin, P., Catling, D. C., 2018. “Detectability of Biosignatures in Anoxic Atmospheres with the James Webb Space Telescope: A TRAPPIST-1e Case Study.” *The Astronomical Journal*, 156.
- Kristensen, L. E., et al. 2017. Origin of warm and hot gas emission from low-mass protostars: Herschel-HIFI observations of CO $J = 16-15$. I. Line profiles, physical conditions, and H₂O abundance. *Astronomy and Astrophysics*. 605, A93.
- Kronberg, P. K. 1994, Extragalactic magnetic fields. *Rep. Prog. Phy.* 325-328
- Kueppers, M., O’Rourke, L., Bockelee-Morvan, D., et al, 2014, ”Localized sources of water vapour on the dwarf planet (1) Ceres,” *Nature*, 505, 525
- Kurth, D., Belfiore, C., Gorriti, M. F., Cortez, N., Farias, M. E., & Albarracín, V. H., 2015. “Genomic and proteomic evidences unravel the UV-resistome of the poly-extremophile *Acinetobacter* sp. Ver3”. *Frontiers in microbiology*, 6, 328.
- Lambert, D. K. and Richards, P. L., 1978, “Martin-puplett interferometer: an analysis,” *Appl. Opt.* 17, 1595–1602.
- Lansbury, G.B., Alexander, D.M., Aird, J., Gandhi, P., Stern, D., et al. 2017 “The NuSTAR Serendipitous Survey: Hunting for the Most Extreme Obscured AGN at >10 keV.” *The Astrophysical Journal*, 846, 20
- Latif, M. A. et al. “Black hole formation in the early Universe”. In: *MNRAS*, 433.2 (Aug. 2013), pp. 1607-1618. doi: 10.1093/mnras/stt834. arXiv: 1304.0962 [astro-ph.CO].
- Lecar, M., et al. 2006. On the Location of the Snow Line in a Protoplanetary Disk. *The Astrophysical Journal*. 640, 1115.
- Lederberg, J., 1965. “Signs of Life: Criterion-System of Exobiology,” *Nature* 207, 9.
- Lee, C., Chattopadhyay, G., Jung, C., Reck, T., Cooper, K., Peralta, A., Lin, R., Mehdi, I., del Pino, M.A. and Juan, N.L., 2013, April. “Silicon microlens antenna for multi-pixel THz heterodyne detector arrays.” In 2013 7th European Conference on Antennas and Propagation (EuCAP) (pp. 1745-1746). IEEE.
- Lesaffre, P., Pineau des Forêts, G., Godard, B., et al. 2013, *A&A*, 550, A106
- Li, P. S., McKee, C. F., Klein, R. I. 2015, Magnetized interstellar molecular clouds. I. Comparison between simulations and Zeeman observations. arXiv:1506.08228

- Line, M. R., Parmentier, V., 2016. "The Influence of nonuniform Cloud Cover on Transit Transmission Spectra," *The Astrophysical Journal*, 820, 78.
- Line, M. R., Yung, Y.L., 2013a. "A Systematic Retrieval Analysis of Secondary Eclipse Spectra. III. Diagnosing Chemical Disequilibrium in Planetary Atmospheres," *The Astrophysical Journal*, 779, 3L.
- Line, M. R., Knutson, H., Deming, D., Wilkins, A., Desert, J.-M., 2013b. "A Near-infrared Transmission Spectrum for the Warm Saturn HAT-P-12b," *The Astrophysical Journal*, 778, 183.
- Line, M. R., Knutson, H., Wolf, A., Yung, Y. L. 2014. A Systematic Retrieval Analysis of Secondary Eclipse Spectra. II. A Uniform Analysis of Nine Planets and their C to O Ratios. *The Astrophysical Journal*, 783, 70.
- Line, M.I R., Stevenson, K. B., Bean, J., Desert, J.-M., Fortney, J. J., Kreidberg, L., Madhusudhan, N., Showman, A. P., Diamond-Lowe, H., 2016. "No Thermal Inversion and a Solar Water Abundance for the Hot Jupiter HD 209458b from HST/WFC3 Spectroscopy," *The Astronomical Journal*, 152, 203.
- Lines, S., Manners, J., Mayne, N. J., Goyal, J., Carter, A. L., Boutle, I. A., Lee, G. K. H., Helling, C., Drummond, B., Acreman, D. M., 2018. "Exonephology: transmission spectra from a 3D simulated cloudy atmosphere of HD 209458b", *Monthly Notices of the Royal Astronomical Society*, 481.
- Linsky, Jeffrey L. 1998. Deuterium Abundance in the Local ISM and Possible Spatial Variations. *Space Science Reviews*. 84, 285.
- Linsky, Jeffrey L., et al. 2007. Chandra Observations of the Eagle Nebula. I. Embedded Young Stellar Objects near the Pillars of Creation. *The Astrophysical Journal*. 654, 347.
- Lis, D., et al., 2014. Widespread Rotationally Hot Hydronium Ion in the Galactic Interstellar Medium. *The Astrophysical Journal*. 785, 135.
- Liu, X., Guo, W., Wang, Y., Dai, M., Wie, L.F., Dober, B., McKenney, C.M., et al. 2017, "Superconducting micro-resonator arrays with ideal frequency spacing," *Applied Physics Letters*, 111, 260
- Liu, D., Daddi, E., Dickinson, M., et al. 2018, "Super-deblended Dust Emission in Galaxies. I. The GOODS-North Catalog and the Cosmic Star Formation Rate Density out to Redshift 6" , *The Astrophysical Journal*. 853, 172
- Lodders, Katharina 2003. Solar System Abundances and Condensation Temperatures of the Elements. *The Astrophysical Journal*. 591, 1220.
- Lopez-Rodriguez, E., Dowell, C.D., Jones, T.J., et al. 2019, "SOFIA/HWC+ traces the magnetic fields in NGC 1068," eprint arXiv:1907.06648
- Lopez-Sanchez, A.R., Dopita, M.A., Kewley, L.J., Zahid, H.J., Nicholis, D.C., Scharwachter, J. 2012, "Eliminating error in the chemical abundance scale for extragalactic HII regions", *Monthly Notices of the Royal Astronomical Society*, 426, 2630
- Lourie, N.P., Ade, P.A.R., Angile, F.E. et al. 2018, "Preflight characterization of the BLAST-TNG receiver and detector arrays," *Proceedings of the SPIE*, 10708, 0
- Love, P.J., Hoffman, A.W., Lum, N.A., Ando, K.J., Rosbeck, J., Ritchie, W.D., Therrien, N.J., Holcombe, R.S. and Corrales, E., 2005. 1024 x 1024 Si: As IBC detector arrays for JWST MIRI. In *Proc. SPIE* (Vol. 5902, pp. 58-66).
- Lovelock, J. E., 1965. "A Physical Basis for Life Detection Experiments," *Nature*, 207, 568.

- Lloyd, R. O. P., France, K., Youngblood, A., Schneider, C., Brown, A., Hu, R., Linsky, J., Froning, C. S., Redfield, S., Rugheimer, S., Tian, F., 2016. "The MUSCLES Treasury Survey. III. X-Ray to Infrared Spectra of 11 M and K Stars Hosting Planets," *The Astrophysical Journal*, 824, 102.
- Luger, R., Barnes, R., 2015. "Extreme Water Loss and Abiotic O₂ Buildup on Planets Throughout the Habitable Zones of M Dwarfs," *Astrobiology*, 15, 119.
- Lum, N.A., Asbrock, J.F., White, R., et al. 1993, "Low-noise, low-temperature 256x256 Si:As IBC staring FPA," *Proceedings of the SPIE*, 1946, 100
- Lutz, D., et al. 1998. "The Nature and Evolution of Ultraluminous Infrared Galaxies: A Mid-Infrared Spectroscopic Survey", *The Astrophysical Journal*, 505, L103.
- Lutz, D. et al. 2003. "ISO spectroscopy of star formation and active nuclei in the luminous infrared galaxy NGC 6240", *Astronomy & Astrophysics*, 409, 867.
- Ma, Hopkin & Garrison-Kimmel, 2018. Simulating galaxies in the reionization era with FIRE-2: galaxy scaling relations, stellar mass functions, and luminosity functions. *MNRAS* 478, 1694
- MacDonald, R. J., Madhusudhan, N., 2017. "HD 209458b in new light: evidence of nitrogen chemistry, patchy clouds and sub-solar water," *Monthly Notices of the Royal Astronomical Society*, 469, 1979.
- MacKenzie, T.P., Scott, D., Swinbank, M., 2016, "SEDEBLEND: a new method for deblending spectral energy distributions in confused imaging," *Monthly Notices of the Royal Astronomical Society*, 463, 10.
- Madau, P., & Dickinson, M., 2014. "Cosmic Star-Formation History", *Annual Review of Astronomy & Astrophysics*, 52, 415.
- Madhusudhan, N., Agúndez, M., Moses, J. I., Hu, Y., 2016. "Exoplanetary Atmospheres – Chemistry, Formation Conditions, and Habitability." *Space Science reviews*, 205.
- Madhusudhan, N., Lee, K., Uts, I., Mousis, O., 2013. "Chemical characterization of Extrasolar Super-Earths - Interiors, Atmospheres, and Formation Conditions," *American Astronomical Society Meeting* 221, 126.04.
- Madhusudhan, Nikku 2012. C/O Ratio as a Dimension for Characterizing Exoplanetary Atmospheres. *The Astrophysical Journal*. 758, 36.
- Magorrian, J., et al., 1998. "The Demography of Massive Dark Objects in Galaxy Centers", *The Astronomical Journal*, 115, 2285.
- Mainzer, A., Bauer, J., Grav, T., et al. 2011, *The Astrophysical Journal*, 731, 53
- Mairs, S. et al. 2017, *The JCMT Transient Survey: Data Reduction and Calibration Methods*, *The Astrophysical Journal*, 843, 55
- Majeau, C., Agol, E., Cowan, N., B., 2012. "A Two-dimensional Infrared map of the Extrasolar Planet HD 189733b," *The Astrophysical Journal Letters*, 747, L20.
- Malfait, K., et al. 1998. The spectrum of the young star HD 100546 observed with the Infrared Space Observatory. *Astronomy and Astrophysics*. 332, L25.
- Mandel, K., Agol, E., 2002. "Analytic Light Curves for Planetary Transit Searches," *The Astrophysical Journal*, 580, L171.
- Manser, Christopher J., et al. 2016. Doppler imaging of the planetary debris disc at the white dwarf SDSS J122859.93+104032.9. *Monthly Notices of the Royal Astronomical Society*. 455, 4467.

- Marconi, A., and Hunt, L.K., 2003. "The Relation between Black Hole Mass, Bulge Mass, and Near-Infrared Luminosity", *The Astrophysical Journal*, 589, L21.
- Martin, D. and Puplett, E., 1970, "Polarised interferometric spectrometry for the millimetre and sub-millimetre spectrum," *Infrared Physics* 10(2), 105 – 109.
- Martin, C.L. 1999, "Properties of Galactic Outflows: Measurements of the Feedback from Star Formation," *The Astrophysical Journal*, 513, 156
- Martin, C.L., Shapley, A.E., Coil, A.L., Kornei, K.A., Bundy, K., Wiener, B.J., Noeske, K.G., Schiminovich, D. 2012, "Demographics and Physical Properties of Gas Outflows/Inflows at $0.4 < z < 1.4$ ", *The Astrophysical Journal*, 760, 127
- Marty, Bernard 2012. The origins and concentrations of water, carbon, nitrogen and noble gases on Earth. *Earth and Planetary Science Letters*. 313, 56.
- Masi, S., de Berardis, P., Paiella, A., Piacentini, F., Lamagna, L., Coppolecchia, A., et al. 2019, "Kinetic Inductance Detectors for OLIMPO experiment: in-flight operation and performance," *Journal of Cosmology and Astroparticle Physics*, 2019, July 2019
- Masunaga, H. & Inusuka, S. 2000, A Radiation Hydrodynamic Model for Protostellar Collapse, The Second Collapse and the Birth of a Protostar, *The Astrophysical Journal*, 531, 350
- Matsuo, T., Ito, S., Shibai, H., Sumi, T., Yamamuro, T., 2016. "A New Concept for Spectrophotometry of Exoplanets with Space-borne Telescopes," *The Astrophysical Journal*, 823, 139.
- Matsuo, T., Greene, T., Roellig, T. L., McMurray, R.E., Johnson, R.R., Kashani, A., Goda, S., Ido, M., Ito, S., Tsuboi, T., Yamamuro, T., Ikeda, Y., Shibai, H., Sumi, T., Sakon, T., Ennico-Smith, K., 2018, "A highly stable spectrophotometric capability for the Origins Space Telescope mid-infrared spectrometer and camera," *SPIE*, 10698, 44.
- Mauskopf, P.D., 2018. Transition Edge Sensors and Kinetic Inductance Detectors in Astronomical Instruments. *PASP*, 130, 2001
- McCormick, A., Veilleux, S., Rupke, D.S.N. 2013, "Dusty Winds: Extraplanar Polycyclic Aromatic Hydrocarbon Feature of Nearby Galaxies.", *The Astrophysical Journal*, 774, 126
- McClure, M. K., et al. 2015. Detections of Trans-Neptunian Ice in Protoplanetary Disks. *The Astrophysical Journal*. 799, 162.
- McClure, M. K., et al. 2016. Mass Measurements in Protoplanetary Disks from Hydrogen Deuteride. *The Astrophysical Journal*. 831, 167.
- McCullough, P. R., Crouzet, N., Deming, D., Madhusudhan, N., 2014. "Water Vapor in the Spectrum of the Extrasolar Planet HD 189733b. I. The Transit," *The Astrophysical Journal*, 791, 55.
- McKenney, C.M., Leduc, H.G., Swenson, L., Day, P.K., Eom, B.H., Zmuidzinas, J., 2012, "Design considerations for a background limited 350 micron pixel array using lumped element superconducting microresonators," *Proceedings of SPIE*, 8452, 0
- McMurtry, C.W., Forrest, W.J., Moore, A., Pipher, J.L., 2003, "Next Generation Space Telescope: NIR InSb array development," *Proceedings of SPIE*, 4850, 847
- McMurtry, C.W., Forrest, W.J., Pipher, J.L., 2005, "James Webb space telescope: noise results for the mutlplexers of the mid-infrared instrument (MIRI)," *Proceedings of SPIE*, 5902, 45
- McMurtry, C.W., Cabrera, M.S., Dorn, M.L., Pipher, J.L., Forrest, W.J., 2016, "13 micron cutoff Hg-CdTe detector arrays for space and ground-based astronomy," *Proceedings of SPIE*, 9915, 0

- McQuinn, M. 2016 “The Evolution of the Intergalactic Medium.” *Annual Review of Astronomy and Astrophysics*, 54, 313
- Meadows, V. S., 2017. “Reflections on O₂ as a Biosignature in Exoplanetary Atmospheres,” *Astrobiology*, 17, 1022.
- Meadows, Victoria S., Reinhard, Christopher T., Arney, Giada N., Parenteau, Mary N., Schwieterman, Edward W., Domagal-Goldman, Shawn D., Lincowski, Andrew P., Stapelfeldt, Karl R., Rauer, Heike, DasSarma, Shiladitya, Hegde, Siddharth; Narita, Norio, Deitrick, Russell, Lustig-Yaeger, Jacob, Lyons, Timothy W., Siegler, Nicholas, Grenfell, J. Lee, 2018. “Exoplanet Biosignatures: Understanding Oxygen as a Biosignature in the Context of Its Environment.” *Astrobiology*, 18.
- Meeus, G., et al. 2012. Observations of Herbig Ae/Be stars with Herschel/PACS. The atomic and molecular contents of their protoplanetary discs. *Astronomy and Astrophysics*. 544, A78.
- Megeath, S. T., et al. 2012. The Spitzer Space Telescope Survey of the Orion A and B Molecular Clouds. I. A Census of Dusty Young Stellar Objects and a Study of Their Mid-infrared Variability. *The Astronomical Journal*. 144, 192.
- Meijerink, R., et al. 2009. Radiative Transfer Models of Mid-Infrared H₂O Lines in the Planet-Forming Region of Circumstellar Disks. *The Astrophysical Journal*. 704, 1471.
- Melendez, M., Veilleux, S., Martin, C., Engelbracht, C., Bland-Hawthorn, J., Ceil, G., Heitsch, F., McCormick, A., Muller, T., Rupke, D., Teng, S.H. 2015, “Exploring the Dust Content of Galactic Winds with Herschel. I. NGC 4631”, *The Astrophysical Journal*, 804, 46
- Menendez-Delmestre, K., et al. 2007. “Mid-Infrared Spectroscopy of High-Redshift Submillimeter Galaxies: First Results”, *The Astrophysical Journal*, 655, L65.
- Milam, Stefanie N., et al. 2016. The James Webb Space Telescope’s Plan for Operations and Instrument Capabilities for Observations in the Solar System. *Publications of the Astronomical Society of the Pacific*. 128, 018001.
- Min, M., et al. 2011. The thermal structure and the location of the snow line in the protosolar nebula: Axisymmetric models with full 3-D radiative transfer. *Icarus*. 212, 416.
- Min, M., et al. 2016. The abundance and thermal history of water ice in the disk surrounding HD 142527 from the DIGIT Herschel Key Program. *Astronomy and Astrophysics*. 593, A11.
- Naftaly, M. and Dudley, R. 2011, “Terahertz reflectivities of metal-coated mirrors,” *Appl. Opt.* 50, 3201-3204.
- Mizusawa, H., Kazuyuki, Nishi, R., 2005, “Primordial Molecular Emission in Population III Galaxies,” *PASJ*, 57, 951.
- Molinari, S., et al. 1999. “Detection of the 62 micron crystalline H₂O ice feature in emission toward HH7 with the Infrared Space Observatory Long Wavelength Spectrometer.” *The Astrophysical Journal*, 521, L71.
- Montazeri, S., Wong, W. T. , Coskun, A. H. and Bardin, J. C. “Ultra-Low-Power Cryogenic SiGe Low-Noise Amplifiers: Theory and Demonstration,” in *IEEE Transactions on Microwave Theory and Techniques*, vol. 64, no. 1, pp. 178-187, Jan. 2016.
- Moorwood, A.F.M., 1999. “ISO observations of active galaxies”, *ESASP*, 427, 825.
- Morbidelli, A., et al. 2000. Source regions and time scales for the delivery of water to Earth. *Meteoritics and Planetary Science*. 35, 1309.

- Morris, B. M., Agol, E., Hebb, L., Hawley, S. L., Gillon, M., Ducrot, E., Delrez, L., Ingalls, J., Demory, B.-O., 2018. “Non-detection of Contamination by Stellar Activity in the Spitzer Transit Light Curves of TRAPPIST-1,” *The Astrophysical Journal Letters*, 863, L32.
- Moss, D., et al. 2013, The relation between magnetic and material arms in models for spiral arms. *A&A*, 556, 147
- Moster, B.P., et al., 2010. “Constraints on the Relationship between Stellar Mass and Halo Mass at Low and High Redshift”, *The Astrophysical Journal*, 710, 903.
- Muller, T., Balog, Z., Nielbock, M., et al. 2014, “Herschel celestial calibration sources. Four large main-belt asteroids as calibrators for the far-IR/sub-mm range,” *Experimental Astronomy*, 37, 253
- Mumma, Michael J. and Charnley, Steven B. 2011. The Chemical Composition of Comets—Emerging Taxonomies and Natal Heritage. *Annual Review of Astronomy and Astrophysics*. 49, 471.
- Murphy, E.J., et al. 2011. “Calibrating Extinction-free Star Formation Rate Diagnostics with 33 GHz Free-free Emission in NGC 6946”, *The Astrophysical Journal*, 737, 67.
- Najita, Joan R., et al. 2013. The HCN-Water Ratio in the Planet Formation Region of Disks. *The Astrophysical Journal*. 766, 134.
- Neufeld, D.A. and Melnick, G.J. 1991. Excitation of millimeter and submillimeter water masers. *Astronomical Journal*, 368, 215. And Erratum: 1991 *The Astrophysical Journal* 374 784
- Neufeld, D. A., & Wolfire, M.G., 2017. The cosmic-ray ionization rate in the Galactic disk, as determined from observations of molecular ions. *The Astrophysical Journal*. 845, 163.
- Noll S. et al., 2009. “Analysis of galaxy spectral energy distributions from far-UV to far-IR with CIGALE: studying a SINGS test sample”, *A&A* 507, 1793.
- Noroozian, O., Day, P.K., Eom, B.H., Leduc, H.G., Zmuidinas, J. 2012, “Crosstalk Reduction for Superconducting Microwave Resonator Arrays.” *IEEE Transactions on Microwave Theory and Techniques*, 60, 1235-1243
- Notsu, Shota, et al. 2016. Candidate Water Vapor Lines to Locate the H₂O Snowline through High-dispersion Spectroscopic Observations. I. The Case of a T Tauri Star. *The Astrophysical Journal*. 827, 113.
- Öberg, K. I., Murray-Clay, R., Bergin, E. A., 2011. “The Effects of Snowlines on C/O in Planetary Atmospheres,” *The Astrophysical Journal Letters*, 743, L16.
- Öberg, Karin I., et al. 2011. The Effects of Snowlines on C/O in Planetary Atmospheres. *The Astrophysical Journal*. 743, L16.
- Paganini, L., et al. 2017. Ground-based Detection of Deuterated Water in Comet C/2014 Q2 (Lovejoy) at IR Wavelengths. *The Astrophysical Journal*. 836, L25.
- Oberst, T. E.; Parshley, S. C.; Nikola, T.; Stacey, G. J.; Löhr, A.; Lane, A.P.; Stark, A.A.; Kamenetzky, J. 2011, “A 205 micron [NII] Map of the Carina Nebula”, *The Astrophysical Journal*, 739, 100.
- Ogle, P., Boulanger, F., Guillard, P., Evans, D. A., Antonucci, R., Appleton, P. N., Nesvadba, N., and Leipski, C., 2010. “Jet-powered Molecular Hydrogen Emission from Radio Galaxies” *The Astrophysical Journal*, 724, 1193.
- Olsson, K. S., Klimovich, K., An, K., Sullivan, S., Weathers, A., Shi, L., and Li, Z “Temperature Dependence of Brillouin Light Scattering Spectra of Acoustic Phonons in Silicon.” *Applied Physics Letters*. 106, 051906 (2015).

- Olson, J.R., Moore, M., Champagne, P., Roth, E., Evtimov, B., Jensen, J., Collaço, A., Nast, T. 2005, "Development of a Space-Type 4-Stage Pulse Tube Cryocooler For Very Low Temperature", *Advances in Cryogenic Engineering* 51. pp 623-631.
- Omont, A., et al. 1990. "Observations of the 40–70 micron bands of ice in IRAS 09371+1212 and other stars." *The Astrophysical Journal*, 355, L27.
- Omukai, K., Kitayama, T., 2003, "Observing H₂ Emission in Forming Galaxies," *The Astrophysical Journal*, 599, 738
- Ordoñez, O. F., Flores, M. R., Dib, J. R., Paz, A., & Farías, M. E. 2009. "Extremophile culture collection from Andean lakes: extreme pristine environments that host a wide diversity of microorganisms with tolerance to UV radiation." *Microbial ecology*, 58(3), 461-473
- Origins Space Telescope Mission Concept Study Team 2018, "The Origins Space Telescope Mission Concept Study Interim Report", 2018arXiv180909702T
- Orton, G.S., Fletcher, L.N., Moses, J.I. et al. 2014 Mid-infrared spectroscopy of Uranus from the Spitzer Infrared Spectrometer: 1. Determination of the mean temperature structure of the upper troposphere and stratosphere. *Icarus*, 243, 494
- Oshagh, M., Santos, N. C., Ehrenreich, D., Haghighipour, N., Figueira, P., Santerne, A., Montalto, M., 2014. "Impact of occultations of stellar active regions on transmission spectra. Can occultation of a plane mimic the signature of a blue sky?" *Astronomy & Astrophysics*, 568, A99.
- Pakmor, R., Springel, V. 2013, Simulations of magnetic fields in isolated disc galaxies. *MNRAS*, 432, 176
- Parmentier, V., Crossfield, I. J. M., 2018. "Exoplanet Phase Curves: Observations and Theory", *Handbook of Exoplanets*, ISBN 978-3-319-55332-0
- Parmentier, V., Fortney, J. J., Showman, A. P., Morley, C., Marley, M. S., 2016. "Transitions in the Cloud Compositions of Hot Jupiters," *The Astrophysical Journal*, 828, 22.
- Pascucci, I., et al. 2013. The Atomic and Molecular Content of Disks around Very Low-mass Stars and Brown Dwarfs. *The Astrophysical Journal*. 779, 178.
- Pearson W. J., et al. 2017. "De-blending deep Herschel surveys: A multi-wavelength approach," *A&A*, 603, A102.
- Perez, L. M. et al. 2014. Large-scale Asymmetries in the Transitional Disks of SAO 206462 and SR 21. *The Astrophysical Journal*, 783, L13.
- Perez, L.M. et al. 2016, Spiral density waves in a young protoplanetary disk, *Science*, 353, 1519
- Pereira-Santaella, M., Rigopoulou, D., Farrah, D., Lebouteiller, V., Li, J., 2017, "Far-infrared metallicity diagnostics: application to local ultraluminous infrared galaxies," *Monthly Notices of the Royal Astronomical Society*, 470, 1218
- Petach, M.; Michaelian, M. 2014, "Mid InfraRed Instrument (MIRI) Cooler Cold Head Assembly Acceptance Testing and Characterization," *Cryocoolers* 18, ICC Press, Boulder, CO, pp. 11-18.
- Pierrehumbert, R. T., 2010. "Principles of Planetary Climate." Cambridge University Press. ISBN: 9780521865562, 2010.
- Pineda, J.L., Langer, W.D., Goldsmith, P.F. 2014, "A Herschel [CII] Galactic plane survey. III. [CII] as a tracer of star formation", *A&A*, 570, 121

- Pinte, C., et al. 2016. Dust and Gas in the Disk of HL Tauri: Surface Density, Dust Settling, and Dust-to-gas Ratio. *The Astrophysical Journal*. 816, 25.
- Pipher, J.L., McMurtry, C.W., Forrest, W.J., et al., 2004, “Comparison of laboratory and in-flight performance of infrared array camera (IRAC) detector arrays on Spitzer Space Telescope,” *Proceedings of SPIE*, 5487, 234
- Planck Collaboration, et al. 2011, “Planck early results. II. The thermal performance of Planck” *Astronomy & Astrophysics*, 536, A2.
- Planck Collaboration et al. 2015, Planck intermediate results. XIX. An overview of the polarized thermal emission from Galactic dust, *Astronomy & Astrophysics*, 576, 104
- Poglitsch, A., Waelkens, C., Geis, N., et al. 2010, “The Photodetector Array Camera and Spectrometer (PACS) on the Herschel Space Observatory,” *Astronomy & Astrophysics*, 518, 2
- Pont, F., Knutson, H., Gilliland R. L., Moutou, C., Charbonneau, D., 2008. “Detection of atmospheric haze on an extrasolar planet: the 0.55-1.05 μm transmission spectrum of HD 189733b with the Hubble Space Telescope,” *Monthly Notices of the Royal Astronomical Society*, 385, 109.
- Pont, F., Sing D. K., Gibson, N. P., Aigrain, S., Henry, G., Husnoo, N., 2013. “The prevalence of dust on the exoplanet HD 189733b from Hubble and Spitzer Observations,” *Monthly Notices of the Royal Astronomical Society*, 432, 2917.
- Pontoppidan, Klaus M., et al. 2009. A New Raytracer for Modeling AU-Scale Imaging of Lines from Protoplanetary Disks. *The Astrophysical Journal*. 704, 1482.
- Pontoppidan, Klaus M., et al. 2010a. A Spitzer Survey of Mid-infrared Molecular Emission from Protoplanetary Disks. I. Detection Rates. *The Astrophysical Journal*. 720, 887.
- Pontoppidan, Klaus M., et al. 2010b. Spectrally Resolved Pure Rotational Lines of Water in Protoplanetary Disks. *The Astrophysical Journal*. 722, L173.
- Pontoppidan, Klaus M., et al. 2014. Volatiles in Protoplanetary Disks. *Protostars and Planets VI*, University of Arizona Press, 363.
- Pope, A., et al. 2008. “Mid-Infrared Spectral Diagnosis of Submillimeter Galaxies”, *The Astrophysical Journal*, 675, 1171.
- Popp, M., Schmidt, H., Marotzke, J., 2016. “Transition to a Moist Greenhouse with CO₂ and solar forcing.” *Nature Communications*, 7, 10627.
- Poteet, C. A. et al. 2011. “A Spitzer Infrared Spectrograph detection of crystalline silicates in a protostellar envelope.” *The Astrophysical Journal*, 733, L32.
- Poteet, C. A. et al. 2013. “Anomalous CO₂ ice toward HOPS-68: A tracer of protostellar feedback.” *The Astrophysical Journal*, 766, 117.
- Pottasch, S.R., et al. 2001. “Abundances of planetary nebulae NGC 7662 and NGC 6741”, *Astronomy & Astrophysics*, 380, 684.
- Quanz, S. P., Crossfield, I., Meyer, M. R., Schmalzl, E., Held, J., 2015. “Direct detection of exoplanets in the 3-10 μm range with E-ELT/METIS,” *International Journal of Astrobiology*, 14, 279.
- Rackham, B. V., Apai, D., Giampapa, M. S., 2018. “The Transit Light Source Effect: False Spectral Features and Incorrect Densities for M-dwarf Transiting Planets,” *The Astrophysical Journal*, 853, 122.

- Rackham, B., Espinoza, N., Apai, D., López-Morales, M., Jordán, A., Osip, D. J., Lewis, N. K., Rodler, F., Fraine, J. D., Morley, C. V., Fortney, J. J., 2017. "ACCESS I: An Optical Transmission Spectrum of GJ1214b Reveals a Heterogeneous Stellar Photosphere," *The Astrophysical Journal*, 834, 151.
- Ramirez, R. M., Craddock, R. A., Kaltenegger, L., 2018. "The Role of Methane on an Icy Early Mars and in Exoplanetary Atmospheres." *Comparative Climatology of Terrestrial Planets III: From Stars to Surfaces*.
- Raymond, Sean N. et al. 2004. Making other earths: dynamical simulations of terrestrial planet formation and water delivery. *Icarus*. 168, 1.
- Raymond G., Isaak, K.G., Clements, D., Rykala, A., and Pearson, C. 2010. "The Effectiveness of Mid IR / Far IR Blind, Wide Area, Spectral Surveys in Breaking the Confusion Limit," *PASJ*, 62, 697.
- Raymond, S. N. and Cossou, C. 2014. No universal minimum-mass extrasolar nebula: evidence against in situ accretion of systems of hot super-Earths.. *Monthly Notices of the Royal Astronomical Society*. 440, L11.
- Redford, J., Wheeler, J., Karkare, K., et al. 2018, "The design and characterization of a 300 channel, optimized full-band millimeter filterbank for science with SuperSpec," *Proceedings of SPIE*, 10708, 0
- Reed, D., Gardner, J., Quinn, T., Stadel, J., Fardal, M., Lake, G., Governato, F., 2003, "Evolution of the mass function of dark matter haloes," *Monthly Notices of the Royal Astronomical Society*, 346, 565
- Ressler, M.E., Cho, H., Lee, R.A.M., Sukhatme, K.G., Drab, J.J., Domingo, G., McKelvey, M.E., McMurray, R.E., Jr., Dotson, J.L., 2008, "Performance of the JWST/MIRI Si:As detectors," *High Energy Optical, and Infrared Detectors for Astronomy III*, ed. Dorn, D.A., Holland, A.D., *Proceedings of the SPIE*, Vol. 7021, 0
- Ricci, L., et al. 2010. Dust properties of protoplanetary disks in the Taurus-Auriga star forming region from millimeter wavelengths. *Astronomy and Astrophysics*. 512, A15.
- Richards, P.L. 1994, "Bolometers for infrared and millimeter waves," *Journal of Applied Physics*, 76, 1-24
- Richards, S.N. et al., 2018. SOFIA-HIRMES: Looking Forward to the HIGH-Resolution Mid-infrared Spectrometer. *JAI*. 7, 1840015.
- Ricker, G. R., et al., 2015. "Transiting Exoplanet Survey Satellite (TESS)." *Journal of Astronomical Telescopes, Instruments, and Systems*, 1, 014003.
- Riechers, D.A., et al. 2014. "Polycyclic Aromatic Hydrocarbon and Mid-Infrared Continuum Emission in a $z > 4$ Submillimeter Galaxy", *The Astrophysical Journal*, 786, 31.
- Rieke, G. H., Young, E. T., Engelbracht, C. W., Kelly, D. M., Low, F. J., Haller, E. E., ... & Cadien, J. (2004). The multiband imaging photometer for Spitzer (MIPS). *The Astrophysical Journal Supplement Series*, 154(1), 25.
- Rieke, G.H., Ressler, M.E., Morrison, J.E., et al. 2015, "The Mid-Infrared Instrument for the James Webb Space Telescope, VII: The MIRI Detectors," *Publications of the Astronomical Society of the Pacific*, 127, 665
- Rigby, J.R., et al. 2008. "Mid-Infrared Spectroscopy of Lensed Galaxies at $1 < z < 3$: The Nature of Sources Near the MIPS Confusion Limit", *The Astrophysical Journal*, 675, 262.

- Risacher et al. 2016, “The upGREAT 1.9 THz multi-pixel high resolution spectrometer for the SOFIA Observatory” *A&A* 595, 34
- Risacher et al, 2017, “The upGREAT THz heterodyne arrays for SOFIA: 1.9 THz and 4.7 THz first results,” in Proc. 28th Int. Symp. Space THz Tech., Cologne, Germany.
- Ritva A. Keski-Kuha, Charles W. Bowers, Manuel A. Quijada, James B. Heaney, Benjamin Gallagher, Andrew McKay, Ian Stevenson, 2012, “James Webb Space Telescope optical telescope element mirror coatings,” Proc. SPIE 8442, Space Telescopes and Instrumentation 2012: Optical, Infrared, and Millimeter Wave, 84422J
- Riviere-Marichalar, P., et al. 2012. Detection of warm water vapour in Taurus protoplanetary discs by Herschel. *Astronomy and Astrophysics*. 538, L3.
- Roberge, Aki, et al. 2006. Stabilization of the disk around β Pictoris by extremely carbon-rich gas. *Nature*. 441, 724.
- Robert, François, et al. 2000. The Solar System d/h Ratio: Observations and Theories. *Space Science Reviews*. 92, 201.
- Robinson, B. S. et al. “TeraByte InfraRed Delivery (TBIRD): a demonstration of large volume direct-to-Earth data transfer from low-Earth orbit”. eng. In: vol. 10524. SPIE, 2018, pp. 105240V-105240V-6. isbn: 9781510615335.
- Robinson, T. D., et al, 2011. “Earth as an Extrasolar Planet: Earth Model Validation Using EPOXI Earth Observations,” *Astrobiology*, 11, 393.
- Rodler, F., López-Morales, M., 2014. “Feasibility Studies for the Detection of O₂ in an Earth-like Exoplanet,” *The Astrophysical Journal*, 781, 54.
- Rogers, L. A., 2015. “Most 1.6 Earth-radius Planets are Not Rocky,” *The Astrophysical Journal*, 801, 41.
- Ros, K. and Johansen, A. 2013. Ice condensation as a planet formation mechanism. *Astronomy and Astrophysics*. 552, A137.
- Roseboom I. G, et al. 2010. “The Herschel Multi-Tiered Extragalactic Survey: source extraction and cross-identifications in confusion-dominated SPIRE images,” *MNRAS*, 409, 48.
- Ross, R.G., Johnson, D.L., 2006, “NASA’s Advanced Cryocooler Technology Development Program (ACTDP),” *Advances in Cryogenic Engineering: Transactions of the Cryogenic Engineering Conference – CEC*. AIP Conference Proceedings, 823, 607-614
- Ross, R.G., 2007, “Aerospace Coolers: A 50-Year Quest for Long-Life Cryogenic Cooling in Space,” *Cryogenic Engineering, International Cryogenics Monograph Series*, ISBN 978-0-387-33324-3, Springer, 225
- Rostem, K. , D. T. Chuss, K. L. Denis, E. Wollack, Wide-Stopband Aperiodic Phononic Filters, *J. Phys. D: Appl. Phys.*, 49, 255301 (2016)
- Roussel, H., Helou, G., Hollenbach, D.J. et al., 2007. Warm Molecular Hydrogen in the Spitzer SINGS Galaxy Sample. *The Astrophysical Journal*, 669, 959
- Rubio, M., Elmegreen, B.G., Hunter, D.A. et al., 2015. Dense cloud cores revealed by CO in the low metallicity dwarf galaxy WLM. *Nature*. 525, 218.

- Rudie, G.C., et al. 2012. “The Gaseous Environment of High- z Galaxies: Precision Measurements of Neutral Hydrogen in the Circumgalactic Medium of $z \sim 2-3$ Galaxies in the Keck Baryonic Structure Survey”, *The Astrophysical Journal*, 750, 67.
- Ruszkowski, M., Karen Yang, H.-Y., Zweibel, E. 2017, Global simulations of galactic winds including cosmic-ray streaming. *The Astrophysical Journal*, 834, 208
- Safron, E.J. et al. 2015, Hops 383: an Outbursting Class 0 Protostar in Orion, *The Astrophysical Journal*, 800, 5
- Sakon, I., Roellig, T.L., Ennico-Smith, K., Matsuo, T., Ikeda, Y., Yamamuro, T., Fujshiro, N., Enya, K., Takahashi, A., Wada, T., Guyon, O., Kotani, T., Nishikawa, J., Murakami, N., Sarugaku, Y., Burgarella, D., 2018, “The mid-infrared imager spectrometer, coronagraph (MISC) for the Origins Space Telescope,” *SPIE*, 10698, 17
- Salyk, Colette, et al. 2015. Detection of Water Vapor in the Terrestrial Planet Forming Region of a Transition Disk. *The Astrophysical Journal*. 810, L24.
- Sanders, D.B., Soifer, B.T., Elias, J.H., Madore, B.F., Matthews, K., Neugebauer, G., Scoville, N.Z. 1988, “Ultraluminous Infrared Galaxies and the Origin of Quasars.” *The Astrophysical Journal*, 325, 74
- Sanders, R.L., Shapley, A.E., Kriek, M., Reddy, N.A., Freeman, W.R., Coil, A.L., Siana, B., Mobasher, B., Shivaie, I., Price, S.H., de Groot, L., 2015, “The MOSDEF Survey: Mass, Metallicity, and Star-formation Rate at $z \sim 2.3$.” *The Astrophysical Journal*, 799, 138
- Sandstrom, K., et al. 2012. The Spitzer Spectroscopic Survey of the Small Magellanic Cloud (S4MC): Probing the Physical State of Polycyclic Aromatic Hydrocarbons in a Low-metallicity Environment. *The Astrophysical Journal*. 744, 20.
- Santoro, F., and Shull, J. M. 2006, *The Astrophysical Journal*, 643, 26
- Sarkar, S., Argyriou, I., Vandenbussche, B., Papageorgiou, A., Pascale, E., 2018. “Stellar pulsation and granulation as noise sources in exoplanet transit spectroscopy in the ARIEL space mission,” *Monthly Notices of the Royal Astronomical Society*, 481, 2871.
- Scarrott, S. M., et al. Imaging polarimetry of the galaxy NGC 1068 1991, *MNRAS*, 249, 16
- Schlegel, D.J., Finkbeiner, D.P., and Davis, M. 1998. “Maps of Dust Infrared Emission for Use in Estimation of Reddening and Cosmic Microwave Background Radiation Foregrounds,” *The Astrophysical Journal*, 500, 525.
- Schmalzl, M. et al., 2014. “Water in low-mass star-forming regions with Herschel. The link between water gas and ice in protostellar envelopes,” *Astronomy & Astrophysics*, 572, 81.
- Schnittman, J.D., and Krolik, J.H. 2008, “The Infrared Afterglow of Supermassive Black Hole Mergers,” *The Astrophysical Journal*, 684, 835
- Schoonenberg, Djoeka and Ormel, Chris W. 2017. Planetesimal formation near the snowline: in or out?. *Astronomy and Astrophysics*. 602, A21.
- Schruba, A., et al., 2017. Physical Properties of Molecular Clouds at 2 pc Resolution in the Low-Metallicity Dwarf Galaxy NGC 6822 and the Milky Way. *The Astrophysical Journal*. 835, 278.
- Schulz, B., Bock, J.J., Lu, N., Nguyen, H.T., Xu, C.K., Zhang, L., Dowell, C.D., Griffin, M.J., Laurent, G.T., Lim, T.L. and Swinyard, B.M., 2008, August. Noise performance of the Herschel-SPIRE bolometers during instrument ground tests. In *SPIE Astronomical Telescopes+ Instrumentation* (pp. 702022-702022). International Society for Optics and Photonics.

- Seager, S., Bains, W., Hu, R., 2013. "Biosignature Gases in H₂-dominated Atmospheres on Rocky Exoplanets." *The Astrophysical Journal*, 777, 95.
- Seager, S., Bains, W., Petkowski, J. J., 2016. "Toward a List of Molecules as Potential Biosignature Gases for the Search for Life on Exoplanets and Applications to Terrestrial Biochemistry." *Astrobiology*, 16.
- Seager, S., Deming, D., 2010. "Exoplanet Atmospheres," *Annual Review of Astronomy and Astrophysics*, 48.
- Segura, A., Krelow, K., Kasting, J. F., Sommerlatt, D., Meadows, V., Crisp, D., Cohen, M., Mlawer, E., 2003. "Ozone Concentrations and Ultraviolet Fluxes on Earth-Like Planets Around Other Stars," *Astrobiology*, 3, 689.
- Serindag, D. B., Snellen, I. A. G., 2019. "Testing the Detectability of Extraterrestrial O₂ with the Extremely Large Telescopes Using Real Data with Real Noise," *The Astrophysical Journal Letters*, 871, L7.
- Shapley, A.E., et al. 2003. "Rest-Frame Ultraviolet Spectra of z~3 Lyman Break Galaxies", *The Astrophysical Journal*, 588, 65.
- Shields, A. L., Ballard, S., Johnson, J. A., 2016. "The habitability of planets orbiting M-dwarf stars." *Physics Reports*, 663.
- Shipley, H.V., Papovich, C., Rieke, G.H., Brown, M. J. I., Moustakas, J., 2016 "A New Star Formation Rate Calibration from Polycyclic Aromatic Hydrocarbon Emission Features and Application to High-redshift Galaxies," *The Astrophysical Journal*, 818, 60
- Shirron, P. J., Canavan, E. R., DiPirro, M. J., Tuttle, J. G., and Yeager, C. J., 2000, "A Multi-Stage Continuous- Duty Adiabatic Demagnetization Refrigerator", 1629–1638, Springer US, Boston, MA.
- Shirron, P.J., Canavan, E.R., Dipirro, M.J., Jackson, M., Panek, J., Tuttle, J.G. 2002, "A continuous low-temperature magnetic refrigerator," *Low Temperature Detectors: 9th International Workshop AIP Conf. Proceedings*, 605, 379-382
- Shirron, P.J., Kimball, M.O., DiPirro, M.J., Biaslas, T.G., 2015, "Performance Testing of the Astro-H Flight Model 3-stage ADR," *Physics Procedia*, 67, 250-257
- Shirron, P. J., Kimball, M. O., James, B. L., Muench, T., DiPirro, M. J., Letmate, R. V., Sampson, M. A., Bialas, T. G., Sneiderman, G. A., Porter, F. S., and Kelley, R. L., 2016, "Operating modes and cooling capabilities of the 3-stage adr developed for the soft-x-ray spectrometer instrument on astro-h," *Cryogenics* 74, 2 – 9 (2016). 2015 Space Cryogenics Workshop, June 24-26, 2015, Phoenix, AZ Hosted by NASA Glenn Research Center, Cleveland, OH, USA.
- Shu, F. H. 1977. Self-similar collapse of isothermal spheres and star formation.. *The Astrophysical Journal*. 214, 488.
- Shu, F.H., Adams, F.C., & Lizano, S. 1987, Star formation in molecular clouds – Observation and theory, *Annual Review of Astronomy and Astrophysics*, 25, 23.
- Shu, S., Calvo, M., Goupy, J. et al. 2018, "Increased multiplexing of superconducting microresonator arrays by post-characterization adaption of the on-chip capacitors," *Applied Physical Letters*, 113, 2603
- Siess, L., et al. 2000. An internet server for pre-main sequence tracks of low- and intermediate-mass stars. *Astronomy and Astrophysics*. 358, 593.

- Simon, J. I., et al. 2011. Oxygen Isotope Variations at the Margin of a CAI Records Circulation Within the Solar Nebula. *Science*, 331, 1175.
- Sing, D. K., Fortney, J. J., Nikolov, N., Wakeford, H. R., Kataria, T., Evans, T. M., Aigrain, S., Ballester, G. E., Burrows, A. S., Deming, D., Désert, J.-M., Gibson, N. P., Henry, G. W., Huitson, C. M., Knutson, H. A., Lecavelier Des Etangs, A., Pont, F., Showman, A. P., Vidal-Madjar, A., Williamson, M. H., Wilson, P. A., 2016. “A continuum from clear to cloudy hot-Jupiter exoplanets without primordial water depletion,” *Nature*, 529, 59.
- Sing, D. K., Pont, F., Aigrain, S., Charbonneau, D., Désert, J.-M., Gibson, N., Gilliland, R., Hayek, W., Henry, G., Knutson, H., Lecavelier Des Etangs, A., Mazeh, T., Shporer, A., 2011. “Hubble Space Telescope transmission spectroscopy of the exoplanet HD 189733b: high-altitude atmospheric haze in the optical and near-ultraviolet with STIS,” *Monthly Notices of the Royal Astronomical Society*, 416, 1443.
- Sloan, G. C., et al., 2003. A Uniform Database of 2.4 - 45.4 Micron Spectra from the Infrared Space Observatory Short Wavelength Spectrometer. *The Astrophysical Journal Supplement*, 147, 379.
- Smith, J.D.T., et al. 2004. “Mid-Infrared IRS Spectroscopy of NGC 7331: A First Look at the Spitzer Infrared Nearby Galaxies Survey (SINGS) Legacy”, *The Astrophysical Journal Supplement Series*, 154, 199.
- Smith, J.D.T., Draine, B. T., Dale, D. A., Moustakas, J., Kennicutt, Jr., R. C., Helou, G., Armus, L., Roussel, H., Sheth, K., Bendo, G. J., Buckalew, B. A., Calzetti, D., Engelbracht, C. W., Gordon, K. D., Hollenbach, D. J., Li, A., Malhotra, S., Murphy, E. J., and Walter, F., 2007. “The Mid-Infrared Spectrum of Star-forming Galaxies: Global Properties of Polycyclic Aromatic Hydrocarbon Emission”, *The Astrophysical Journal*, 656, 770.
- Smith, R. G., et al. 1994. Molecular ices as temperature indicators for interstellar dust: the 44- and 62- μ m lattice features of H₂O ice.. *Monthly Notices of the Royal Astronomical Society*. 271, 481.
- Snellen, I., de Kok, R., Birkby, J. L., Brandl, B., Brogi, M., Keller, C., Kenworthy, M., Schwarz, H., Stuik, R., 2015. “Combining high-dispersion spectroscopy with high contrast imaging: Probing rocky planets around our nearest neighbors.” *Astronomy & Astrophysics*, 576, A59.
- Snellen, I. A. G., de Kok, R. J., le Poole, R., Brogi, M., Birkby, J., 2013. “Finding Extraterrestrial Life Using Ground-based High-dispersion Spectroscopy,” *The Astrophysical Journal*, 764, 182.
- Somerville, R.S., & Dave, R., 2015. “Physical Models of Galaxy Formation in a Cosmological Framework”, *Annual Review of Astronomy and Astrophysics*, 53, 51.
- Sousa-Silva, C., Seager, S., Petkowski, J. J., Ranjan, S., Zhan, Z., Hu, R., & Bains, W. 2019. “On Phosphine as a Biosignature Gas in Exoplanet Atmospheres.” *Astrobiology*
- Spergel, D.N., Verde, L., Peiris, H.V. et al., 2003, “First-Year Wilkinson Microwave Anisotropy Probe (WMAP) Observations: Determination of Cosmological Parameters”, *The Astrophysical Journal Supplement Series*, 148, 175.
- Spoon, H.W.W., & Holt, J., 2009a. “Discovery of Strongly Blueshifted Mid-Infrared [Ne III] and [Ne V] Emission in ULIRGs”, *The Astrophysical Journal*, 702, L42.
- Spoon, H.W.W., et al. 2009b. “High-Velocity Neon Line Emission From the ULIRG IRAS F00183-7111: Revealing the Optically Obscured Base of a Nuclear Outflow”, *The Astrophysical Journal*, 693, 1223.

- Springel, V., Di Matteo, T., and Hernquist, L., 2005. "Modelling feedback from stars and black holes in galaxy mergers", *Monthly Notices of the Royal Astronomical Society*, 361, 776.
- Stacey, G.J., Parshley, S., Nikola, T., et al. 2014, "SWCam: the short wavelength camera for the CCAT Observatory," *Proceedings of SPIE*, 9153,0
- Stacey, G.J., Hailey-Dunsheath, S., Nikola, T., Oberst, T.E., Parshley, S.C., Benford, D.J., Staguhn, J.G., Moseley, S.H., Tucker, C. 2007, "ZEUS: the Redshift (z) and Early Universe Spectrometer," *ASPC*, 375, 52
- Staguhn, J. G., Benford, D. J., Allen, C. A., et al. 2006, *Proc. SPIE*, 6275, 62751D
- Staguhn, J. G.; Benford, D. J.; Dowell, C. D.; Fixsen, D. J.; Hilton, G. C.; Irwin, K. D.; Jhabvala, C. A.; Maher, S. F.; Miller, T. M.; Moseley, S. H.; Sharp, E. H.; Runyan, M. C.; Wollack, E. J., 2016, "Performance of Backshort-Under-Grid Kilopixel TES Arrays for HAWC+," *Journal of Low Temperature Physics*, 184, 811
- Staguhn, J.G., 2018, "FIR Detector Sensitivity, Dynamic Range, and Multiplexing Requirements for the Origins Space Telescope," *Journal of Low Temperature Physics*, 193, 908-915
- Stahl et al., *Opt. Eng.*, 52(9) 091805 (2013)
- Stark, C.c., Belikov, R., Bolcar, M., et al. 2019, 'ExoEarth yield landscape for future direct imaging space telescopes,' *Journal of Astronomical Telescopes, Instruments and Systems*, 5, 24009
- Steidel, C.C., Dickinson, M., and Persson, S.E., 1994 "Field galaxy evolution since Z approximately 1 from a sample of QSO absorption-selected galaxies", *The Astrophysical Journal*, 437, L75.
- Steirwalt, S., et al. 2014. "Mid-infrared Properties of Luminous Infrared Galaxies. II. Probing the Dust and Gas Physics of the GOALS Sample", *The Astrophysical Journal*, 790, 124.
- Stevenson, David J. and Lunine, Jonathan I. 1988. Rapid formation of Jupiter by diffusive redistribution of water vapor in the solar nebula. *Icarus*. 75, 146.
- Strandet et al. 2017. "ISM Properties of a Massive Dusty Star-forming Galaxy Discovered at $z \sim 7$ ", *The Astrophysical Journal*, 842, L15.
- Sturm, E., et al. 2011. "Massive Molecular Outflows and Negative Feedback in ULIRGs Observed by Herschel-PACS", *The Astrophysical Journal*, 733, L16.
- Sullivan, Peter W., Winn, Joshua N., Berta-Thompson, Zachory K., Charbonneau, David, Deming, Drake, Dressing, Courtney D., Latham, David W., Levine, Alan M., McCullough, Peter R., Morton, Timothy, Ricker, George R., Vanderspek, roland, Woods, Deborah, 2015. "The Transiting Exoplanet Survey Satellite: Simulations of Planet Detections and Astrophysical False Positives," *The Astrophysical Journal*, 809, 77.
- Suzuki, T., Khosropanah, P., Ridder, M.L., Hijmering, R.A., Gao, J.R., Akamatsu, H., Gottardi, L., van der Kuur, JI, Jackson, B.D., 2016, "Development of Ultra-Low-Noise TES Bolometer Arrays," *Journal of Low Temperature Physics*, 184, 52.
- Swain, M. R., Line, M. R., Deroo, P., 2014. "On the Detection of Molecules in the Atmosphere of HD 189733b Using HST NICMOS Transmission Spectroscopy," *The Astrophysical Journal*, 784, 133.

- Swenson, L. J., Day, P. K., Dowell, C. D., Eom, B. H., Hollister, M. I., Jarnot, R., Kovacs, A., Leduc, H. G., McKenney, C. M., Monroe, R., Mroczkowski, T., Nguyen, H. T., and Zmuidzinas, J., 2012, “MAKO: a pathfinder instrument for on-sky demonstration of low-cost 350 micron imaging arrays,” in [Society of Photo-Optical Instrumentation Engineers (SPIE) Conference Series], Society of Photo-Optical Instrumentation Engineers (SPIE) Conference Series 8452, 0.
- Swinyard, B. M., Rieke, G.H., Ressler, M., Glasse, A., Wright, G.S., Ferlet, M., Wells, M., 2004, “Sensitivity estimates for the mid-infrared instrument (MIRI) on the JWST,” SPIE, Optical, Infrared, and Millimeter Space Telescopes, ed. Mater, J.C., Vol 5487, 785
- Tacconi, L., et al. 1999 “Gasdynamics in the Luminous Merger NGC 6240”, The Astrophysical Journal, 524, 732.
- Tanaka & Menou 2010, “Time-dependent Models for the Afterglows of Massive Black Hole Mergers”, The Astrophysical Journal. 714, 404
- Tian, F., 2009. “Thermal Escape from Super Earth Atmospheres in the Habitable Zones of M Stars,” The Astrophysical Journal, 703, 905.
- Tian, F., Ida, S., 2015. “Water contents of Earth-mass planets around M dwarfs,” Nature Geoscience, 8, 177.
- Trapman, L., et al. 2017. Far-infrared HD emission as a measure of protoplanetary disk mass. Astronomy and Astrophysics. 605, A69.
- Tremonti, C.A., et al. 2004 “The Origin of the Mass-Metallicity Relation: Insights from 53,000 Star-forming Galaxies in the Sloan Digital Sky Survey”, The Astrophysical Journal, 613, 898.
- Trotta, R., 2008. “Bayes in the sky: Bayesian inference and model selection in cosmology,” Contemporary Physics, 49, 71.
- Trotta, R., Ruiz de Austri, R., Pérez de los Heros, C., 2009. “Prospects for dark matter detection with IceCube in the context of the CMSSM,” Journal of Cosmology and Astroparticle Physics, 08, 034.
- Turbet, M., Leconte, J., Selsis, F., Belmont, E., Forget, F., Ribas, I., Raymond, S. N., Anglada-Escudé, G., 2016. “The habitability of Proxima Centauri b. II. Possible climates and observability.” Astronomy & Astrophysics, 596, A112.
- Turner, M.L., et al. 2014 “Metal-line absorption around $z \approx 2.4$ star-forming galaxies in the Keck Baryonic Structure Survey”, Monthly Notices of the Royal Astronomical Society, 445, 794.
- Tuttle, J., DiPirro, M., Canavan, E., Hait, T., 2008, “Thermal Properties of Double-Aluminized Kapton at Low Temperatures”, Advances in Cryogenic Engineering Materials Transactions of ICMC, 54, 34
- Tuttle, J., Canavan, E., DiPirro, M. et al. 2014, “The area-density-dependence of Ball IR Black’s low-temperature emissivity,” Cryogenics, 64, 240.
- Tuttle, J., Canavan, E., DeLee, H., et al. 2017, “Development of a space-flight ADR providing continuous cooling at 50 mK with heat rejection at 10 K,” IOP Conf. Ser.: Materials Science and Engineering 278 012009.
- Valiante, E., et al. 2007 “A Mid-Infrared Spectroscopic Study of Submillimeter Galaxies: Luminous Starbursts at High Redshift”, The Astrophysical Journal, 660, 1060.
- van der Marel, N., et al. 2016. Resolved gas cavities in transitional disks inferred from CO isotopologs with ALMA. Astronomy and Astrophysics. 585, A58.

- van der Marel, Nienke, et al. 2013. A Major Asymmetric Dust Trap in a Transition Disk. *Science*. 340, 1199.
- van Dishoeck, E. F., et al. 2011. Water in Star-forming Regions with the Herschel Space Observatory (WISH). I. Overview of Key Program and First Results. *Publications of the Astronomical Society of the Pacific*. 123, 138.
- Van Dishoeck, E.F., Bergin, E.A., Lis, D.C., Luninie, J.I. 2014. Water: From Clouds to Planets. In *Protostars and Planets VI*, Henrik Beuther, Ralf S. Klessen, Cornelis P. Dullemond, and Thomas Henning (eds.), University of Arizona Press, Tucson, 914 pp., p.835-85.
- Veilleux, S., Cecil, G., BlandPawthorn, J. et al. 2005, Galactic Winds. *Annual Review of Astronomy and Astrophysics*. 43, 769-826
- Veilleux, S., Melendez, M., Sturm, E., Gracia-Carpio, J., Fischer, J. et al. 2013. Fast Molecular Outflows in Luminous Galaxy Mergers: Evidence for Quasar Feedback from Herschel. *The Astrophysical Journal*, 776, 27
- Visser, R., et al. 2009. “The chemical history of molecules in circumstellar disks: I. Ices.” *Astronomy & Astrophysics*, 495, 881.
- Visser, Ruud, et al. 2013. Hot Water in the Inner 100 AU of the Class 0 Protostar NGC 1333 IRAS2A. *The Astrophysical Journal*. 769, 19.
- Vitense, Ch. et al., 2012. An improved model of the Edgeworth-Kuiper debris disk. *Astronomy and Astrophysics*, 540, 30.
- Vito, F., et al. 2018 “High-redshift AGN in the Chandra Deep Fields: the obscured fraction and space density of the sub- L^* population”, *Monthly Notices of the Royal Astronomical Society*, 473, 2378.
- Vogt Peter, Birk Manfred, Wagner Georg, Geiger Felix, Lange Gert, Golstein Hans, Kiselev Oleg, Emrich Anders, 2010, “Characterisation of the TELIS autocorrelator spectrometer”, 21st International Symposium on Space Terahertz Technology.
- Wakeford, H. R., Lewis, N. K., Fowler, J., Bruno, G., Wilson, T. J., Moran, S. E., Valenti, J., Batalha, N. E., Filippazzo, J., Bourrier, V., Hörst, S. M., Lederer, S. M., de Wit, J., 2019. “Disentangling the Planet from the Star in Late-Type M Dwarfs: A Case Study of TRAPPIST-1g,” *The Astronomical Journal*, 157, 11.
- Wakeford, H. R., Sing, D. K., 2015. “Transmission spectral properties of clouds for hot Jupiter exoplanets,” *Astronomy & Astrophysics*, 573, A122.
- Walch, S., et al., 2015. The SILCC (SIMulating the LifeCycle of molecular Clouds) project - I. Chemical evolution of the supernova-driven ISM. *Monthly Notices of the Royal Astronomical Society*. 454, 238.
- Walsh, Catherine, et al. 2014. Complex organic molecules in protoplanetary disks. *Astronomy and Astrophysics*. 563, A33.
- Wang, Yuwei; Tian, Feng; Hu, Yongyun. 2014, “Climate Patterns of Habitable Exoplanets in Eccentric Orbits Around M Dwarfs., *The Astrophysical Journal Letters*, 791, L12
- Watson, D., et al. 2015 “A dusty, normal galaxy in the epoch of reionization”, *Nature*, 522, 402.
- Watson, Dan M., et al. 2007. The development of a protoplanetary disk from its natal envelope. *Nature*. 448, 1026.

- Werk, J.K., et al. 2014 “The COS-Halos Survey: Physical Conditions and Baryonic Mass in the Low-redshift Circumgalactic Medium”, *The Astrophysical Journal*, 792, 8.
- Whitaker, K.E., et al., 2017 “The Constant Average Relationship between Dust-obscured Star Formation and Stellar Mass from $z = 0$ to $z = 2.5$ ”, *The Astrophysical Journal*, 850, 208.
- Whittet, D. C. B., et al. 1983. Interstellar ice grains in the Taurus molecular clouds. *Nature*. 303, 218.
- Wiedner et al. “A Proposed Heterodyne Receiver for the Origins Space Telescope” *IEEE Transactions on Terahertz Science and Technology* (Volume: 8 , Issue: 6 , Nov. 2018) Page(s): 558 - 571 DOI: 10.1109/TTHZ.2018.2876093
- Williams, Jonathan P. and Best, William M. J. 2014. A Parametric Modeling Approach to Measuring the Gas Masses of Circumstellar Disks. *The Astrophysical Journal*. 788, 59.
- Williams, Jonathan P. and Cieza, Lucas A. 2011. Protoplanetary Disks and Their Evolution. *Annual Review of Astronomy and Astrophysics*. 49, 67.
- Windhorst, R.A., Mather, J., Clampin, M. et al. 2009, “Galaxies Across Cosmic Time with JWST,” *Astro2010: The Astronomy and Astrophysics Decadal Survey*, Science White Papers, no. 317
- Winn, J. N., 2010. “Transits and Occultations,” from *EXOPLANETS*, ed. S. Seager, University of Arizona Press (Tucson, AZ).
- Woitke, P., et al. 2009. Radiation thermo-chemical models of protoplanetary disks. I. Hydrostatic disk structure and inner rim. *Astronomy and Astrophysics*. 501, 383.
- Wolf, E. T., 2017. “Assessing the Habitability of the TRAPPIST-1 System Using a 3D Climate Model.” *The Astrophysical Journal Letters*, 839, L1.
- Wolf, E. T., Toon, O. B., 2015. “The evolution of habitable climates under the brightening Sun,” *Journal of Geophysical Research: Atmospheres*, 120.
- Wolfgang, A., Lopez, E., 2015. “How Rocky Are They? The Composition Distribution of Kepler’s Sub-Neptune Planet Candidates within 0.15 AU,” *The Astrophysical Journal*, 806, 183.
- Wolfire, M. G., Hollenbach, D. and McKee, C. F., 2010. The Dark Molecular Gas. *The Astrophysical Journal*. 716, 1191.
- Wordsworth, R. D., Schaefer, L. K., Fischer, R. A., 2018. “Redox Evolution via Gravitational Differentiation on Low-mass Planets: Implications for Abiotic Oxygen, Water Loss, and Habitability”, *The Astronomical Journal*, 155, 195.
- Wordsworth, R., 2015. “Atmospheric Heat Redistribution and Collapse on Tidally Locked Rocky Planets,” *The Astrophysical Journal*, 806, 180.
- Wright, E.L 1998, “Angular Power Spectra of the COBE DIRBE Maps,” *The Astrophysical Journal*, 496, 1
- Yan, L., et al. 2005 “Spitzer Detection of Polycyclic Aromatic Hydrocarbon and Silicate Dust Features in the Mid-Infrared Spectra of $z \sim 2$ Ultraluminous Infrared Galaxies”, *The Astrophysical Journal*, 628, 604.
- Yang, J., Cowan, N. B., Abbot, D. S., 2013. “Stabilizing Cloud Feedback Dramatically Expands the Habitable Zone of Tidally Locked Planets,” *The Astrophysical Journal Letters*, 771, L45.
- Yang, Le, Ciesla, F.J., and Alexander, C.M.O.D., 2013. The D/H ratio of water in the solar nebula during its formation and evolution. *Icarus*. 226, 256.

- Yang, Y.-L., et al., 2017. The Class 0 Protostar BHR71: Herschel Observations and Dust Continuum Models, *The Astrophysical Journal*, Volume 835, Issue 2, article id. 259, 27
- Yang, Y.-L., et al., 2018. CO in Protostars (COPS): Herschel-SPIRE Spectroscopy of Embedded Protostars, *The Astrophysical Journal*, Volume 860, Issue 2, article id. 174, 32
- Yates, S.J.C., Baryshev, A.M., Yurduseven, O., et al. 2017, “Surface Wave Control for Large Arrays of Microwave Kinetic Inductance Detectors,” *IEEE Transactions on Terahertz Science and Technology*, &, 789-799
- Yoo, H. et al. 2017, The JCMT Transient Survey: Detection of Submillimeter Variability in a Class I Protostar EC 53 in Serpens Main, *The Astrophysical Journal*, 849, 69
- Youngblood, A., France, K., Loyd, R.O.P., et al. 2017 “The MUSCLES Treasury Survey. IV. Scaling Relations for Ultraviolet, Ca II K, and Energetic Particle Fluxes from M Dwarfs,” *The Astrophysical Journal*, 843, 31
- Yu M, et al., 2017. “The Effects of Protostellar Disk Turbulence on CO Emission Lines: A Comparison Study of Disks with Constant CO Abundance versus Chemically Evolving Disks,” *The Astrophysical Journal*, 850, 169.
- Zahid, H. J., Dima, G.I., Kudritzki, R-P, Kewlwy, L.J., Geller, M.J., Hwang, H.S., Silverman, J.D., Kashino, D. 2014, “The Universal Relation of Galactic Chemical Evolution: The Origin of the Mass-Metallicity Relation.” *The Astrophysical Journal*, 791, 130
- Zahnle, K. J., Marley, M. S., 2014. “Methane, Carbon Monoxide, and Ammonia in Brown Dwarfs and Self-Luminous Giant Planets,” *The Astrophysical Journal*, 797, 41.
- Zailer, E., Belostotski, L. and Plume, R. 2016, “8-GHz, 6.6-mW LC-VCO with Small Die Area and FOM of 204 dBc/Hz at 1-MHz Offset,” *IEEE Microwave and Wireless Components Letters*, vol. 26, no. 11, pp. 936-938.
- Zakhvatkin, M. V. et al. “RadioAstron orbit determination and evaluation of its results using correlation of space-VLBI observations”. In: arXiv e-prints, arXiv:1812.01623 (Dec. 2018), arXiv:1812.01623. arXiv: 1812.01623 [astro-ph.IM].
- Zellem, R. T., Griffith, C. A., Pearson, K. A., Turner, J. D., Henry, G. W., Williamson, M. H., Ryleigh F., M., Teske, J. K., Biddle, L. I., 2015. “XO-2b: A Hot Jupiter with a Variable Host Star That Potentially Affects Its Measured Transit Depth,” *The Astrophysical Journal*, 810, 11.
- Zellem, R. T., Swain, M. R., Roudier, G., Shkolnik, E. L., Creech-Eakman, M. J., Ciardi, D. R., Line, M. R., Iyer, A. R., Bryden, G., Llama, J., Fahy, K. A., 2017. “Forecasting the Impact of Stellar Activity on Transiting Exoplanet Spectra,” *The Astrophysical Journal*, 844, 27.
- Zeng, L., et al. 2018. “Survival function analysis of planet size distribution with Gaia Data Release 2 updates.” *Monthly Notices of the Royal Astronomical Society*, 479, 4.
- Zmuidzinas, J., 2012. Superconducting microresonators: Physics and applications. *Annu. Rev. Condens. Matter Phys.*, 3(1), pp.169-214.
- Zmuidzinas, J. and Richards, P.L., 2004. Superconducting detectors and mixers for millimeter and submillimeter astrophysics. *Proceedings of the IEEE*, 92(10), pp.1597-1616.
- Zubko, V., Dwek, E., and Arendt, R.G. 2004. “Interstellar Dust Models Consistent with Extinction, Emission, and Abundance Constraints,” *The Astrophysical Journal Supplements*, 152, 211.
- Zuckerman, B. and Song, Inseok 2012. A 40 Myr Old Gaseous Circumstellar Disk at 49 Ceti: Massive CO-rich Comet Clouds at Young A-type Stars. *The Astrophysical Journal*. 758, 77.